ESL-TR-87-73
VOL I

SCALING PROBLEMS FOR WAVE PROPAGATION IN LAYERED SYSTEMS VOLUME I

F.Y. SORRELL, Y. HORIE, J.K. WHITFIELD,
S.H. LEE, J.K. PARK

NORTH CAROLINA STATE UNIVERSITY
DEPARTMENT OF MECHANICAL & AEROSPACE ENGINEERING
RALEIGH NC 27695-7910

SEPTEMBER 1989

FINAL REPORT

MARCH 1985 — MARCH 1988

AIR FORCE ENGINEERING & SERVICES CENTER
ENGINEERING & SERVICES LABORATORY
TYNDALL AIR FORCE BASE, FLORIDA 32403

NOTICE

PLEASE DO NOT REQUEST COPIES OF THIS REPORT FROM HQ AFESC/RD (ENGINEERING AND SERVICES LABORATORY). ADDITIONAL COPIES MAY BE PURCHASED FROM:

NATIONAL TECHNICAL INFORMATION SERVICE
5285 PORT ROYAL ROAD
SPRINGFIELD, VIRGINIA 22161

FEDERAL GOVERNMENT AGENCIES AND THEIR CONTRACTORS REGISTERED WITH DEFENSE TECHNICAL INFORMATION CENTER SHOULD DIRECT REQUESTS FOR COPIES OF THIS REPORT TO:

DEFENSE TECHNICAL INFORMATION CENTER
CAMERON STATION
ALEXANDRIA, VIRGINIA 22314

REPORT DOCUMENTATION PAGE

Form Approved OMB No. 0704-0188

1a. REPORT SECURITY CLASSIFICATION UNCLASSIFIED	1b. RESTRICTIVE MARKINGS
2a. SECURITY CLASSIFICATION AUTHORITY	3. DISTRIBUTION/AVAILABILITY OF REPORT Approved for public release. Distribution unlimited.
2b. DECLASSIFICATION/DOWNGRADING SCHEDULE	
4. PERFORMING ORGANIZATION REPORT NUMBER(S) Contract F08635-85-K-0052	5. MONITORING ORGANIZATION REPORT NUMBER(S) ESL-TR-87-73 Vol I
6a. NAME OF PERFORMING ORGANIZATION North Carolina State University 6b. OFFICE SYMBOL (If applicable)	7a. NAME OF MONITORING ORGANIZATION Air Force Engineering and Services Center
6c. ADDRESS (City, State, and ZIP Code) Department of Mechanical & Aerospace Engineering Raleigh NC 27695-7910	7b. ADDRESS (City, State, and ZIP Code) HQ AFESC/RDCS Tyndall AFB FL 32403-6001
8a. NAME OF FUNDING/SPONSORING ORGANIZATION 8b. OFFICE SYMBOL (If applicable)	9 PROCUREMENT INSTRUMENT IDENTIFICATION NUMBER Contract F08635-85-K-0052
8c. ADDRESS (City, State, and ZIP Code)	10. SOURCE OF FUNDING NUMBERS PROGRAM ELEMENT NO. 6.2 / PROJECT NO. 2673 / TASK NO 0046 / WORK UNIT ACCESSION NO.

11. TITLE (Include Security Classification)
Scaling Problems for Wave Propagation in Layered Systems Vol I

12. PERSONAL AUTHOR(S)
Sorrell,F.Y.;Horie,Y.;Whitfield,J.K.;Lee,S.H.;Park,J.K.

13a. TYPE OF REPORT	13b. TIME COVERED	14. DATE OF REPORT (Year, Month, Day)	15 PAGE COUNT
Final	FROM Mar85 TO Mar88	September 1989	262

16. SUPPLEMENTARY NOTATION
Availability of this report is specified on reverse of front cover

17. COSATI CODES			18. SUBJECT TERMS (Continue on reverse if necessary and identify by block number)
FIELD	GROUP	SUB-GROUP	Gas gun, Scaling, Layered systems, Buried model structures, Ground-shock loading, Coventional, Wave propagation

19. ABSTRACT (Continue on reverse if necessary and identify by block number)

This Technical Report consists of three volumes. Volume I, Executive Summary, Introduction and Laboratory Test Program, describes the gas gun facility and technique and correct scaling for test models. Volume II, Wave-Analysis Program for the Response of Buried Model Structures describes the computer code for wave propagation analysis of buried model structures under ground-shock loading. Volume III, Experimental and Numerical Program, covers methods of laboratory simulation of ground shock loading from a conventional weapon and develops a unified numerical simulation of ground-shock loading and structural response.

20. DISTRIBUTION/AVAILABILITY OF ABSTRACT ☒ UNCLASSIFIED/UNLIMITED ☐ SAME AS RPT ☐ DTIC USERS	21. ABSTRACT SECURITY CLASSIFICATION UNCLASSIFIED
22a. NAME OF RESPONSIBLE INDIVIDUAL Diane B. Miller, Capt, USAF	22b. TELEPHONE (Include Area Code) (904)-283-3728 22c. OFFICE SYMBOL HQ AFESC/RDCS

DD Form 1473, JUN 86 Previous editions are obsolete.

(The reverse of this page is blank).

PREFACE

This report was prepared by North Carolina State University, Raleigh, NC 27695-7910, under contract number F08635-85-K-0052, for the Air Force Engineering and Services Center, Engineering and Services Laboratory, Airbase Structures and Weapons Effects Branch (AFESC/RDCS), Tyndall AFB, FL 32403-6001. Lt Col Robert J. Majka and Capt Diane B. Miller were the government technical program managers. This report summarizes work accomplished between 1 March 1985 and 1 March 1988.

This report has been reviewed by the Public Affairs office and is releasable to the National Technical Information Service (NTIS). At NTIS, it will be available to the general public, including foreign nations.

This technical report has been reviewed and is approved for publication.

Diane B Miller

DIANE B. MILLER, Capt, USAF
Project Officer

Robert J. Majka

ROBERT J. MAJKA, Lt Col, USAF
Chief, Engineering Research Division

William S. Strickland

WILLIAM S. STRICKLAND
Chief, Airbase Structures and
Weapons Effects Branch

James R. VanOrman

JAMES R. VAN ORMAN, Deputy Director
Engineering and Services Laboratory

A-1

(The reverse of this page is blank.)

TABLE OF CONTENTS

TABLE OF CONTENTS (CONCLUDED)

LIST OF FIGURES

LIST OF FIGURES

(Concluded)

LIST OF TABLES

(The reverse of this page is blank.)

SECTION I

INTRODUCTION

A. OBJECTIVES

The major objective was the development of an experimental technique and of necessary facilities for testing reduced-scale models to study the dynamic response behavior of protective structures against conventional weapons. Special emphasis was placed upon the behavior of layered systems such as buried structures under high dynamic loading that results from close-in detonations. This work includes the development and verification of scaled-model systems, and the development of computational capabilities for conducting wave propagation analysis of the layered systems. The latter is required for evaluation and use of the test data.

B. BACKGROUND

A broad perspective of protective structural design against conventional weapons had been given in a recent review article by N. H. Abramson (Reference 1). He finds: (1) that because of improvements in guidance techniques, expected loads are increased by orders of magnitudes, (2) because of this, the traditional design methodologies and data base are inadequate for severe loadings from bombs directly impacting or detonating very close to their targets, and (3) there is a need for new design concepts as well as new and different materials to neutralize this emerging threat.

Full-scale testing of new designs and materials and the development of instrumentation to determine loads accurately from close-in detonations are expensive and time consuming. One effective approach is to use scale models (Reference 2). Scale models have been successfully used in developing approximate solutions and gaining physical insight into problems where theory is inadequate to obtain a complete solution or where full-scale tests are too expensive. The model testing of tall structures is such

an example (Reference 3). Other examples in hydrodynamics, aerodynamics, and elasticity are widely known (References 4-8). Recent examples and progress dealing with protective structures for conventional weapons may be found in References 7 and 9.

Model testing is also an effective and inexpensive means of initially screening new ideas and new materials. The use of models is not restricted to conservative phenomena; thus, there is no restriction on the mode of deformation. For example, structural models have been tested successfully under both impact and explosive loading involving plastic deformation and fracture (Reference 9). It has also been shown that if the primary concern is the modeling of the ultimate strength of structures, similitude requirements can be somewhat relaxed, depending upon the mode of failure (Reference 10).

The novelty of the proposed program is the use of compressed-gas guns for the simulation of close-in detonations and their interactions with protective structures. Conceptually, the proposed gun facility is similar to those that employ a shock tube (Reference 11), a high-pressure gas (Reference 12), or a drop-weight (Reference 13) to generate dynamic loads. The difference lies in the technique of generating and controlling critical parameters such as peak pressure, pressure-time relation, and impulse-peak pressure relationship. The gun system has capabilities that cannot be duplicated by other techniques including explosives. It has the advantages of precise repeatability of the loading and the capability to produce a wide range of loading conditions, including very high peak pressures.

C. SCOPE

The first phase of the proposed research program is the modeling of the response of buried structures loaded by the ground shock from close-in detonations. The scaling of the wave propagation was accomplished in terms of geometric similitude where the geometric dimensions of a prototype are scaled by a constant factor, S. The reason is that the governing

differential equations including those for the description of shocks are invariant under this scaling (Reference 2). The restriction which must be applied is that strain rate effects are negligible. Fortunately, many porous energy-absorbing materials are known to satisfy this condition (References 14 and 15). Additional benefits of the geometric scaling are: (1) that the same solid material may be used in a model as in a prototype and (2) that impact velocity and loading pressure will be identical in model and prototype. Table 1 shows a selected list of variables that are invariant or scaled geometrically by S. Section III.A.2 gives a complete analysis of scaling considerations, as well as how the correct scaled loading is achieved with the gas gun.

Experimental facility development comprises the construction of four major components: (1) a gun (a projectile launcher), (2) a soil test chamber, (3) a model structure, and (4) instrumentation. The ground shock loading device was constructed to simulate pressure waves in the ranges of 1-100 ksi and 1 μs - 10 ms in duration. The magnitude of these parameters is controlled by such parameters as projectile impact velocity and geometry, mechanical impedance, and protective soil cover, etc. A complete description of how these parameters are controlled in a gas gun is given in Section III.A. The test chamber and model must be large enough to minimize boundary effects. In the present studies the maximum soil chamber is limited to 30-inch diameter. With this test chamber, geometric scale factors need to be 15 or less for a panel of 15 feet by 15 feet. The generic structures used in the preliminary tests were limited to a concrete slab with and without steel reinforcement. The construction of model slabs were based upon the technique developed in References 7 and 8. The loading on the model was measured by Manganin gages and in some cases by polymer gages developed by the National Bureau of Standards. Structural failures were studied in terms of scaled loads and load profiles. These tests, without instrumentation, are referred to as recovery tests, and were conducted to study qualitatively the correlation between failure modes and load profiles. These were used to demonstrate the capability of the gas gun to provide the desired loading conditions. A limited number of

instrumented tests were conducted to further verify the capability of achieving the correct scaling in peak loads and load profiles.

TABLE 1. SCALING OF SELECTED VARIABLES

Quantity	Ideal Scale	SI Units
Length	S	M
Displacement	S	M
Scaled Distance	1	$M/Kg^{1/3}$
Strain	1	mm/M
Stress	1	MPa (KBar)
Time	S	sec
Velocity	S	M/s
Density	1	Kg/M^3
Elastic Moduli	1	MPa
Loading Impulse	S^3	$MPa-M^2-sec$
Unit Impulse (Areal)	S	MPa-sec

The development of computational capabilities focused on the construction of a two-dimensional wave propagation code to study ground shock and structure interactions in a unified fashion. Of particular interest was the investigation of the short-time stress-wave response of buried structures under high dynamic loading. A central problem is the description of material response in the form of constitutive equations. The current effort utilized the development of simple constitutive equations for various soil types in a unified structure to improve understanding of shock loading on buried structures. Concrete behavior was described by a model based upon plasticity theory and tensile failure in the direction of maximum tension (Reference 16 and 17).

Parametric numerical studies were conducted on generic concrete structures to guide and aid in the analysis of the experiments, and to identify the relative importance of different parameters that govern structural failure under close-in detonations.

D. REPORT ORGANIZATION

The report is organized in two volumes. Volume I describes the gas gun facility development and use, including the construction details of the guns used in this work. It also contains a description of the instrumentation currently used. In addition it gives the results of a number of experiments that are used to demonstrate the capability of the gas gun technique to produce scaled loading on test models. This volume includes the methodology for producing the scaled test models. It also describes the correct scaling of ground shock loads from conventional weapons, in order to assure the model is correctly loaded.

Volume II describes the computational model. This volume provides a description of the code. Also, description applications of the code are given for the simplified test geometry used in the experiments. In addition, the code is also used to simulate results for a more realistic model structure. Finally, this volume discusses the usefulness of the code for evaluation of general ground shock loading on protective structures.

SECTION II

FACILITY DEVELOPMENT

A. GAS GUNS

1. General Description

As stated in the Introduction, the major objective was the development of an experimental technique and the necessary facilities to evaluate the technique for testing reduced scale models. This testing is to study and improve the dynamic response behavior of protective structures against conventional weapons. Of particular interest is the ability to conduct scale-model testing of the layered systems typical of those in buried structures. The goal of the testing is to simulate the high dynamic loading that occurs from close-in detonations. The loading from such detonations is characterized by rapid, and high loading. Typically the peak normal stress under such conditions ranges from 100 KPa (0.1 KBar) to 500 MPa (5 KBar) with loading rise times of 0.05 to 5 milliseconds. Scale loading on a test model should be at the same stress levels, and with the loading time scaled down or shortened by the geometry scale factor, S. A full discussion of the correctly scaled loading is given in Section III.A.

A number of experimental techniques were considered for producing this type of loading. In addition to producing the loading mentioned above, the method should be repeatable and easily controlled. A review of the techniques considered is not given here. The decision was made to use the light-gas gun to produce the loading in a controlled laboratory environment. The Shock Physics laboratory at North Carolina State University (NCSU) has considerable experience with powder guns and some experience with light-gas guns. With gas guns a light (low-molecular weight) -driver gas is used to accelerate projectiles to a high speed. The loading described above can generally be achieved with a "medium" -weight driver gas, such as Nitrogen or air. Therefore,the present tests are with what should be strictly called a gas gun. The use of a light-driver gas is always possible if higher-

loading conditions are desired. Two facilities were used in the present work. The first is a 3.8 cm bore gun, that was initially a powder gun, i.e., the projectile was accelerated by a conventional powder burn. This gun was converted to a medium pressure gas gun and used for preliminary experiments. A brief description of this gun is given in the next section.

Because of the small bore of the 3.8 cm gun, the geometric scale ratio between a full-scale structure and the test model is quite large. The standard scale ratio used in the present tests was 30. This scale factor was so large as to make some of the test model structural parameters questionable. Of particular question is the correct scaling of a sand or soil layer with a scale factor this large. A larger gas gun, dedicated to ground shock simulation, was constructed to work with a larger test model, and has a smaller geometric scale ratio. A 6-inch bore diameter gun was chosen to meet this objective. (Because this gun is made of 6-inch bore steel tube, it is referred to as a 6-inch gun although this report uses the SI system of units.) A determination of the projectile speed required to produce the desired ground shock pressures indicated that a projectile speed of 300 m/s (1000 ft/s) would be required. The isentropic theory for the gas expansion was applied via an interactive computer program to determine the proper barrel length to achieve this speed. A 1.4 meter (4.5 foot) barrel was found to be required to achieve the desired speed range with a maximum reservoir (breech) pressure of 20 MPa (3000 Psi). A description of the design conditions for the 6 inch gun are given in the section following the 3.8 cm gun (Section II.A.3). This section includes the results of preliminary tests to evaluate the performance of the gun. A detail design description of the gun and the operating procedures is given in Appendix A.

2. 3.8 Cm Gun

The 3.8 cm gun was used for many of the initial experiments to simulate ground shock. This gun was developed by modification of an existing 2 cm powder gun which had been used on previous projects. The modification consisted of replacing the 2 cm diameter barrel with a 3.8 cm diameter barrel which was available. In addition, the powder breech was

replaced with a low volume gas breech. A diagram of this gun is shown in Figure 1, and shows the major components which are:

a. A manually operated gas breech which is limited to a maximum gas pressure of 5 MPa (800 Psig).

b. A 3.8 cm bore diameter barrel which is 2.1 meters long. The barrel includes ports that can be used to make projectile speed measurements.

c. A rectangular target chamber that houses the test model and has electrical feed-through connections for instrumentation.

d. A catcher tank filled with shock-absorbing material in case the test model does not stop the projectile.

The target chamber will allow a test model, including mount, of approximately 18 cm (6 inch) on a side, with a maximum total length of 35 cm (14 inch). The gun uses both Aluminum or Lexan® projectiles, with a typical projectile mass of 37 to 175 gram. The lower limit on projectile mass is set by having a projectile long enough that it does not tumble or bind in the barrel. The upper limit on projectile mass is set by the speed that can be achieved, lower mass projectiles can be accelerated to higher speeds. For the low mass projectiles the maximum speed that can be obtained is approximately 225 m/s.

Because this gun was a retrofit of an existing system, it was modified and available for experiments relatively early in the project. The gun has a limited range of projectile mass and speed, which makes the data that can be obtained from it somewhat limited. However, a much more serious limitation is the small-size test model that must be used. The smallest scale ratio for structures of interest is about 30. This scale ratio is so small that there are some concerns the scale effects may be distorting the results. Of particular concern is the modeling of soil layers with this large scale ratio. Because of this, a larger facility was deemed necessary.

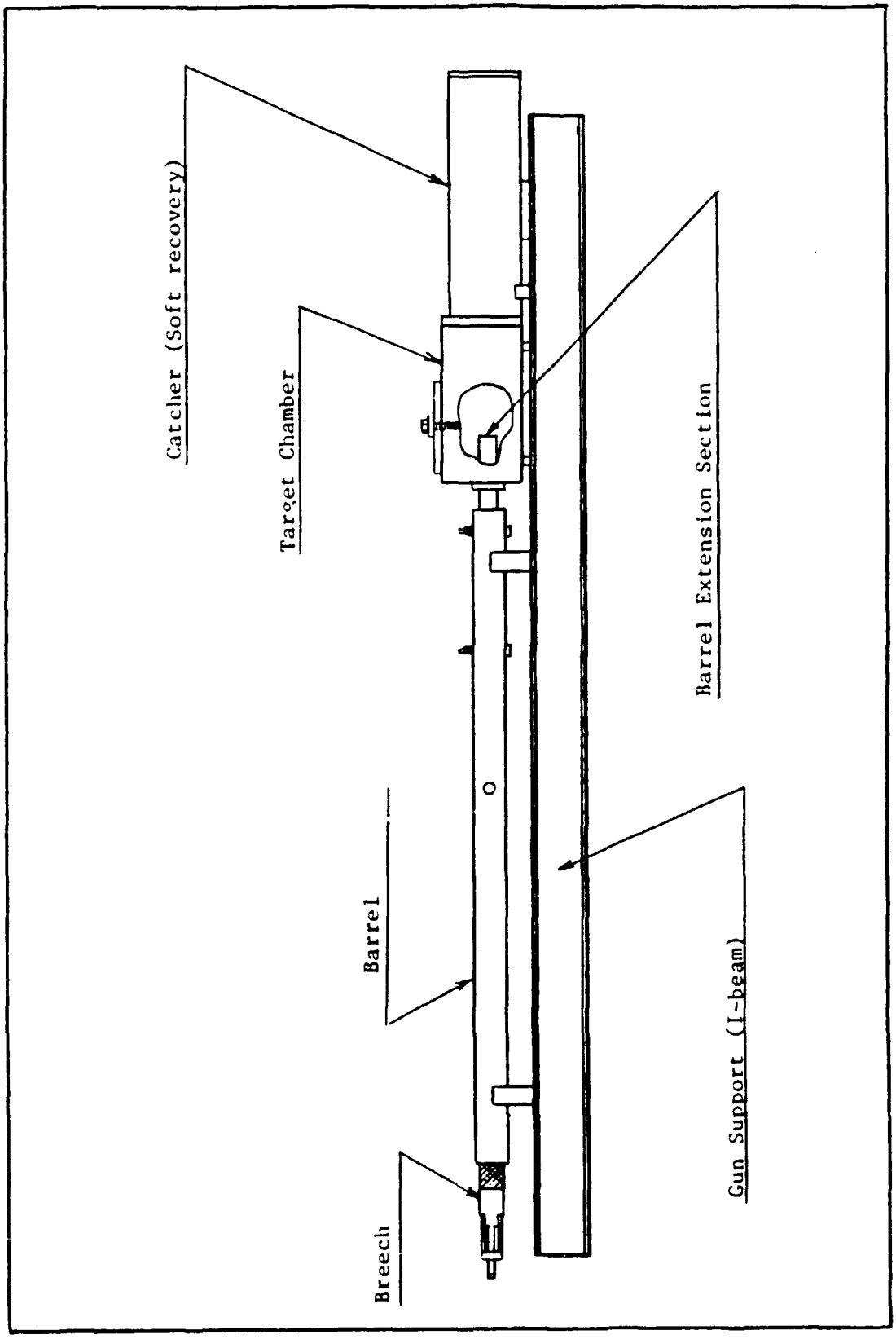

Figure 1. Overall View of the 3.8 cm Light-Gas Gun

3. Six-Inch Gun

a. General

Because a 6-inch gun was specifically developed for the testing of scale models of buried hardened structures, the design started from basic scientific performance considerations. The practical velocity range of a single-stage gas gun, up to 1500 m/sec as shown in reference 18, is more than adequate for this research program (this fact will be expanded on in the shock wave theory discussion). Additionally, gas guns are relatively safe and can be operated by a small laboratory staff in a campus environment. Furthermore, the Shock Physics Laboratory has been operating a 50 mm diameter bore light gas gun since 1983.

Although this laboratory also has experience with powder-driven guns which can be shorter for given projectile velocities and therefore less expensive, they are less satisfactory for precisely controlled impact studies due to problems of cleanliness and large recoil forces. Also of primary concern was the problem of proper storage and handling of gunpowder in a densely populated campus atmosphere.

Designed for a maximum projectile mass of 3 Kg (6 pounds weight) with a maximum velocity of 500 m/sec (1600 ft/sec), the gun has produced a velocity of 200 m/sec (670 ft/sec) with a breech pressure as low as 2 Mpa (300 psi), which is one-tenth of the maximum design pressure on a 1.6 Kg (3.5 pound weight) projectile. The gun system is comprised basically of a "wrap-around" breech attached to one end of a three section, smooth bore barrel. Compressed gas such as helium is employed to accelerate projectiles. The projectile, acting as its own release valve in the breech, accelerates down the barrel to the muzzle end, where the target is placed. Impact with the target occurs at the muzzle end of the barrel which is located in a tank serving as a dual- purpose impact chamber and catcher. The catcher stops and contains the results of the impact. In terms of safety, the entire system was designed with a minimum of 1.5 factor of safety, based on yield, for all components.

b. Theoretical Considerations

To achieve this performance, a number of variations in design were considered. The major design parameters are barrel length, barrel diameter, operating pressure, gas reservoir volume, and system vacuum. Probably the most important of these parameters is the barrel diameter which obviously determines the projectile diameter.

The bore diameter of 6 inch was determined based upon two factors: the scaling factor S and the practical limits of gas-driven systems (Reference 18). Once the diameter is chosen, a projectile length of no less than the bore diameter is implied to keep the length-to-diameter ratio (L/D) at a minimum of one. Sufficient projectile length must be maintained to provide good tilt control (impact surface angular misalignment) at the target end of the barrel.

Operating pressure and barrel length are interdependent and have direct bearing on the velocities obtainable for a given projectile and projectile mass. The maximum operating pressure is basically limited by: (1) the expense of constructing a gas reservoir capable of withstanding the pressure, and (2) the gas expansion volume available which is limited by the barrel volume and catcher volume. These physical restraints are further restricted by the amount of available laboratory space. If the barrel is made too long, the frictional and gas dynamic effects lower the average propelling pressure. For ideal circumstances, one would want a propellant capable of propelling the projectile for its entire travel at a constant pressure equal to the initial pressure of the gas reservoir (Reference 19). As such, a propellant known as a "constant-base pressure propellant," is only idyllic. The method of achieving high velocities is to increase the average propelling pressure by finding a balance between breech (gas reservoir) dimensions and capabilities, and suitable barrel length. However, while increasing the average pressure, attention must be given to all gun components in terms of pressure rise so as not to damage the components. Seigel (Reference 19) reported that, in practice, barrels and gas reservoirs can be designed to withstand static

pressures up to 900 Mpa (130,000 psi) without permanent deformation. This research program does not require such extreme gas pressures to achieve the needed shock loads.

The gas reservoir volume depends both on the desired velocity range and the available space for the facility. A light-gas gun having its gas reservoir or chamber diameter greater than its barrel diameter is described as a "chambered" facility or a facility with "chamberage." As the projectile moves down the barrel, a rarefaction disturbance is created behind the projectile by its acceleration and the evacuation of a small space behind it. A rarefaction disturbance is characterized by the fact that it decreases the pressure and density of the gas through which it passes. In a chambered facility the rarefaction travels in the barrel toward the breech, and upon reaching the increased area section gas flows from a larger volume layer into the evacuated space. As a result, the pressure in that space is raised to a higher pressure than if the gas had moved from a constant-diameter chamber. Therefore, the rarefaction disturbance from the projectile, upon reaching the change in area section, is partially reflected as a compression disturbance traveling back toward the projectile. Consequently, the pressure behind the projectile is raised and therefore the projectile velocity is raised above the value of a facility having no chamberage. The transmitted portion of the rarefaction continues into the breech and is reflected as a rarefaction; at the change in area, a portion is reflected as a rarefaction and the remainder travels toward the projectile as a rarefaction. Therefore, increased chamberage is more conducive to maintaining a constant average base pressure and leads to higher velocities. Due to rarefaction characteristics, increasing chamber diameter increases velocity to a greater extent than increasing chamber length. For a more complete treatment of this entire phenomenon see Reference 19. The above discussion is beneficial to this particular design as space is limited in the laboratory. In light of these facts, the gas reservoir volume should be designed with an emphasis on maximum chamber diameter and minimum chamber length within the constraints of space and velocity requirements.

A properly designed vacuum system provides for a more reliable response from the instrumentation and, therefore, more accurate and interpretable results. The most important volume to be evacuated is the barrel as any air in front of the projectile reduces the projectile velocity as the air is compressed, and the consequent air shock produced is recorded by the instruments. Provisions for both drawing the vacuum and measuring it must be incorporated into the design process.

The motion of a projectile in a barrel is calculated, based on the assumption that the gas expansion is one-dimensional and isentropic. Consider the model presented in Figure 2, where M denotes the projectile mass, L denotes the barrel length, and A denotes the cross-sectional area of the barrel. The gas pressure at the rear of the projectile is given by P_p and X_p is the distance traveled by the projectile at an instantaneous projectile velocity given by V_p. Newton's law applied to the projectile at any instant of time yields:

$$F = Ma = \frac{MdV_p}{dt} = \frac{MV_p dV_p}{dxp} = P_p A \qquad (1)$$

Rewriting Equation (1):

$$MV_p dV_p = P_p A dx_p \qquad (2)$$

Now integrating:

$$\frac{1}{2} MV^2 = A \int_0^{L_p} P_p dx \qquad (3)$$

The left-hand side of Equation (3) should be recognized as the kinetic energy of the projectile. The right-hand side of Equation (2) is the incremental work done by the expanding gas at the instant in question. Namely,

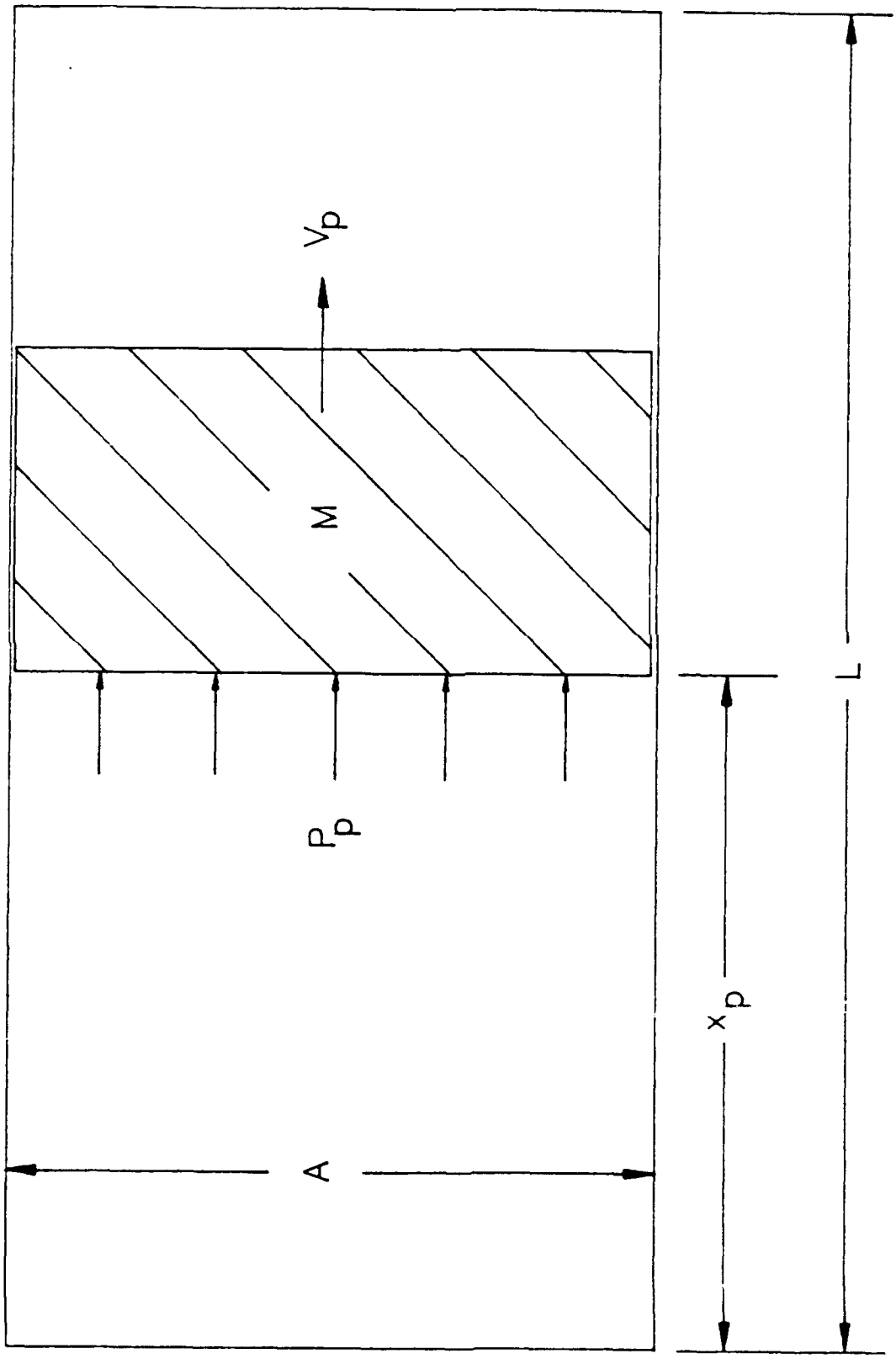

Figure 2. Work Done by the Movement of a System Boundary

$$\delta_W = P_p A dx_p = P_p \, dV \; . \tag{4}$$

Then, assuming we are dealing with a isentropic process, the total work done by the expanding gas on the projectile is

$$W_{12} = \int_1^2 \delta W = \int_1^2 P_p dV \tag{5}$$

where W_{12} symbolizes the work done during the process from State 1 to State 2.

One standard computational procedure for solving the integral in Equation (5) is to assume the polytropic equation.

$$PV^n = \text{constant } (C) \tag{6}$$

The value of n may be any value from -1 to +1 depending on the particular process. For this class of processes, the integration of Equation (6) is

$$\therefore \int_1^2 P_p dV = \frac{P_2V_2 - P_1V_1}{1 - n} \tag{7}$$

This is valid for every case except n=1. For n=1, the integral is given by

$$\int_1^2 P_p dV = P_1V_1 \text{Ln} \left[\frac{V_2}{V_1}\right] \tag{8}$$

If the gas is ideal, then n is the specific heat ratio, k, defined as the ratio of the constant-pressure specific heat to the constant-volume specific

heat at zero pressure. Finally, an expression for projectile velocity can be obtained from Equations (8) and (3).

$$\frac{1}{2} MV_p^2 = \frac{P_2V_2 - P_1V_1}{1 - k} \tag{9}$$

Or:

$$V_p = \left[\frac{2(P_2V_2 - P_1V_1)}{M(1 - k)}\right]^{1/2} \tag{10}$$

Both the breech and barrel are treated as thick-walled cylinders subjected to an internal pressure. The projectile is a moving boundary at one end of the barrel and the breech essentially serves as a closed other end. The preceding section shows that the pressure behind the projectile decreases as it moves down the barrel (the work of the expanding gas being converted into the kinetic energy of the projectile). However, the barrel is designed to withstand the maximum pressure introduced into the barrel. Therefore, all barrel sections will be designed as if they are subjected to the maximum pressure.

For both the breech and barrel, the external pressure (P_o) is taken to be zero; therefore, the internal pressure (P_i) is represented simply as P. The longitudinal stress exists because the internal pressure acts on the closed ends of the vessel. The force acting against the ends must be equated to the longitudinal stress times the area over which it acts. Thus,

$$P\pi a^2 = \sigma_a(\pi Dt) = \sigma_a(\pi 2at)$$

$$\therefore \sigma_a = \frac{Pa}{2t} \tag{11}$$

where a is the inner radius of the cylinder and t is the wall thickness.

Differing from a closed, thick-walled cylinder, an open-ended, thick-walled cylinder experiences only tangential and radial stresses when external or internal pressures are exerted on it. These stress components are given by References 21 and 22.

$$\sigma_t = \frac{P_l a^2 - P_o b^2 - a^2 b^2 (P_o - P_i)/r^2}{b^2 - a^2} \tag{12}$$

$$\sigma_r = \frac{P_l a^2 - P_o b^2 + a^2 b^2 (P_o - P_i)/r^2}{b^2 - a^2} \tag{13}$$

As is the usual sign convention, positive stresses are taken to indicate tension and negative stresses indicate compression. Again, we take the external pressure to be zero and simply call the internal pressure P. Therefore, the longitudinal stress (defined by Equation (11)) and the tangential stress are tensile components, and the radial stress is a compressive component. Since there are no shear forces acting on the cylinder, the principal stresses are equivalent to the normal stresses defined as σ_t, σ_r, and σ_a. The following definitions will be used for the remainder of this discussion:

$$\sigma_1 = \sigma_{t,max} = \bar{P}_{max} \left[\frac{b^2 + a^2}{b^2 - a^2}\right] \tag{14}$$

$$\sigma_2 = \sigma_{a,max} = \frac{P_{mas}}{b - a} \tag{15}$$

$$\sigma_3 = \sigma_{r,max} = -P_{max} \tag{16}$$

With the maximum stresses defined above, a failure theory is applied to predict the onset of plastic deformation. Several theories have

been developed to predict failure of ductile materials. The distortion-energy theory is used in this design.

The theory predicts that yielding begins whenever the distortion energy equals the distortion energy at yield in simple tension. The beginning of yield for a triaxial stress state is predicted by:

$$\sigma' = \left[\sigma_t^2 + \sigma_a^2 + \sigma_r^2 - (\sigma_t\sigma_a + \sigma_a\sigma_r + \sigma_t\sigma_r)\right]^{1/2} \tag{17}$$

This expression is referred to as a von Mises stress or equivalent stress, σ'. Therefore, failure by yielding is predicted whenever $\sigma'=S_y$ and a factor of safety, n, is predicted by:

$$n = \frac{S_y}{\sigma} \tag{18}$$

Many investigators have observed that gun barrels do not show any signs of plastic deformation when fired at pressures much higher than the pressures which produce yield under hydrostatic tests, i.e., materials exhibit much higher yield strength under dynamic loading than that under static loading (Reference 22). Therefore, for designing components such as a gun barrel, dynamic yield strength, a function of strain-rate, may be used. Use of the static yield strength, S_y , results in a conservative design, making it safer than the calculated factor of safety indicates.

c. Performance

The prediction curves for the 6-inch gun were plotted from theoretical data obtained by using Equations (7) and (10). Computer programs were written to give the projectile velocities, breech pressures, catcher pressures, and travel distances for projectile weights varying from 8 N (2 pound) to 25 N (6 pound). The curves presented on the following pages are all based on helium as the propellant gas. This is because helium is

currently available in the laboratory. Additionally, Reference 8 indicates that theoretical and experimental data are in better agreement when helium is used as the driver gas rather than nitrogen.

Figure 3 shows the projectile velocity-breech pressure curves for different projectile weights. These and subsequent curves show that projectile weight plays a large role in the performance of the gun. This set of curves can be used to predict the projectile velocity at a given breech pressure and projectile weight. Curves showing the increase in projectile velocity as different weight projectiles move down the barrel at a maximum breech pressure of 20 MPa (3000 psi) are shown in Figure 4. These are the projectile Velocity-Travel Distance Curve. These curves show that the velocity begins to increase linearly with distance about half-way down the barrel and that the curves are actually beginning to flatten, suggesting that a constant velocity is being approached as the projectile reaches the muzzle end of the barrel. Because the catcher tank pressure is limited, the final pressure in the catcher chamber was calculated. Figure 5 contains the curve of final catcher pressure versus breech pressure for varying weight projectiles. This curve shows that the catcher chamber is capable of handling the final expansion pressure experienced for the entire operational pressure range. In fact, for many of the shot combinations, the final pressure is below atmospheric pressure.

The 6-inch diameter gun has been used successfully for producing projectile velocities from 185 m/s (610 ft/s) to 220 m/s (730 ft/s). Projectiles weighing from 15 N (3.35 pounds) to 33 N (7.35 pounds) have been accelerated by the system and have been stopped in the catcher with the use of the stripping mechanism described in the appendix A. Projectile velocity predictions made via the analytical velocity equation derived previously and used in a computer code have proved reliable. The percent difference between the calculated projectile velocity and the measured projectile velocity has ranged from 1 percent to 3.5 percent. These percent differences agree with the results reported in Reference 19, which also used the theory of isentropic expansion to predict projectile

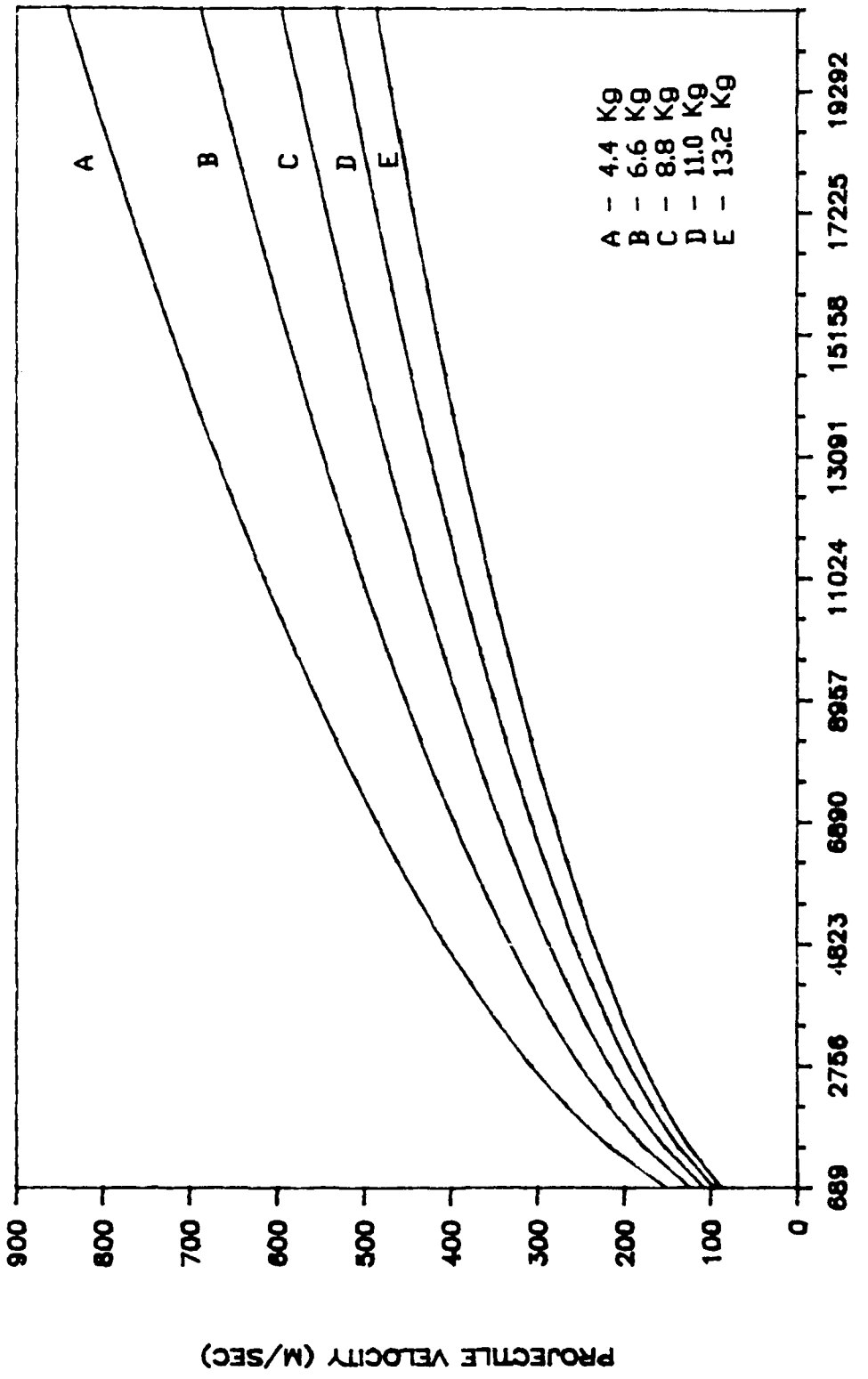

Figure 3. Projectile Velocity as a Function of Breech Pressure - Helium Driver Gas.

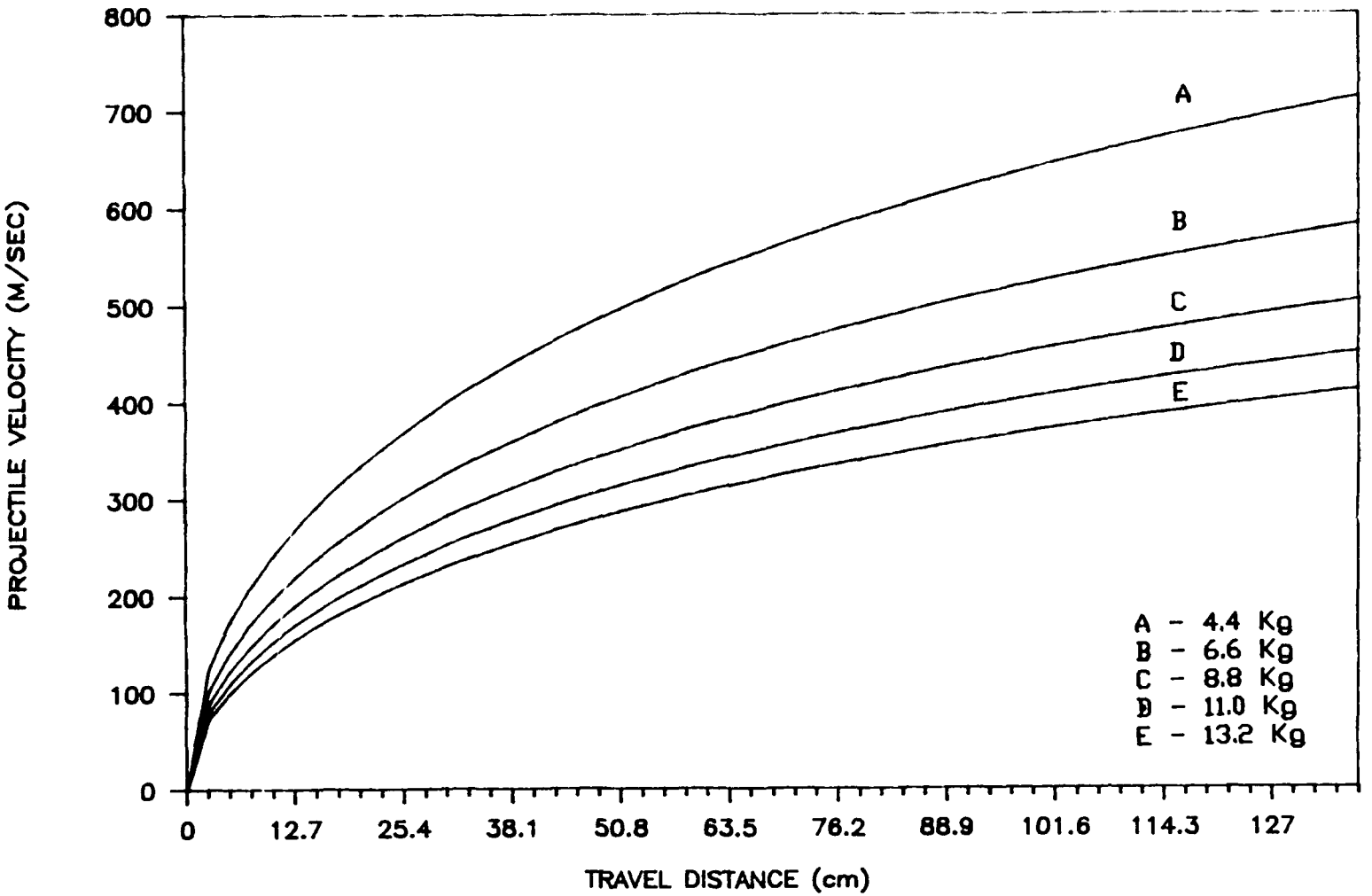

Figure 4. Projectile Velocity as a Function of Projectile Travel Distance - Helium Driver Gas.

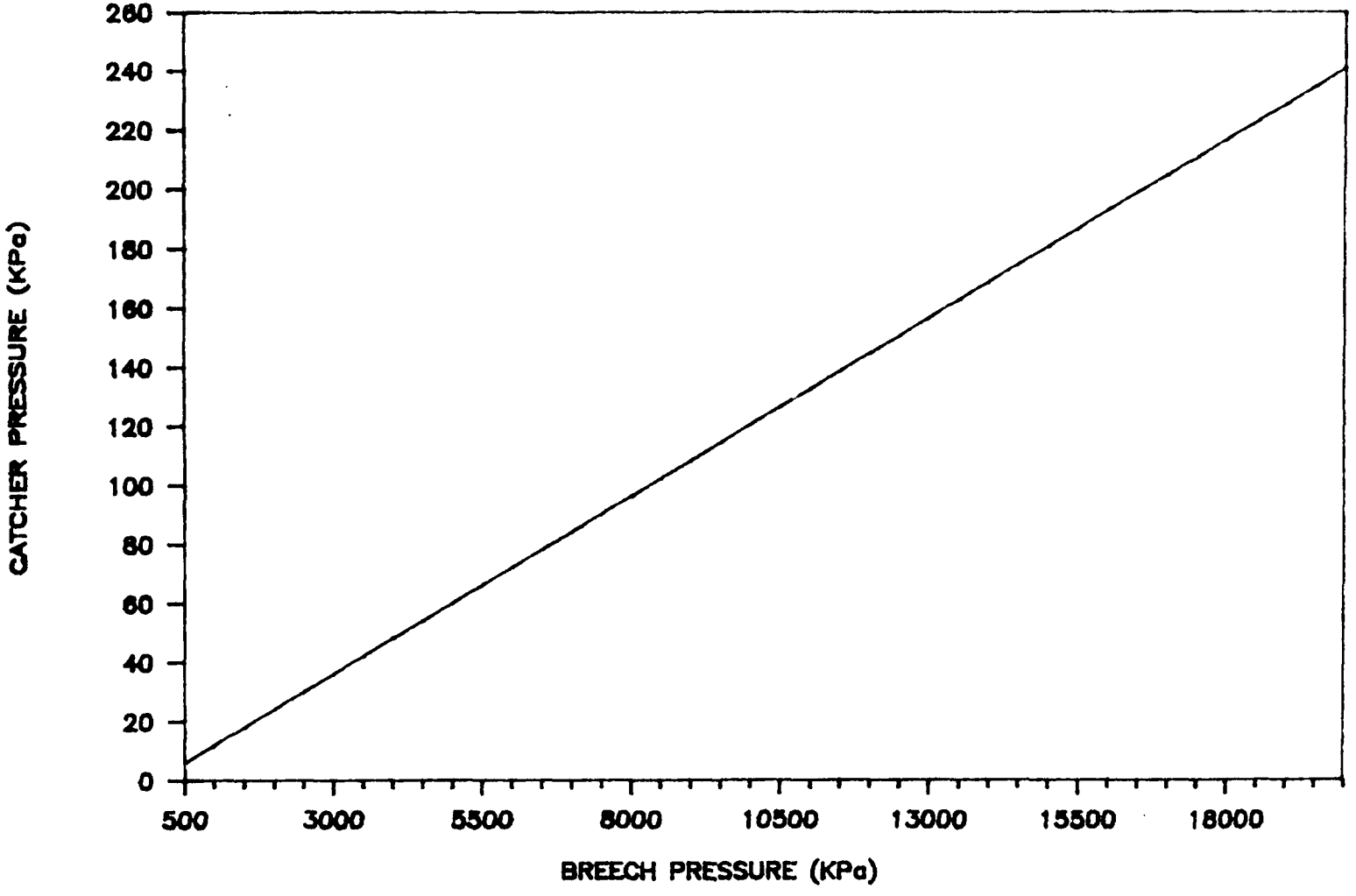

Figure 5. Catcher Tank Pressure as a Function of Breech Pressure - Helium Driver Gas.

velocities. Upper limits on the projectile velocity have not been established to date because of the nature of the research work in progress and because a safety wall for the protection of the gun operators has not yet been erected. However, the prediction curves for projectile velocity versus breech pressure are expected to show good agreement with actual experimental results at even higher projectile velocities. The comparison in Reference 19 showed good agreement with isentropic predictions for velocities as high as 3600 m/s (12,000 ft/s).

Overall performance of the light-gas gun has been good and its relatively quiet operation has not created any noise problems on campus. It has proven to be a clean-operating system with a reasonable turnaround time in terms of actual gun preparation. The gun can be fired as frequently as once a day if several targets and several projectiles are prepared in advance.

The gun barrel was fabricated from a 1018 CD steel tubing which is a relatively soft material, therefore , susceptible to scratching and scoring in the bore diameter. To avoid this type of damage to the barrel, a steel tubing made from an alloy steel such as 4140 or 4340 is recommended since these materials are tougher initially and are also heat-treatable. Another consideration in terms of barrel design is that of barrel length. The 1.4 meter (4.5 feet) long barrel was chosen as it fit best into the limited space available in the laboratory and was of sufficient length to produce the projectile velocities needed for this research. However, if the barrel could be longer, the same projectile velocities could be produced at lower breech pressures thereby, reducing the cost per shot. When the projectile exits the barrel in the gun now in use, it is still accelerating (i.e., the projectile has not reached a constant velocity). In fact, for a maximum pressure shot of 20 MPa with a 2.75 kg projectile, the projectile velocity is still increasing as it exits the barrel approximately 2 m/s for every cm of additional travel. If the barrel was as long as 6 m, the velocity would be almost constant as it exited the barrel. Therefore, a compromise can be made between the additional initial cost of a longer barrel and the cost of operation per

shot by optimizing the gun barrel length. If additional space is provided for this research work in the future, the existing barrel could be lengthened by simply adding barrel sections.

Also, as a consequence of limited space, the catcher tank has a stopping distance of 1 m. Although this has proven sufficient for the experiments performed to date, a larger stopping distance would provide flexibility for future experiments and future research applications in terms of recovery and nonrecovery experiments. To provide additional experimental flexibility the catcher could be allowed to have some recoil motion, as opposed to being rigidly mounted, to help dissipate the large sums of kinetic energy associated with high-speed projectiles.

B. INSTRUMENTATION

1. Velocity Measurement

Even in the recovery tests, when no measurements of the shock loading stress is made, the projectile velocity must be known. Therefore, instrumentation to measure the projectile velocity is required. As this is required for all tests, the present system of projectile velocity measurement is described first. This is followed by a description of two different gages used to measure the loading profile, Manganin and polyvinylidene fluoride (PVDF) gages.

Projectile velocity was measured on both the 3.8 cm and 6-inch guns through use of charged pins connected to a set of timing counters. Upon contact with the projectile face, the sets of charged pins are used to first start and then stop the counters (Fluke Model 7261A and NCSU-built "Triune" counters). By carefully measuring the pin spacings before the shot, the average velocity of the projectile over the pin-spacing distance can be readily computed by dividing by the transit time required. Several locations for the pins have been utilized, depending both upon the experiment and gun being employed. For both guns, mounting the pins at the end of the barrel or on the target itself provides the best accuracy, on the

order of 1-2 percent in the velocity measurements. Alternatively, in some of the experiments on the 3.8 cm gun, the pins were placed 15 and 30 cm from the end of the barrel in ports which were already machined into the barrel. In this case the velocity measurement is not as accurate, usually around 5 percent.

2. Manganin Gages

The loading profile was measured with both Manganin and PVDF gages. In selecting an appropriate transducer, the following criteria were established based on the scale-modeling requirements:

a. Stress range: 5 MPa to 500 Mpa.

b. Rise time: < 1 μs

c. Shock-state duration: 5 to 500 μs

d. Physical size of transducer must not be so large as to disturb the stress wave profile

e. Reasonable cost

f. Ready availability

g. Ability to withstand the rapid loading and unloading

Although no available transducer fully meets the above criterion, Manganin pressure gages were first selected as being the most suitable. In appearance and construction, Manganin gages are similar to strain gages; however, unlike conventional strain gages, Manganin gages are designed to respond to pressures normal to the grid surface instead of in-plane strains. In measuring pressures, Manganin gages can easily handle the upper end of the required pressure range; the lower end presents more of a problem due to the relatively low sensitivity of the gages. As such, high-excitation

voltages are necessary to provide adequate signal level. Like strain gages, manganin gages are very thin (.05-.08 mm thick), and therefore,have a very fast risetime (50-100 ns). In addition, the glass fiber-epoxy backing provides a fairly good impedance match with many of the layering materials used in these experiments. The net result of this is that manganin gages offer little disturbance to the stress wave profile.

Since relatively high excitation voltages (50-100 volts) are necessary to provide adequate signal levels, it is necessary to employ pulsed power supplies for gage excitation. By providing a constant level current pulse with a maximum duration of approximately 180 μs, overheating of the Manganin gages can be avoided. Of course, use of such a power supply requires careful coordination between the impact of the projectile and the delivery of the excitation current to the Manganin gage sensing elements. To provide the necessary pulsed power source, two Piezoresistive Pulsed Power Supplies (Model CK-50-300) were purchased from Dynasen, Inc. (Goletta, California). These power supplies are built around the Wheatstone bridge concept, in which either one or two manganin gages are used as the active sensing elements for completing the bridge. A variable voltage, capacitor-discharge circuit is used to provide the necessary current pulse. The excitation voltage is adjustable from 30 to 300 volts, and the pulse duration is adjustable up to a maximum of approximately 180 μs. Output to these units with 50 ohm gages is approximately 30-40 mV/kbar at 100 volts excitation. Triggering of the power supplies is accomplished by shorting (by projectile impact of trigger pins) of an NCSU-built trigger circuit which provides a positive-going 5-volt trigger pulse.

The output voltage signal from the Wheatstone bridge circuit is sent directly to the recording oscilloscopes via coaxial cable. The primary oscilloscopes employed for this purpose were a 400 MHz Dual-Beam Oscilloscope (Tektronix Model 7844) and a 200 MHz Single Beam Oscilloscope (Tektronix Model 7704). Cameras (Tektronix Model C-51) were used to permanently record the oscilloscope beam traces. Additional scopes and cameras available for stress-wave profile recording were two B&K Model 1500 oscilloscopes and two Tektronix Model C-30B cameras, one of which was equipped with a writing-speed enhancer.

As previously mentioned, the output of manganin gages is relatively low; therefore, strict measures must be taken to ensure that unwanted electrical noise does not interfere with the output signal. As such, the use of coaxial cables and shielding is required throughout. The primary cables employed in this work were Belden-Type RG-58/U shielded coaxial cables, although the smaller diameter RG-174/U cables were used within the target chamber itself to prevent damage to the BNC feed-through connectors upon shearing of the cable.

Manganin gages require calibration to ensure the accuracy of the results. This calibration must be dynamic; hence, the earliest shots conducted in this project were calibration shots to characterize the output response of the Manganin gages, and provide experience in their usage. A total of five calibration records were obtained on the 3.8 cm gun. The gages employed in these tests were manufactured by the Micro-Measurements Group and were of the open-face variety with a nominal resistance of 48.5 j (Type LM-SS-110FB-0485). A known loading was applied to the gages by mounting three or less gages between Plexiglass (PMMA) layers. This configuration was then shock loaded with a PMMA projectile whose velocity was carefully measured. Because the shock Hugoniot curves for PMMA are well known, the stress in the layers can be very accurately calculated. Using the measured gage output and the known input stress conditions, the gage factor for each gage was be calculated.

For the gages used here, the average gage factor is 1.68 mohm/ohm/kbar, with a variation between the individual gages of 5.4 percent. This gage factor is somewhat lower than the value of 2 mohm/ohm/Kbar nominal value usually given for manganin gages. This is probably because previous use of Manganin gages has been almost exclusively in a much higher pressure range (10's of kbars) than is being used in this work.

Manganin gages do have some important drawbacks. The two most important are signal output at the lower stress levels here, and the early failure of the gage leads caused by shear. The low output signal level of these gages has already been discussed; the low signal level requiring the

use of pulsed power supplies (with associated timing problems), and shielding from electrical noise. The second problem, that of early lead failure, occurs after the initial compression pulse has passed, and the gage is subjected to a variety of interacting tensile and shear waves. To minimize this problem, the "sandwiching" of the gages between PMMA layers with epoxy has proven to be somewhat effective, particularly at the lower stress levels. Nevertheless, the overall fragility of the gages remains a matter of concern.

3. Polyvinylidene Fluoride (PVDF) Gages

The above shortcomings of the Manganin gages point out the need for a more suitable transducer when conducting scaled stress-wave experiments with a soil layer. Shock loading of the soil layer results in large particle displacements, relative to those that occur in metals or concrete. This makes use of Manganin gages particularly difficult, as the problem with lead shear is increased. In this regard, the new PVDF or polymer gages being developed by NBS show promise, because they are more rugged and more sensitive than the Manganin gages.

One problem with the use of the polymer gages in scaled experiments has been the availability of a high-frequency (at least 1 MHz) signal conditioning system. Common practice has been to use a charge amplifier to convert the output, which is electrical charge, to a usable voltage signal. This presents two problems. First, charge amplifiers are generally limited to a frequency response of around 250 kHz. While this is adequate for full most full-scale tests, it is a lower frequency than is needed for scale-model testing. Second, charge amplifiers are rather expensive and fragile, particularly those with the above frequency response. Because of this, an emitter follower (or voltage follower) was adapted to convert the charge output from these gages to and acceptable voltage output. This is considerably cheaper than a charge amplifier, and gives a frequency response of 1 MHz. All data using the NBS polymer gages were obtained here with the voltage follower system.

The voltage follower system was checked for operation by a series of drop weigh tests. After the signal conditioning system was operating satisfactorily, it was used in a series of tests before calibration. Because it was not clear that the gages would hold up under shock loading, or that they would even operate properly at the very rapid loadings that occur in the present tests, they were first used under actual test conditions. The use of the gages is described in detail in Section III.B.2. At this time the PVDF or polymer gages appear well-suited for the present tests. They offer two advantages over the Manganin gages. First the polymer gages are much less susceptible to failure when there is large material or particle displacement. The mechanical properties of soil are such that there are large particle displacements under shock loading. The problem with the leads shearing off of the Manganin gages during these large particle motions has never been completely resolved. Second, the lower limit on the sensitivity of the Manganin gages is at or slightly above the stress levels in the present tests. These two factors lead to guarded optimism on the suitability of the polymer gages for making stress measurements in scaled tests.

After preliminary use of the gages proved encouraging, calibration of the gages was addressed. The gages must be calibrated dynamically, because the charge will bleed off in a static calibration. The two gages, designated AF-84 and AF-85, were hydraulically calibrated by the National Bureau of Standards (NBS). As reported in Reference 23, similar gages were also calibrated by NBS under dynamic loading in soil. Reference 23 reports an apparent difference in gage sensitivity, with the gages being approximately 2 to 2.5 times more sensitive in the soil calibration than in the hydraulic calibration. Because the shear strength of soil is low, we expected the stress state behind the shock to be very close to hydrostatic, or to the stress state in the hydraulic calibration. Preliminary data comparing the stress measured by the Manganin gages to that measured by the polymer gages confirms this. That is, the normal stress, as measured by a Manganin gage, was close to that measured by the polymer gage, when the hydraulic calibration constant was used for the polymer gage. It is not

clear why the calibration in Reference 23 is so different than the hydraulic calibration. Further work is necessary before this discrepancy can be resolved.

4. Data Acquisition

In any "single-shot" test, acquiring the data becomes an important consideration. Scaling of the loading for model tests requires that the loading rise time and decay be shortened by the scale factor, S (described in Section III.A.2). Because of this, the data acquisition or recording instrumentation must record signals of very short duration. Typically the rise times are the order of 1-10 μs and total test times are 100-500 μs. At the beginning of the project the main concern was with calibration of the Manganin gages, and measurement of the projectile velocity. Projectile velocity is measured with a counter, using standard counter technology. Gage calibration and data from the first instrumented tests were recorded with two oscilloscopes and attached cameras. This system has worked satisfactorily, however both the record length and the accuracy of data taken by oscilloscope camera is limited. Signal and time accuracies better than 2-5 percent with this system are difficult to obtain. Therefore, as the project progressed toward instrumented tests, the need for a more accurate and flexible data acquisition became apparent.

Unfortunately, the need for improved data acquisition came late in the project when equipment funds were limited. Because of this, the upgrading of the present data acquisition system has just begun. Recent developments in analog-to-digital (A/D) converters allows for rapid conversion of the signal to digital form. After the signal is in digital form, it can easily be stored and reduced by computer. Long-term storage of the data is via soft disk or tape. Most of these facilities are available at NCSU. However, this approach requires an A/D system dedicated to the Laboratory. The faster A/D required in the laboratory, the more expensive. At the data acquisition rates needed here the digital memory must be on board with the A/D system. Because the computer and storage system are relatively invariant for the different speed systems, their cost and

availability are relatively invariant. At present the Shock Physics laboratory has acquired a medium speed A/D data acquisition system. This four-channel system can take simultaneous samples every 2 μs. This system is fast enough to capture data from tests with a soil layer, because the soil disperses the shock wave, and the rise time of the shock loading is around 10 μs. Tests without a soil layer have much faster rise times, on the order of 1-2 μs and the present data acquisition system is not useful for these tests. This system does start the move to digital data acquisition and reduction, which is the direction the laboratory needs to go. Clearly, a future goal is to be able to continue this upgrade to faster systems.

SECTION III

EXPERIMENTAL

A. DESIGN OF EXPERIMENTS

1. Model Design

Experiments were designed with the overall goal of building and demonstrating a facility capable of investigating the response of correctly scaled model structures to the loading from conventional weapons. The models under consideration are to be hardened (buried) structures, hence the loading is from the ground shock produced by the weapon. The ground shock loading from conventional weapons is quite complex, primarily because of the very large number of parameters that can influence it. These include the type of weapon and distance from the structure, the type of soil between the weapon and the structure, and the stiffness of the structure itself. However, certain general characteristics of ground-shock loading can be identified. These are very short loading rise times, typically .05 to 5 msec and high peak loads on the structure, normally ranging from 50 KPa (.05 KBar) to 500 MPa (5 Kbar). Decay times for ground shock loading are more variable, depending on the structure and surrounding geometry as well as the parameters listed above.

Because of this wide range of loading parameters, the present approach was not to attempt to model a specific full-scale experiment or set of experiments, but to demonstrate the capability of the experimental facility to produce the range of loading conditions and failure modes that have been observed in field or full-scale tests. The task is, thus, to build a correctly modeled structure and to develop a technique to load the scaled structure as required by the appropriate modeling considerations. Considerable work has been done on the correct way to model concrete structures and how to construct them. Reference 24 describes the necessary scaling laws for small-scale models of reinforced concrete structures.

Reference 25 is a book on the construction and loading of model reinforced concrete structures. The actual materials and procedures to make scale reinforced concrete models are described in Reference 26.

The above body of work defines the necessary construction procedures to make accurate scale models of reinforced concrete structures. This type of scaling can be considerably simplified if the materials the model is made of, that is the microconcrete and the model-reinforcing rods, have approximately the same yield strength and modulus of elasticity as those in the full-scale structure. This requires that the magnitude of the loading on the model should be approximately the same as that in the full-scale structure. However, the stress within the structure, and, consequently, the failure modes are related not only to the stress levels but to the wave propagation that occurs to produce these stresses. Consequently, even though the peak stress should be the same in the model and the prototype, the loading profile, e.g. the rise and decay time of the loading must be quite different. Scaling of the loading pulse shape or profile is discussed in the next section. Because this scaling depends on the geometry of the model structure, the model geometry is discussed next.

As previously mentioned, the objectives are to demonstrate similar scaled loading and failure modes in the model structures and the full-scale structure. Consequently, the model structure should be an accurate representation of the full-scale structures of interest. The model structures used in the present tests were based on the wall sections used in the one-third-scale studies conducted at the U.S. Army Waterways Experiment Station (WES). These wall sections were reinforced concrete slabs representing a one-third-scale model of a typical command and control center wall. A description of the experiments and the wall sections is given in Reference 27. The model used for the experiments described here were scaled sections of the WES tests, in effect a model of a model. To fit inside the test section of the 3.8 cm gun, the largest model that could be constructed was 15.25 cm (6 inches) in width. The model size was then chosen to be square, with a length and width of 15.25 cm (6 inches sq.). The WES test were on walls with length to thickness ratios of 5 and 10. This corresponds

to a model thickness for the present experiments of 3 cm (1.2 inches) and 1.5 cm (0.6 inch). Construction and dynamic load testing of a reinforced concrete model with a wall thickness of only 1.5 cm was considered to be more difficult and less representative than the thicker wall. In addition, higher loading was required to fail the model with the thicker wall. One of the objectives of these tests was to demonstrate the capability to generate the complete range of loads that may produce failure. Consequently, the model with the thicker wall was also chosen because of the higher loading required to produce failure. The model thus has a length and width of 15.25 cm (6 inches) and a thickness of 3 cm (1.2 inches). A drawing of the test model, with the maximum reinforcing configuration is shown in Figure 6. The model here is approximately one-tenth-scale of the WES experiments. As the WES experiments were one-third-scale, this results in an overall scale ratio of 1-to-30 between the wall for a typical command and control center and the model wall section used in the present experiments.

The reinforcing rods used for the tests are made of black steel wire, prepared as follows. To have the proper bond between the concrete and the model reinforcing rods, the surface of the wire is slightly deformed by passing the wire through a set of knurling wheels. This processes, and the knurling machine itself is described in References 25 and 26. Wire used in the present experiments was knurled in the machine described in Reference 26. After treatment to produce the desired surface deformation, the wire is then preloaded to remove any kinks and curvature. Reference 26 has shown this procedure to be necessary to produce a model reinforcing rod that has the correct modulus of elasticity and does not exhibit hysteresis in the stress-strain curve. The wire used for these tests was prestressed to approximately 344 MPa (50,000 psi) in preparation for use as model reinforcing bars.

The one-third-scale wall sections used in the WES experiments had a ratio of steel reinforcing rods to concrete that ranged from 0.5 percent to 1.0 percent by volume. As indicated in Reference 25, common practice is to give the ratio of steel to concrete by percent of cross-section area. Because we wished to test a model with maximum strength, the present model

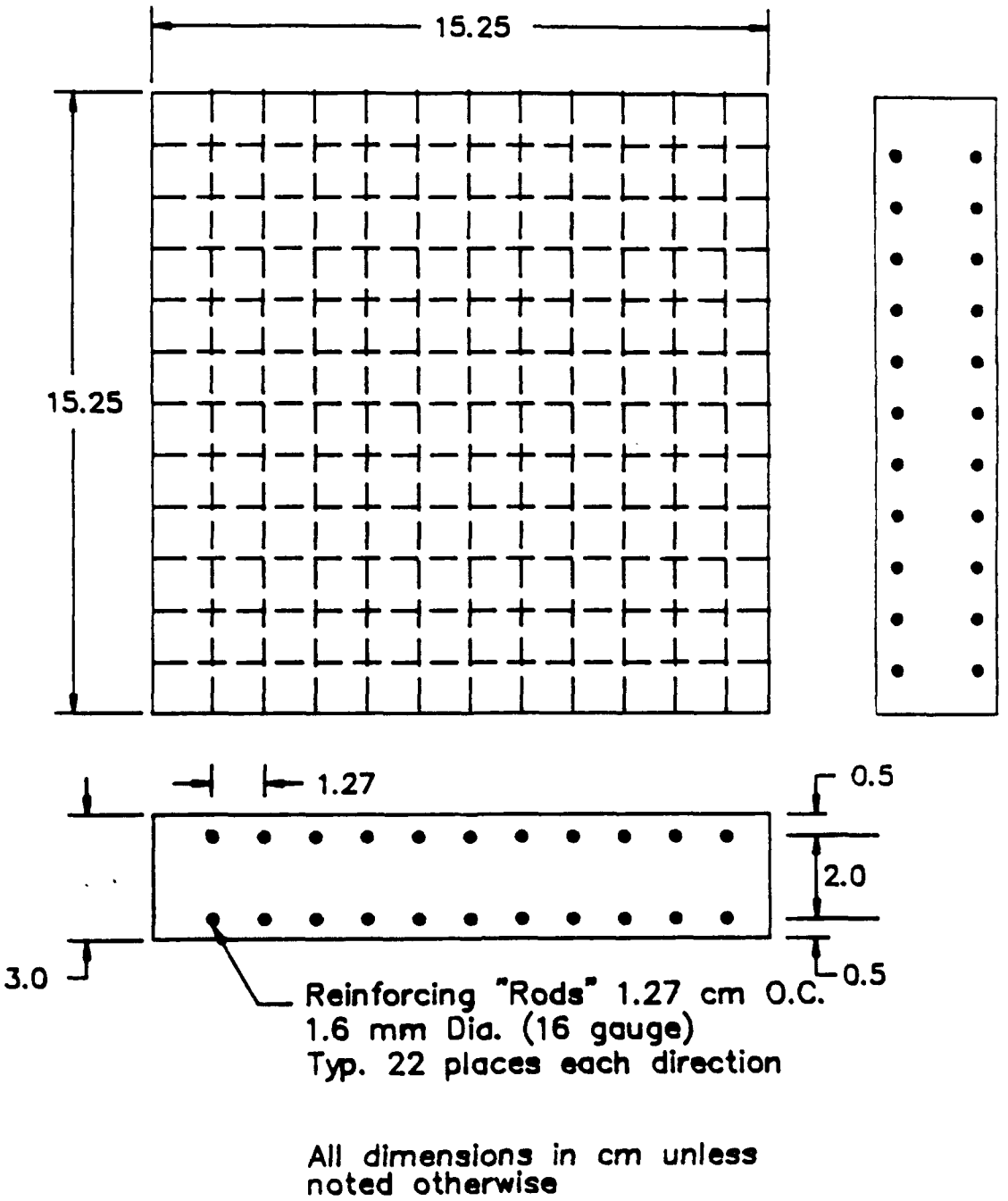

Figure 6. Structural Model Used in the Present Tests.

had a ratio of steel to microconcrete of 1.0 percent of the cross-section area. This results in slightly more than 1 percent by volume, approximately 1.2 percent steel by volume. Because of the small scale of the model, it was not possible to exactly model the size and location of the reinforcing bars in the WES wall section. Consequently a compromise was made by using fewer bars, but of greater size, in order to provide the correct ratio of steel to microconcrete. This was accomplished by using 22 ea, 16 gauge (.0625 inch diameter) steel rods in each direction. This configuration is shown in Figure 6. The rods are stiff enough that they only have to be held in place at the sides of the forms during the microconcrete pour. Forms were made with holes in the sides to hold the model reinforcing rods in place. Model Reinforcing rods were then placed in the holes, which held them in place.

The microconcrete was prepared as described in Reference 26, and poured into the forms, over the reinforcing rods. A check after the pour and the microconcrete had set showed that the reinforcing rods were still located in the correct position. The microconcrete was prepared as described in Reference 26. Both Ultracal 30 and Ultracal 60 were used, however, the Ultracal 60 was used in most of the models. The concrete was prepared in an aggregate to Gypsum (A/G) ratio of 1.0 and a water to Gypsum (W/G) ratio of .35 to .40. One static test was conducted to insure that the strength of the microconcrete was approximately that indicated in Reference 26. The reader can consult Reference 26 for a complete description of how the microconcrete models were constructed, and for the physical properties of the both reinforced and unreinforced microconcrete models.

2. SCALED DYNAMIC LOADING

Proper scaling of the model structure was discussed in Section II. In this section, proper scaling of the dynamic loading or the loading profile is defined. The loading profile can be conveniently defined by the peak loading, the rise time to the peak loading, and the decay time of the loading. These three parameters are shown in Figure 7. This section discusses how each of these parameters should be scaled for model testing.

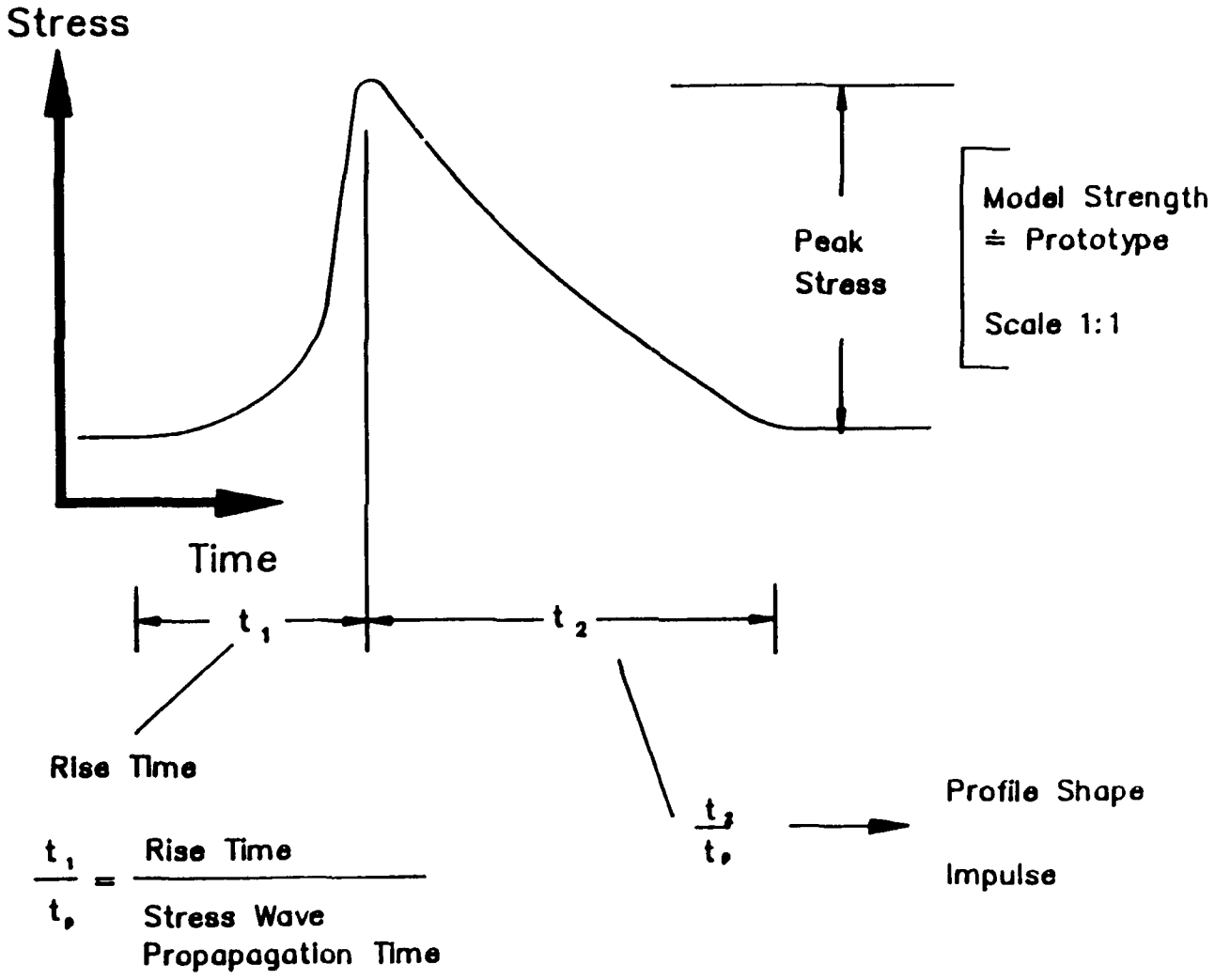

Figure 7. Typical Ground Shock Loading Profile Showing the Scaling Used for Model Tests.

A gas gun was chosen as the best technique to dynamically load the model structures. These facilities are described in Section II. In this section the control of the above mentioned three parameters in a gas gun is also covered. The section thus defines how the parameters are scaled and this scaling is achieved with gas guns.

a. Peak Stress

Both the microconcrete and the reinforcing bars have approximately the same elastic modulus and yield strength as does the full scale structure. Consequently the peak stress, as defined in Figure 7, in the scaled test should be equal to that observed in the prototype or full scale test. The range of maximum stress required in scale model test is, thus the same as that found in full-scale testing.

Therefore, the ability to control the magnitude of the peak stress is necessary in conducting a correctly scaled model test. With the gas gun the peak stress is controlled primarily by the projectile speed. The projectile and impact (target) materials, mainly the material wavespeed and density, also influence the peak stress in the target or model. However, the projectile speed has the most influence on peak stress, and is probably the most easily controlled. The factors that control peak stress in the gas gun are summarized in Figure 8. As described in Section II, the 6-inch gas gun used in this laboratory was designed to operate at a range of projectile speeds that will produce the entire range of peak stresses observed in field tests. One advantage of the gas gun is that the projectile speed is easily and accurately controlled. Consequently, a wide range of conditions be achieved and reproduced accurately and predictably.

b. Rise Time

The peak stress incident on the front surface of a structure can be relieved by stress-wave propagation through and subsequently reflected from the rear of the wall surface. This occurs if the reflected wave arrives at the rear wall surface before the peak pressure occurs.

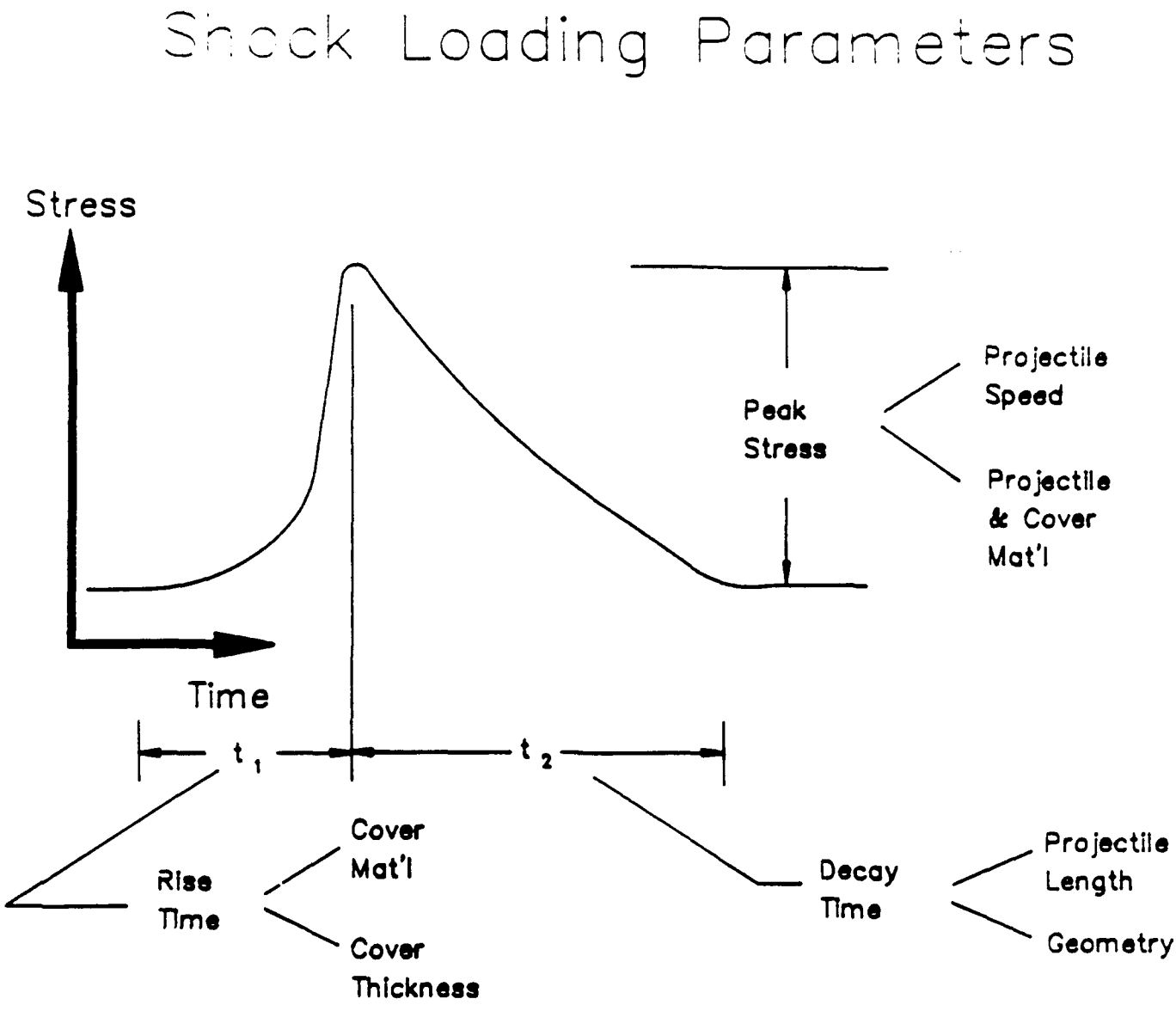

Figure 8. Ground Shock Loading Profile Showing How the Various Loading Parameters can be Controlled in a Light Gas Gun.

Therefore, if the rise time of the loading is slow relative to the wave propagation time through the structural surface, the peak load will be reduced or relieved. Alternatively, if the rise time of the loading is short, compared to the stress-wave propagation time through the wall surface, the loading will not be relieved before the onset of the peak stress, and the structure must sustain the peak load locally. That is, the peak load will not be distributed through the structure, but must be carried by at certain locations in the front of the structure. Indeed, it is this rapid compressive loading, followed by a rapid unloading (tensile stress wave) that leads to spalling. Because of this, the ratio of loading rise time to the stress-wave propagation time through the front of the structure is one important scaling parameter. Alternatively, one may consider the nondimensional rise time to be:

$$Rt/Wt$$

where Rt = the rise time of the loading and Wt = the time for propagation of a stress wave through the front of the structure. This nondimensional parameter is illustrated in Figure 7 for a typical ground shock loading profile. Scaling of the rise time requires equivalence of the two non-dimensional parameters, eg.,

$$Rt_m/Wt_m = Rt_p/Wt_p$$

Here the subscript m indicates the model and p the full-scale or prototype structure. Thus,

$$Rt_m/Rt_p = Wt_m/Wt_p = T_mCo_m/T_pCo_p$$

where T_m and T_p are the wall thickness of the model and prototype, respectively, and Co_m and Co_p the wave propagation speeds in the model and the prototype. The thickness of the wall of the model is scaled by the scale ratio between the model and the full-scale structure, 3. The micro-concrete used in these experiments has a stress wavespeed of approximately

3000 m/s which is about the same as in the full-scale structure. That is, Co_m is approximately equal Co_p. Therefore;

$$Rt_m/Rt_p = T_m/T_p = 1/S$$

where S is the length scale ratio between the model and the prototype. Thus, rise times in the model test should be reduced by this scale ratio. That is

$$Rt_m = (1/S)Rt_p$$

The rise time, Rt_m, of the loading from a gas gun is controlled primarily by the material layers between the location of projectile impact and the model structure. Metals with high density and stress wave speeds exhibit short fast rise times, and powders such as soil will disperse the stress wave and increase the rise time. Consequently, control of the rise time in the gas gun is by the type and thickness of the materials covering the model (the layer or layers between the location of projectile impact and the model). The dependence of the rise time on these parameters is illustrated in the figure showing how the scale parameters are controlled in a gas gun, Figure 8. In general, due to the rise time scaling mentioned above, the rise time of the model loading profile must be very short, usually on the order of microseconds. While control of the rise time in a gas gun is not accomplished as directly as the peak stress of the loading profile, there is usually sufficient variation in cover material properties and thickness that proper scaling can be achieved. As with peak stress, the gas gun will reproduce the rise time, repeatably and with good accuracy.

If the condition occurs where the ratio of rise time to propagation speed in the prototype, Rt_p/Wt_p, is much less than one, eg. $Rt_p/Wt_p << 1$, then this is all that is required in the model test. That is, one does not require that $Rt_p/Rt_m = S$, but only that $Rt_m/Wt_m << 1$. Conversely, if $Rt_p/Wt_p >> 1$ is the condition in the prototype test, then the condition on the model test is only that $Rt_m/Wt_m >> 1$.

c. Decay Time

The third parameter that must be scaled is the impulse loading on the structure. That is, the Impulse on the model should be properly scaled in the experiment. The nondimensional impulse I^* is:

$$I^* = \frac{I}{\sigma_o L^2 \left(\frac{\rho}{E}\right)^{1/2} L'}$$

Where I is the physical impulse, σ_o = the yield stress, L = the length scale, ρ = the structure density, and E = the structure modulus of elasticity. $\sigma_o L^2$ has the dimensions of force and $(\rho/E)^{1/2}L'$ has the dimension of time. For a plate this time is proportional to the natural frequency of the structure if L′ is the length of 1 side of the plate. If L′ is the wall or plate thickness this time is proportional to time for an elastic wave to propagate through the structure. For a fixed geometric configuration, the relation between the wall or plate edge length and the wall thickness is fixed, thus,either dimension can be used. Either will scale as the geometric scale ratio, S. Impulse scaling thus,requires that

$$I^*_m = I^*_p$$

where the subscript m is for the model and p denotes the prototype or full scale structure. This equivalence of nondimensional Impulse gives the following relation between the physical Impulse on the model and that for the prototype.

$$\frac{I_m}{I_p} = \left(\frac{\sigma_{om}}{\sigma_{op}}\right)\left(\frac{L_m}{L_p}\right)^3\left(\frac{\rho_m}{\rho_p}\right)^{1/2}\left(\frac{E_p}{E_m}\right)^{1/2}$$

For microconcrete

$$\frac{\sigma_{om}}{\sigma_{op}} = 1 , \quad \frac{\rho_m}{\rho_p} = 1 , \quad \frac{E_p}{E_m} = 1 .$$

Thus, scaling for models constructed with the microconcrete should have the impulse scale as:

$$\frac{I_m}{I_p} = \frac{(L_m)^3}{(L_p)^3} = \frac{1}{S^3}$$

Ground shock loading typically has a very rapid rise time with a much slower decay. Therefore, the time of the loading is very nearly the decay time, consequently, scales approximately with the decay time. Accordingly the impulse can be approximated by

$$I = KP_o L^2 D_t$$

Where K is a geometric factor relating the peak loading stress, P_o and the decay time D_t to the area of the roughly triangular loading pulse. L^2 is the loading area and scales as S^2. The requirement that the Impulse scale as S^3 give the following scaling for D_t.

$$\frac{P_{om} L_m^2 D_{tm}}{P_{op} L_p^2 D_{tp}} = \frac{1}{S^3}$$

For microconcrete $P_{om} = P_{op}$ and $L_m = (1/S)L_p$, hence:

$$\frac{D_{tm}}{D_{tp}} = \frac{1}{S}$$

Therefore, the decay time, D_t, scales linearly with the model tc prototype scale ratio, S. As was previously covered, the rise time also scales linearly with the scale ratio, and the peak loading stress, P_o scales directly (one-to-one). Thus, the model structure should be loaded with a loading stress profile that has the same peak pressure as observed in the full-scale or prototype structure, and with a time scale compressed (shortened) by the scale ratio, S.

The decay time of the stress loading from a projectile impact is controlled by the geometry of the model and by the projectile geometry. Release waves from either the edges of the model and/or from the back of the projectile reduce the peak loading and cause the decay. Assuming the model geometry is fixed, the loading decay time in the gas gun is controlled by the projectile length. The release waves from the edges of the model and from the rear of the model are difficult to predict analytically or numerically; consequently, the decay time and how it is altered by different projectile lengths must be determined experimentally. This, in turn, requires availability and use of suitable instrumentation to measure the complete (not just the peak) loading profile.

d. Shock Curvature

The ground shock wave from a conventional explosion is roughly spherical, at least until the wave interacts with the structure. The curvature of this shock wave is conveniently described by the radius of the spherical shape at the time the wave first interacts with the structure. The structure typically has a planar or flat wall upon which the ground shock impinges. Although not as important as the peak stress or loading rise time, true geometric similarity requires that the ground shock radius scale with the geometric scale ratio, S. Working with a nondimensional parameter that is a measure of this is often the most convenient way to describe the scaling. Here the shock radius was nondimensionalized by the edge length (vertical height) of the wall. That is the shock radius, Rs, is nondimensionalized by dividing by the edge length of the wall. The nondimensional shock radius is Rs. Values of Rs were taken from Reference 27,

for the case in which the wall first failed. These were nondimensionalized and compared with measured values in the present 1/30 scale tests. Overall, the agreement was deemed good. The calculation procedure is given in the following, and a description of the measured data is given in Section III.B.2.

The shock radius in the tests described in Reference 27 was estimated by assuming a spherical ground shock, with the origin at the location of the explosive used in the test. The shock radius is thus the standoff distance of the explosive. When comparing this field data with laboratory data, the standoff distance that produced failure of the structure is used. This is because the recovery tests (described in Section III.B.1) were conducted to produce failure of the model structure. Shock curvature in the model tests was measured by using two stress gages, one at the center of the model wall and one a known distance off center. The speed of the shock wave and the difference in arrival time at the two locations was measured. This data, combined with distance between the gages, is used to compute the shock radius in the model test. The radius of curvature for both field and laboratory tests is nondimensionalized, and the non-dimensional values are compared.

The radius of curvature of the shock in the model test is controlled by the diameter of the projectile fired from the gas gun. The ratio of the projectile diameter to the edge length of the test model, combined with the thickness of the soil layer, determines the shock radius. This parameter is easily controlled by building larger or smaller models. The projectile diameter can also be changed by using a smaller diameter projectile mounted on a projectile shell that is the bore diameter of the gun. This procedure, referred to as saboting, can be used to decrease the impacting projectile diameter, but not to increase the diameter. This is one of the reasons that a large-bore gas gun was constructed.

3. SUMMARY

This section has described how the scale models were constructed for the experiments, and how the scale ratio was chosen. Loading of the models is by impact of a projectile fired from a gas gun. A description is given of how the peak stress, rise time, and decay time of this loading should be scaled to assure correct similarity between the model and the prototype or full-scale structure. The suitability of the gas gun to produce the desired scaled loading profile could be demonstrated directly by measuring the loading profile on the model. This requires instrumentation capable of making normal stress measurements at the interface of the soil cover and the model. Alternately, because the failure mode of the structure depends directly on the loading profile, a semiqualitative demonstration of the applicability of the loading profile can be shown by evaluation of the failure mode as the gun and soil cover parameters are changed. The failure modes are then correlated with the gun performance to show how the loading profile can be tailored by changing the projectile mass, speed, geometry,and the thickness of soil cover on the model.

The following section on experimental results covers both approaches. First, a number of experiments are described in which different failure modes are achieved by using different gun and layer parameters. The data are the failure mode of the model and the conditions required to produce failure under set conditions. It is necessary to achieve marginal failure, that is, loading that causes the model to fail, but only to the point the structure has local yielding, cracking, and/or spalling. Few useful data are obtained if the model is not stressed above the yield point, or is completely destroyed. Finding the conditions for marginal failure as the parameters are changed can sometimes be difficult and time consuming. Because the data are obtained by inspection of the model failure mode after the model is recovered from the experiment, these are referred to as recovery tests.

In addition to the recovery tests, there is work on the development and utilization of instrumentation to directly measure the

loading profile. Early work used Manganin gages, but difficulty in obtaining measurements in the latter (decreasing stress or as "unloading") part of the loading profile hampered their use. This problem has been addressed, as well as an investigation of the use of polymer gages. The work is still underway, and the further development of this instrumentation is required before the loading profile can be measured with the desired accuracy. However, preliminary tests indicate the capability to control the parameters of the loading profile by the techniques discussed above, and thus to produce the desired loading conditions.

B. RESULTS

This section covers the results from two different approaches. The purpose of each is to demonstrate the capability of producing the desired loading profile (load versus time) on the model. The first approach is a group of experiments which correlate the failure mode of the model and the loading conditions on the model. Because the failure mode is related to the loading profile, information on the loading profile can be indirectly obtained from the failure mode. The data in these experiments are the projectile speed, size, and mass; the configuration of the layers between the projectile impact and the model, and the failure mode of the model. Because the failure mode is determined by recovering the model after the impact test, these are referred to as recovery tests.

The second approach is to measure the load on the model as a function of time, e.g., directly measure the loading profile. This measurement requires suitable instrumentation to measure the rapidly changing and high levels of stress to which to model is subjected. This section reviews the development of the instrumentation and gives the results of preliminary measurements of the load profile. Because of the additional time needed for instrument development, and because the preparation of an instrumented test model requires much more time than preparation of a model without instrumentation, the number of tests with instrumentation is smaller than the number of recovery tests.

The recovery tests were carried out first as a qualitative way to investigate the loading profile on the model and to demonstrate the capability of changing it. These tests could be conducted earlier in the project because they did not require instrumentation development and application. This allowed an evaluation of how well the models could be built and the correct loading achieved, before additional time was spent in developing and utilizing instrumentation. As such, they can be viewed as an intermediate step in achieving the goal of a model tested under desired and predictable loading, and with instrumented measurements. All tests were conducted in a test setup shown in Figure 9. The model was constructed as discussed in the prior section, and the model geometry was not changed. The layers between the projectile impact and the model were changed as a way of controlling the shape and magnitude of the loading profile.

1. Recovery Tests

Recovery tests results are the failure mode of the model and the projectile impact parameters, which are used to estimate the loading conditions. The objective is to demonstrate similar failure modes between the scale model and the full-scale structure. These failure modes are then correlated with the change in loading profile that is expected to occur as the projectile impact parameters are changed. For this approach to work, the scale model must accurately represent the full-scale structure. This consideration, as well as a discussion of how the loading profile parameters can be varied as a function of projectile speed and geometry, is given in Section III.A, which deals with different failure modes and how changes in the load profile cause these different failure modes. A summary of all recovery tests, including the projectile impact data is given in Table 2. In this table, the prefix "M" on the shot number indicates that the test was conducted in the 3.8 cm (1.5 inch) gun. The prefix 6 indicates that the test was conducted in the 6-inch gun.

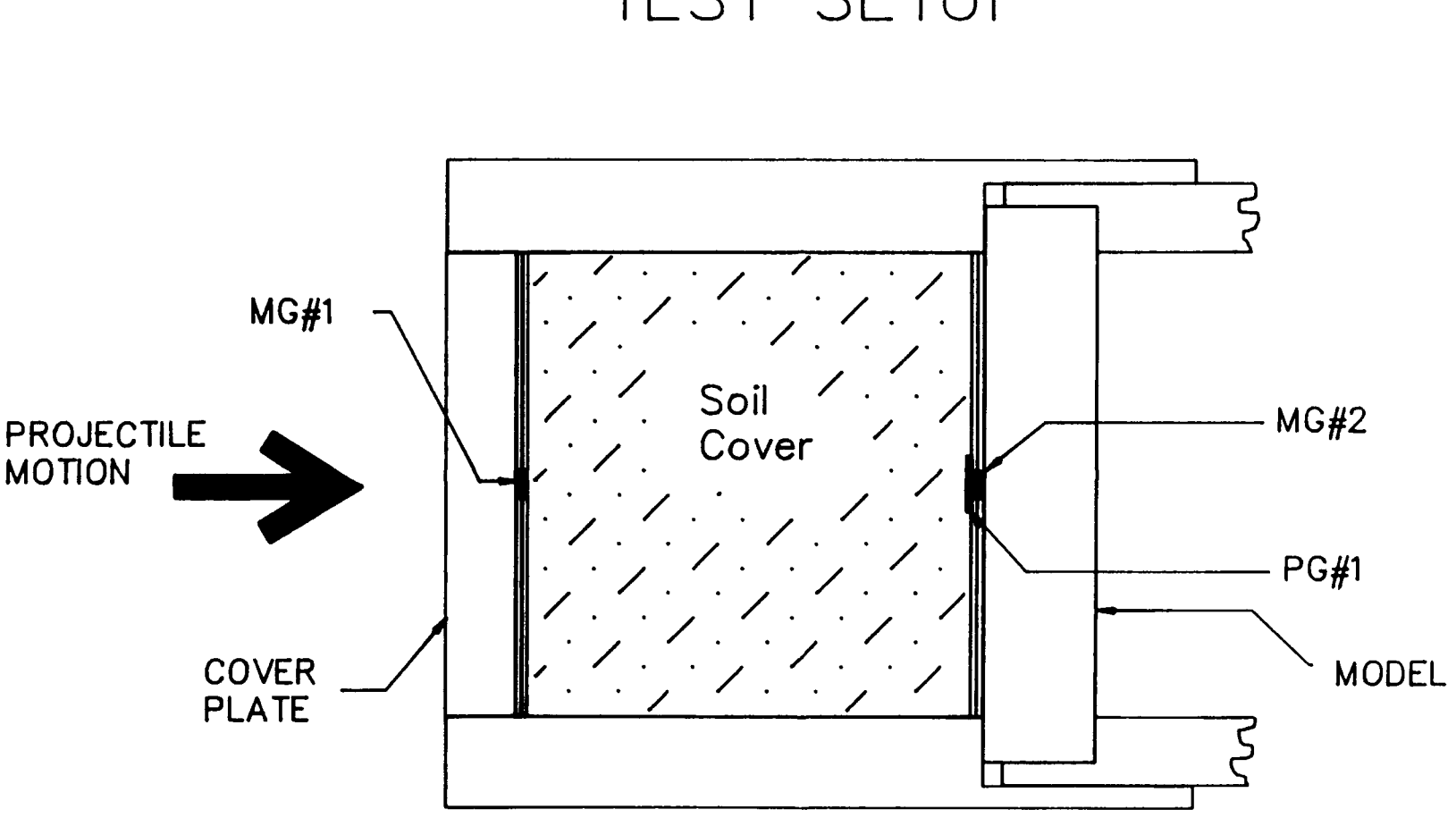

Figure 9. Diagram of the Test Setup.

TABLE 2. SURVEY OF RECOVERY TEST

Shot No.	Projectile			Cover Plate Material	Soil Thickness	Model Reinf.	Official Use Only
	Matl.	Mass	Speed M/S				
M014	Lexan	100	73	Alum	0	No	15,16
M017	Lexan	100	35	Alum	0	No	16
M018	Lexan	100	54	Alum	0	No	16
M019	Lexan	100	63	Alum	0	Yes	16
M020	Lexan	100	158	Alum	3.4	No	16
M021	Lexan	37	227	Alum	3.4	No	16
M022	Lexan	100	154	PMMA	3.4	No	16
M024	Alum	112	178	Lexan	3.4	Yes	
M025	Alum	112	85	Alum	0	No	18
6-04	Alum	415	222	Alum	3.5	Yes	
6-07	Alum	550	550	Alum	4.5	Yes	

a. Spall Failure

The ultimate stress in concrete and microconcrete is much greater in compression, typically 3 - 3.5 MPa (4000 - 5000 Psi), than in tension where the ultimate stress is .3 - .35 MPa (400 - 500 Psi). A commonly observed failure mode is shock loading in compression near the ultimate compressive strength, with this loading followed by tensile waves from either the edge of the structure of reflected from the back of the structure. If both are rapid, the structure can not relieve the stress from the tensile waves. This produces failure in tension, usually near the back of a wall where the reflected tensile waves first develop. In the tests reported here, the static compressive strength had to be exceeded in order to produce the spall failure mode. This is probably caused by the very rapid loading, in which the ultimate stress is a function of strain rate as well as strain (so-called rate effects). The stress levels and the loading times are described below.

A sum of all the tests that gave spall failure is given in Table 3. The time for a stress wave to propagate through the 3 cm thick model wall is approximately 10 μs. Thus, the loading to produce the spall failure mode

TABLE 3. ESTIMATED RECOVERY TEST LOADING

SPALL FAILURES

Shot No.	Est. Peak Stress on Model	Model Reinf.	Failure Description
M014	105 MPa	No	Massive Spall
M017	50	No	None
M018	77	NO	Spall
M019	90	YES	Spall to Reinforcing Rods
M025	100	NO	Massive Spall

BENDING FAILURES

Shot No.	Est. Peak Stress		Soil Thickness cm	Model Reinf.	Failure Description
	Input to Soil	on Model			
M020	24	12	8.6	NO	Minor Cracking
M021	34	17	8.6	NO	None
M022	53	26	8.6	NO	Bending Failure
M024	130	65	8.6	YES	Minor Cracking
6-04	108	54	8.6	YES	Cracks Due Bending Projectile Impact Off-center
6-07	100	50	11.4	YES	Bending Failure

STATIC FAILURE

S01	70	5	8.6	NO	Bending Failure

must be quite rapid, with a rise time of less that 10 μs. The rise time for these tests is estimated to be 1-3 μs, and is always less than 10 μs. This condition is achieved by using only metals or plastic for the cover layer protecting the model, the cover layer for each test is given in the test summary, Table 2. Rise time estimations were made from the type of cover layer material and measured load profiles from similar shots using these materials (described in the section on instrumented tests). This shock

loading and subsequent tensile wave unloading produce the spall failure mode. A brief discussion of the individual recovery tests is given.

A summary of the tests that produced the spall or scabbing failure of the model is given in the upper part of Table 3. As previously mentioned the projectile and coverplate materials were selected to give loading rise times of 1-3 μs. The loading decay time is not known, as no successful measurements were made of the loading profile because the gages failed early in the test. However, in a number of tests the peak stress was measured, and then the gage failed. Although the loading profile was not measured, these measurements do provide the loading rise time and a comparison of the calculated and the measured peak stress. In all cases without soil cover, the rise time was less than 3 μs. In addition, the calculated and measured peak stress were in reasonable agreement, typically within 5 to 8 percent. Because of this, the calculated peak stress given in Table 3 is considered to be an accurate estimate of the peak stress that occurred in the test. The ultimate strength of the concrete is around 27 MPa (4000 Psi), and, with very rapid loading, spalling will not occur until the peak stress is well above the static strength. Test M014, on a model without any steel reinforcing, produced a calculated peak stress of 105 Mpa (3000 Psi) and resulted in a massive spall failure. By massive spall is we mean a very large area of spall material, compromising approximately one/third of the total material in the model. A picture of the model, as recovered after the test, is shown in Figure 10. As shown in the picture, the spall penetrated completely through the front of the model. The model also had diagonal cracks completely through it.

Several tests at lower calculated peak stress were subsequently conducted. Test M017 produced a peak stress of 50 MPa (9,200 Psi) on an unreinforced model, and no damage, spall or otherwise was observed. This appears to be close to the limit were spall failure would be observed for this rapid loading. This was investigated by test M018 which produced a peak stress of 77 MPa (11,000 Psi), in which a spall failure about 2 inches across was observed. Tests M014 and M025, which were instrumented tests, were at projectile speeds considerably higher than

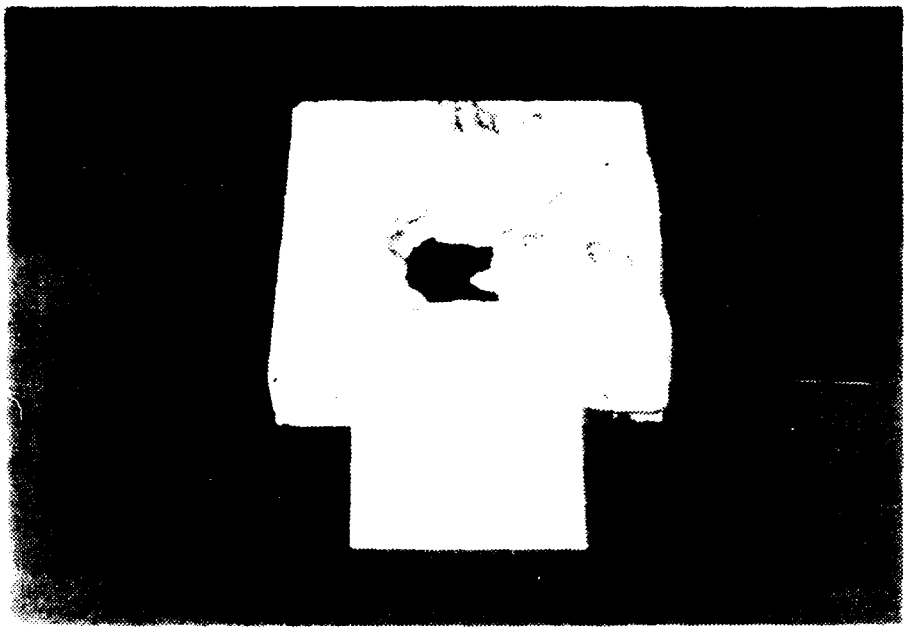

(a) Plan View of Back of Model

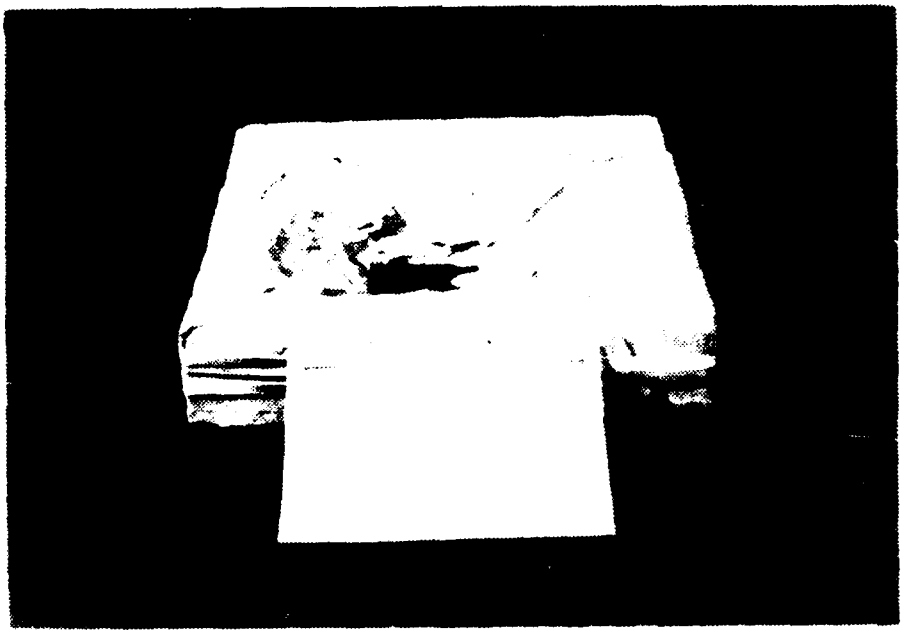

(b) Oblique Side View

Figure 10. Back of Model After Shot M014 Showing the Massive Spall Failure.

planned. Consequently, although load profile data was obtained in M025, the peak stress of 92 Mpa (13,300 Psi) during the test was much higher than needed to produce spall failure. The model failed with a massive spall and was partially destroyed in test M025. This data is consistent with the previous tests, and confirms the approximate peak stress level required to produce spalling.

The effect of steel reinforcing on the spall strength of the model was investigated with test M019. This was a test of a model reinforced, as shown in Figure 6. There is no reinforcing steel within 0.5 cm of the back or front of the model. In addition there was principal steel, but no shear steel in the model reinforcing. Because the model failed from the rear surface in the spall failure mode, there was some question as to whether inclusion of this reinforcing steel pattern would increase the spall strength. Test M019, which was conducted on the reinforced model, showed spall failure at a peak stress of 90 MPa (13,000 Psi). The loading was slightly higher than test M018, where spall failure was observed at a peak stress of 77 MPa (11,000 Psi) in a model that did not have any reinforcing. The recovered model is shown in Figure 11, and the spall extends from the back of the model into the rear reinforcing steel. The model remained intact, except for the spall at the back. The reinforcing steel thus appeared to contribute to the integrity of the model, but did not prevent the spall at the back. For the reasons given above, this is consistent with prior recovery test results.

If time and funding had permitted, additional recovery testing would have been undertaken to investigate different reinforcing steel configurations and to define which of these provided the best protection against the spall type failure. However, the failure mode observed in the one/third third-scale tests, Reference 27 and some full-scale tests, Reference 28 indicates a failure mode, that although showing some spalling, also has failure in bending or shear. Therefore, it was deemed more important to demonstrate that the gas-gun technique could produce the loading and subsequent failure in this mode, rather than investigate loading that produce failure with only the spall component.

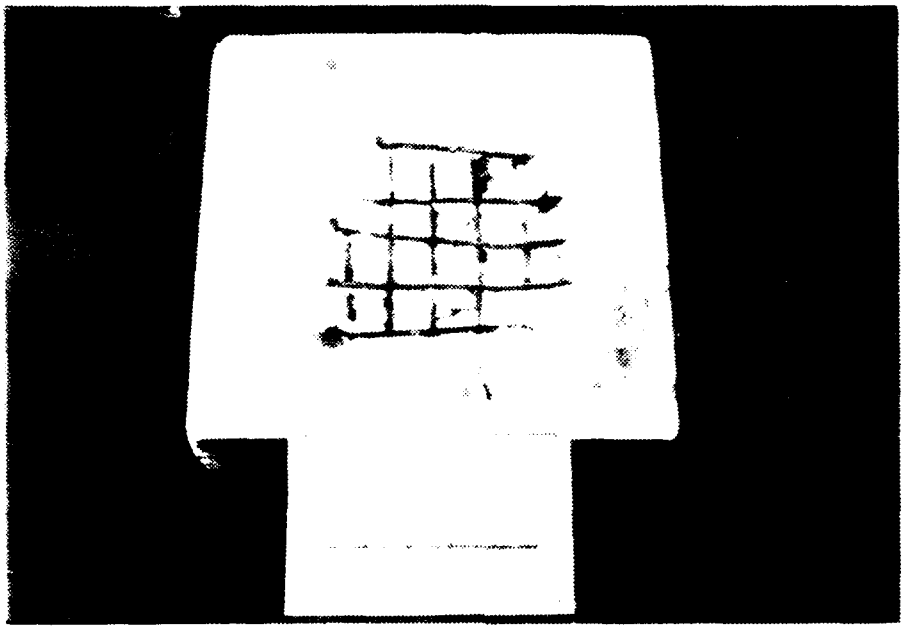

(a) Plan View of Back

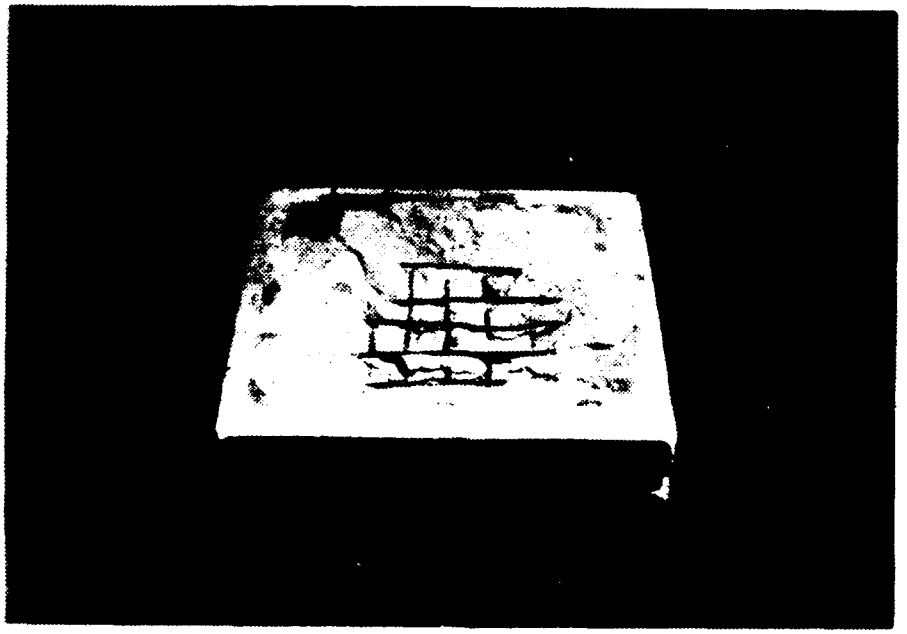

(b) Oblique Side View

Figure 11. Back of Model After Shot M019 Showing Spall Failure into the Reinforcing Rods.

Consequently the layers of material in front of the model were changed to produce a different loading profile.

b. Bending Failures

The primary goal of these test is to demonstrate the capability of producing a wide range of loading profiles sufficient to cover the range of expected scaled loading conditions that would might occur in full scale testing or loading a conventional weapon. Based on the referenced full- and one-third-scale tests, a loading with a ratio of rise time to wave propagation time through the structure greater than produced for the spall recovery tests appears to be required. The scaling of the ratio of rise time to wave propagation time has been discussed in Section III.A.2.c. As indicated in this section, this can be accomplished by introducing a more dispersive layer between the point of projectile impact and the model. Because the loading on the full scale structure is due to ground shock, e.g., from a shock wave propagating through soil, and because soil is a very dispersive medium, soil wave chosen as the material for this layer. Of the different soil types, sand has the most dispersive wave propagation characteristics. For this reason, fine or scaled sand was chosen as the material to use in the layer between the coverplate, or plate that is impacted by the gun projectile, and the model. This is shown in Figure 9. The purpose of this layer is to disperse the wave or lengthen the rise time of the wave. An increase in rise time of the shock loading can be shown by directly measuring the loading profile, which was done and is reported in the next section. Alternately, the increased rise time can be indirectly demonstrated by the type of failure type of the model. This is the approach that is employed in the recovery tests.

A summary of the recovery tests that produced a failure in bending is given at the bottom of Table 3. These models were covered with a layer of fine sand 8.6 cm (3.4 inch) thick. The rise time of the shock loading, as measured from several instrumented tests, is estimated to be 10-12 μs. The time for a stress wave to propagate through the model is approximately 10 μs, thus, the rise time and time for a stress wave to

propagate through the model are about the same. Thus Rt/Wt is approximately one. Again, because of failure of the Manganin gages during the unloading part of the stress profile, the decay time is not well known. However, these data do indicate a decay time of at least 80 μs for the short projectiles used in the 3.8 cm gun. As discussed in Section III..A.2.b, the decay time depends largely on the length of the projectile. Thus, the soil layer produces a loading profile with a much longer rise and decay time.

The magnitude of the peak stress in the loading profile is still controlled by the projectile impact speed, and thus can be viewed as independent of the soil layer. The projectile and coverplate material properties are well known, and as with the spall tests, the peak stress in the coverplate, and thus, at the coverplate-soil interface, can be calculated with reasonable confidence. These values are indicated in Table 3. Also given in Table 3 are estimated values of the normal stress on the model. These values are based on two measurements, and were computed by assuming a constant decay through the soil, thus, the confidence level for them is not nearly as high as the estimated peak stresses given at the coverplate-soil interface. They are included to give an "order of magnitude" estimate of the stress level that produced the bending failure. One important feature of these stress levels and loading rise times is that strain rate effects are no longer seen, or are at least minimal. Therefore, when the loading is more representative of that from a close-in detonation, strain rate effects do not appear significant. The model used in these tests is described in detail in Section III.A.1. It is repeated here that this model is square and clamped on all four edges. Therefore, the strength of this model in bending is greater than a similar rectangular hardened wall section, such as reported in References 27 and 28.

A test model without any reinforcing was tested first. As indicated in Table 3, the first tests conducted at relatively low stress levels produced negligible or no damage on this model. The stress level was increased, and a failure that closely resembled bending failure was observed. This failure is shown in Figure 12, which is a picture of the

model recovered after test M022. Confirmation that this failure mode is similar to static bending failure was obtained by static testing or an identical test model. In this test the model was installed in the same mount, covered with 8,6 cm of soil and a 0.64 cm thick Aluminum coverplate. The coverplate was slowly loaded with a 3.7 cm diameter ram in a Baldwin-Southmark tensile/compression test machine. The model failed at a ram load of 75 KN, or a stress on the coverplate of 70 Mpa. A picture of the model after failure is shown in Figure 13. A comparison of Figures 12 and 13 shows nearly identical diagonal cracks, which are the lines of greatest tensile stress in bending. Therefore, it is concluded that the rise time and possibly the decay time of the stress profile were increased sufficiently that the rapid loading and unloading that produced the spall failure mode does not occur. Instead the loading increases and decreases so slowly that the failure mode is nearly identical with that which occurs with static loading. This type of dynamic loading is sometimes referred to as quasistatic.

As previously mentioned, the length of the decay time is controlled by the length of the projectile. As the projectile diameter is fixed at 3.8 cm (1.5 inch) for the tests in the "M" gun, there is a direct relation between projectile mass and projectile length. Therefore, the larger mass projectiles result in the loading profile having longer decay times. Another way of looking at this is that the higher mass projectile will deliver greater energy into the model. Because the peak stress is fixed by impact speed, this mechanism by which this occurs is a longer loading on the model. There is some indication that the stress level which will produce the bending failure mode depends on the total loading time and hence the decay time. Stress profiles with longer decay times will produce the bending failure mode at lower peak stress. Two sets of data show this. Shot M020 was at an input stress to the soil cover of 20 MPa and produced slight cracking on the back of the test model. To produce a higher stress, a faster but lighter projectile was used in shot M021. Here a stress of 34 MPa was achieved, but because of the lighter (and hence shorter) projectile, the loading decay time was less. The test model had no damage

fig. 12

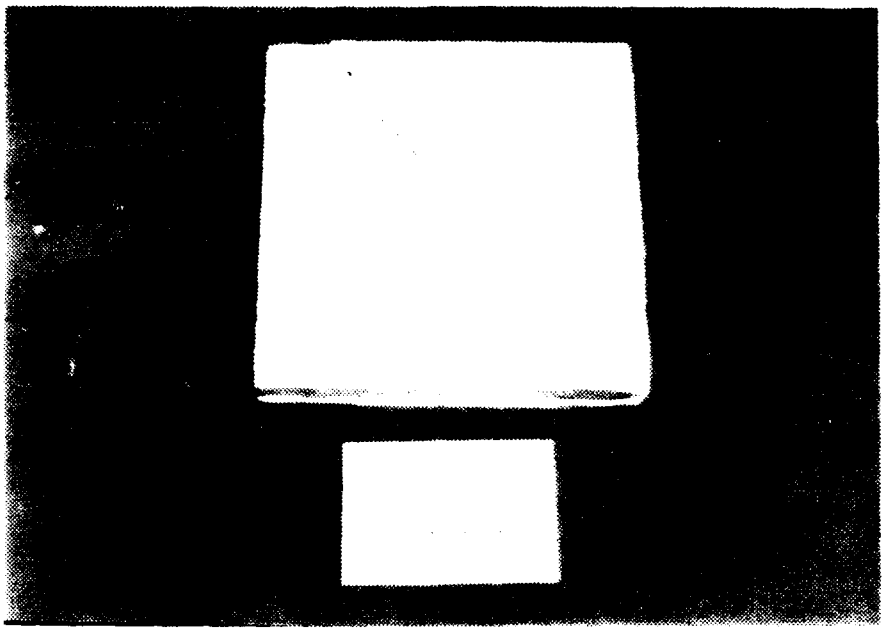

(a) Plan View of Back

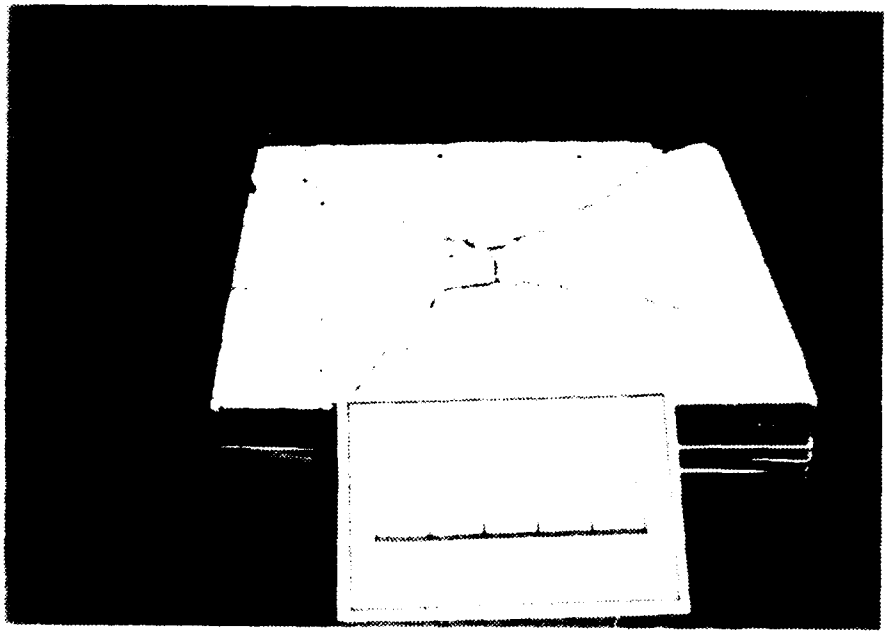

(b) Oblique Side View

Figure 12. Back of Model After Shot M022. The Diagonal Cracks Extend Completely Through the Model.

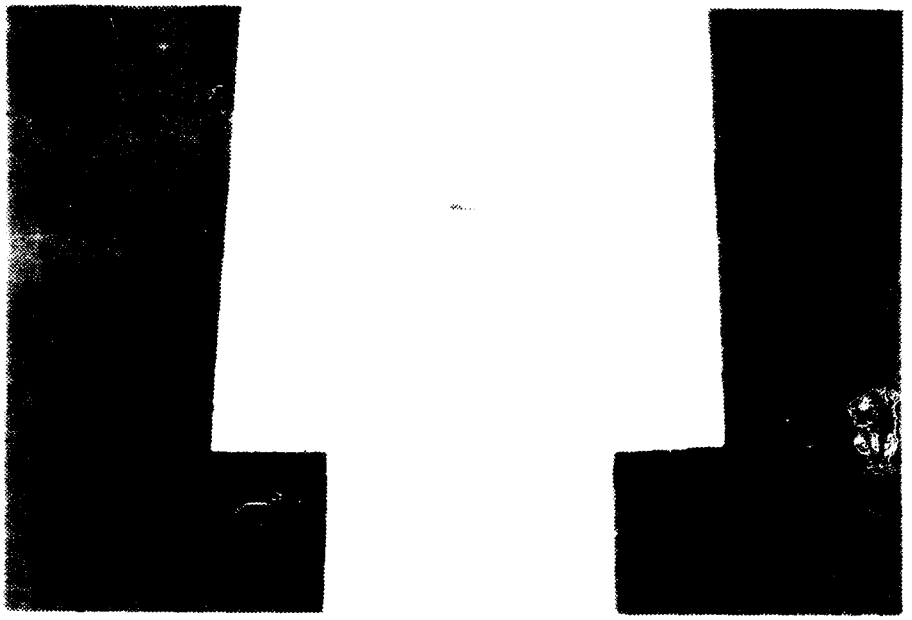

(a) Plan View of the Back of the Model

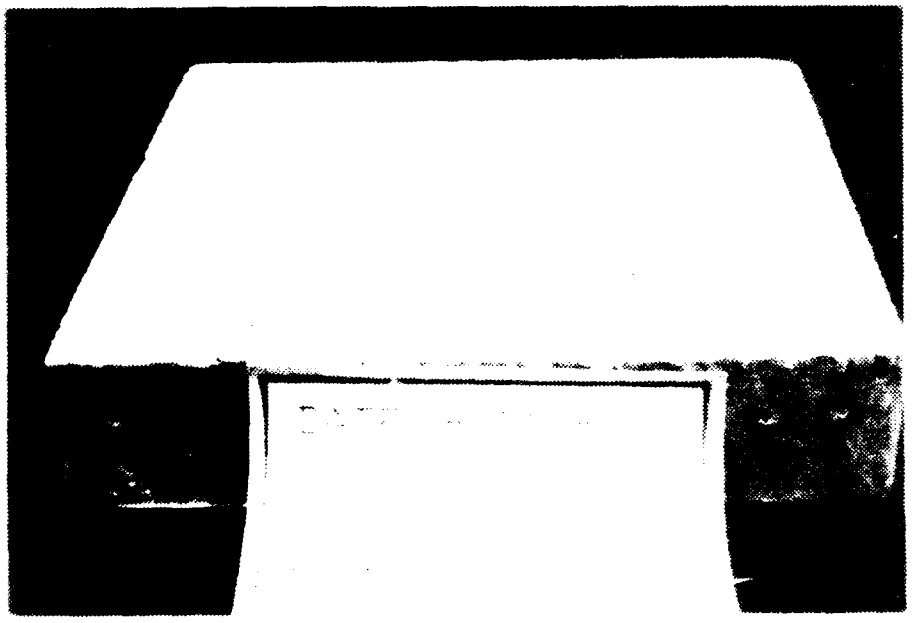

(b) Oblique Side View

Figure 13. Test Model Failed Under Static Loading.

in test M021. A similar situation was found in test M024, which was on a reinforced model. This test, which used a 112 gram Aluminum projectile with a speed of 178 m/s, gave a coverplate-soil stress of 130 MPa and produced on minor damage to the model. This was the highest projectile mass and speed could be obtained with the 3.8 cm gun. The test was moved to the 6-inch gun, and with a 555 gm Aluminum projectile with a speed of 202 m/s was achieved. This produced a stress of 100 MPa. The only slightly higher stress, but much longer loading time produced complete failure of the reinforced model. A picture of the reinforced model after recovery is shown in Figure 14. The interplay between peak loading and the loading time required to produce failure was not investigated further, primarily because the stress on the model could only be estimated in the recovery tests and because there was no direct measurement of the loading time (decay time).

The recovery tests do give data on the amount that the reinforcing steel increases the strength of the structure against ground shock loading. Test M022 produced a loading of 53 MPa at the coverplate-soil interface and resulted in complete bending failure of a model that did not have steel reinforcing. Test M024 was on a reinforced steel model at a coverplate-soil stress of 130 MPa. The model experienced only minor cracking. Both models were "protected" with 8.6 cm of soil cover. Assuming the same shock dispersion for the two tests, these data indicate that the reinforcing steel increases the shock loaded bending strength by at least a factor of three. The reinforced model configuration failed at stress of 100 MPa, but with a much longer loading (higher mass projectile). The interplay of stress level and time of loading in producing failure was discussed above.

In summary, the purpose of the recovery tests was to demonstrate the capability to produce a range of scaled loading conditions on a correctly scaled model. Different loading conditions or loading profiles produce different failure modes. Very rapid loading and unloading, e.g., short rise and decay times, produce the spall failure mode. A loading that increases and decreases very slowly, relative to the wave propagation through the structure, results in a failure mode quite similar to static bending failure. Because both spall and bending failure modes were

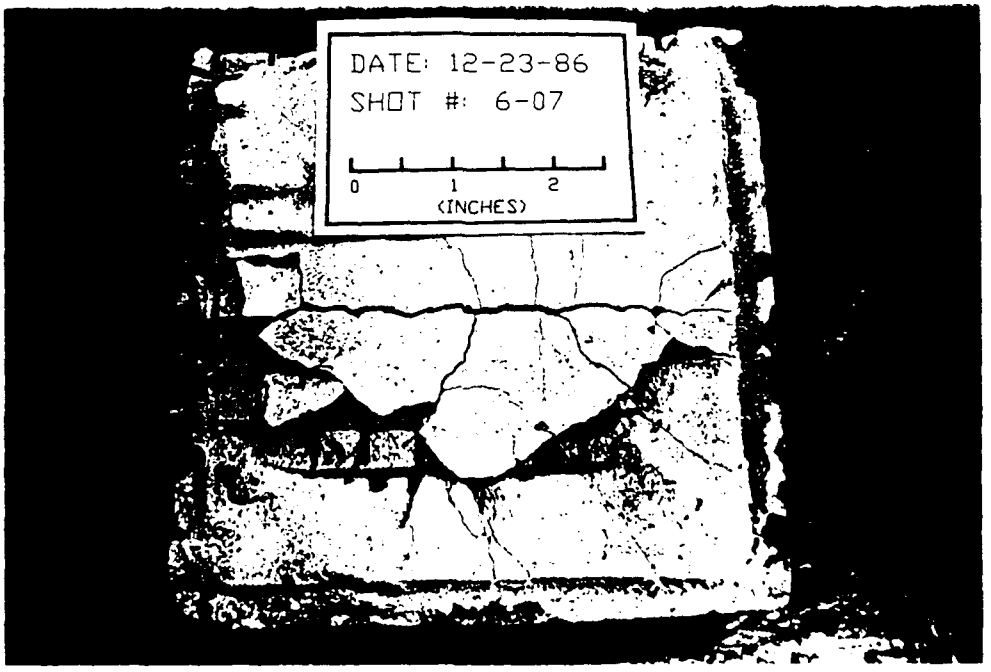

Figure 14. Back of Model After Shot 6-07. The Microconcrete in the Back of the Model has Failed in Bending Tension, but the Reinforcing Rods have Maintained the Models Integrity.

produced, this is used to show the capability of the gas gun technique to produce a broad range of loading parameters. In addition, the capability of controlling the loading conditions by varying the gun parameters is a demonstration of how various desired loading conditions can be achieved. Clearly intermediate loading conditions, those that produce a combination of spall and bending failure mode, can be can be produced using a gas gun. Because the primary purpose of the present recovery tests was to show the capability of producing a complete range of loading parameters, there were very few tests at intermediate conditions.

2. Instrumented Tests

Accompanying the development of suitable facilities to produce the scaled loading on a test model, was the actualization of instrumentation for measuring the pressure-time history or loading profile. This is a part of facility development, and the instrumentation choosen for use and its preliminary testing and calibration are described in Section II.B. This section gives the results of these instrumented tests. The purpose of these tests is twofold: (1) to test and improve the capability of the instrumentation to measure loading profiles, and (2) to measure the loading profile in some of the recovery tests in order to quantify the results. There is a particular need for measured data in the recovery tests that had a soil layer, because the shock dispersion and attenuation through the soil is not well known. As was previously stated, the shock Hugoniot properties of all materials used in the layers are well-known, except for soil. Therefore, as a minimum, the peak stress levels can be accurately calculated if there is no soil layer. However, when a soil layer is present the shock properties are not as well-known, and consequently measured data from instrumented tests are needed.

Loading profile measurements were made using both Manganin gages and Polyvinlylidene Fluoride (PDVF) or polymer gages. The Manganin gages were manufacuted by Dynasen, inc. and the polymer gages were obtained through the AFESC from NBS. The relative merits of the gages, and the signal conditioning and data acquistion system used with each type of gage

has been described in Section II.B. Manganin gages were used first, but problems were encountered with the leads shearing off under tensile loading, and with low sensitivity. Therefore, in the latter measurements the polymer gages were used more extensively. Where possible both types of gages were used together. Because each shot requires considerable setup time, the intrumented tests were conducted to try to accomplish both goals simultaneously. This was not always possible, or even prudent, thus, some of the tests were simply to locate problems in the instrumentation or in the data acquisition system. A summary of those tests that produced useful data is given in Table 4.

The recovery tests that produced the spall failure mode did not have a soil layer. These tests were the first instrumented tests, and were conducted to confirm the estimated peak stress and obtain data on the loading profile, e.g., the rise time and decay time of the loading. As indicated in Table 4, tests M025 and M029 were instrumented tests without a soil layer. Test M025 produced the spall failure, and was instrumented with two Manganin gages, one located on the front of the test model and one poured in place on the rear of the model. Output from the gage located on the front of the model is shown in Figure 15. The gage fails immediately after the peak stress is reached, presumably due to shear of the leads as the tensile waves begin to cause the load to decrease. However, both the rise time and magnitude of the loading can be determined. The peak loading, as measured before the gage fails, is 92 MPa. This agrees well with the calculated value of approximately 100 MPa. This and the data taken from shot M029, given in Table 4, give confidence that the stress levels estimated from the shock Hugoniot properties provides an accurate estimate of the peak stress in the test. The rise time of the loading in Figure 15 is 2-3 μs. Rise times for projectile loading of metals is typically less than 1 μs. When a plastic layer such as Lexan or PMMA is included, the rise time increases slightly to 2-3 μs. This test and test M029 confirm these rise times. This is the basis for the estimated value of rise time given in the discussion of the recovery tests with spall failure, Section III.B.1.a.

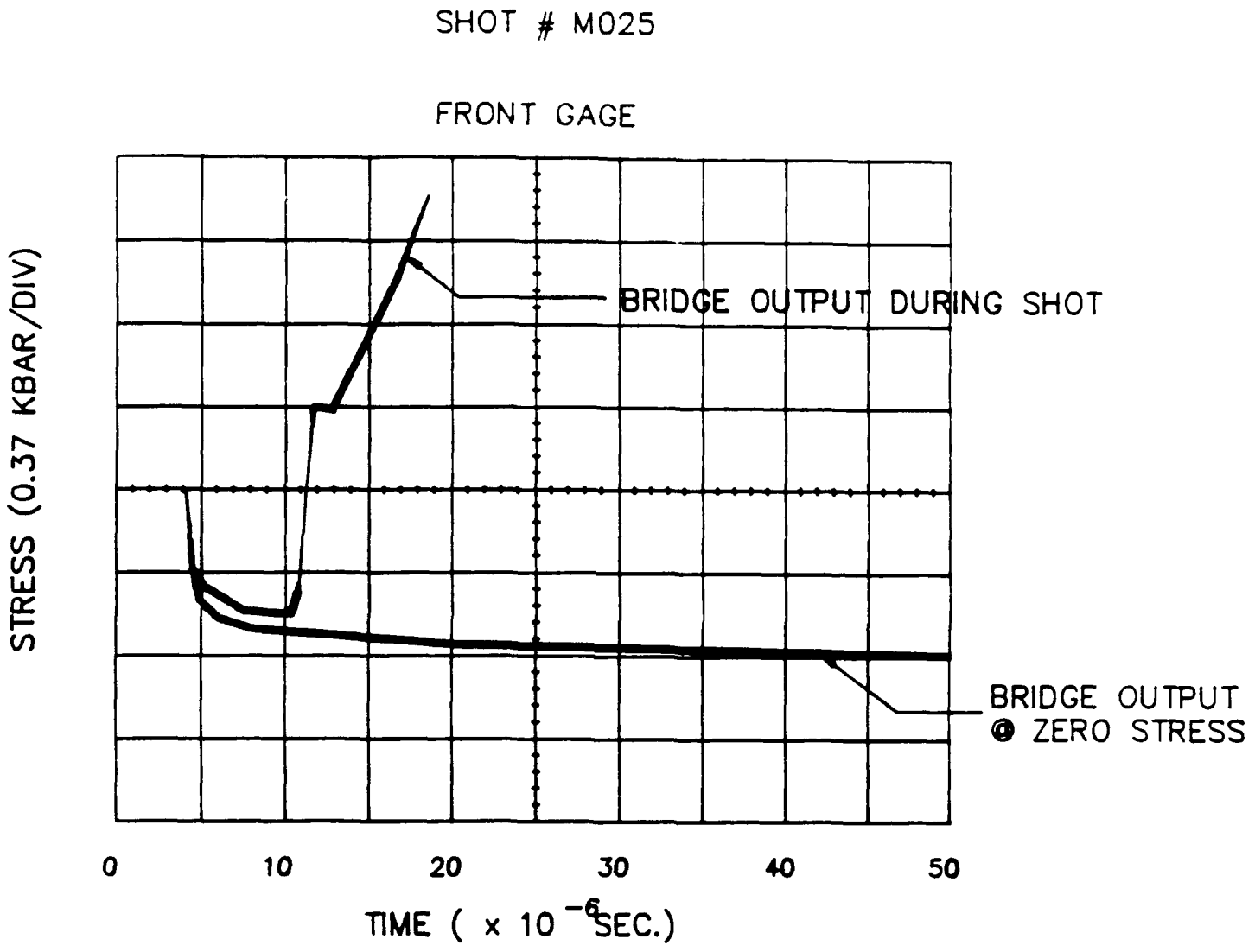

Figure 15. Manganin Gage Output for Shot M025. The Gage is Located on the Front of the Model and Fails Shortly after Reaching the Peak Loading.

TABLE 4. SUMMARY OF INSTRUMENTED TESTS

Shot No.	Soil Thick	Cal Peak Stress		Meas Peak Stress		Other	Stress Profile
		Cover-Pl	Model	Cover-Pl	Model	Gages	
M025	0	---	100	---	92	None	NO
M027	2.3	500	---	540	93	Off-c	on-model
M029	0	---	630	---	646	In layer	In concrete
M030	3.2	83	---	---	48	Plaster Gage	On-model
6-08	2.5	100	---	---	132	None	Initial Profile

Data from tests with a soil layer were harder to obtain using the Manganin gages. This is because the particle motion is greater in soil than with plastics or metals. Any relative displacement between the Manganin gage and the soil will shear off the leads and fail the gage. Several approaches to avoid this happening are described in Section II.B.2. None worked very satisfactorily, and in these tests the Manganin gages still had lead failure unless sandwiched between layers of plastic and mounted on a rigid model. In addition, the lower impedance of the soil layer lowers the stress level. The lower stress level was at or slightly below the level at which the Manganin gages will operate reliabily. Because of this the polymer gages were used with the Manganin gages during the latter tests. As previously mentioned, both the Manganin and the polymer gages had to be calibrated dynamically. A number of Manganin gages were destroyed during calibration, thus, to get maximum use out of the polymer gages, they were used simultaneously with the Manganin gages at higher stress levels. This was to obtain some experience in using them, as well as to provide a dynamic calibration. Calibration of the polymer gages is complicated in that the gage sensitivity may depend on stress state. Reference 23 reports a different sensitivity for calibration in soil than with a hydraulic calibration. Thus, the present tests were directed not only at measuring the loading profile when a soil layer was present, but also at the dynamic response of the polymer gages under shock loading in soil. Tests M027, M030, and 6-08, listed in Table 4, were instrumented tests with a soil layer. Test M027 was at a much higher stress level than needed to produce the

bending failure mode. Test M030 was on an Aluminum model to avoid failure of the model and damage to the gages. Test 6-08 was at the conditions that produce the bending failure mode, but because of a thin coverplate, the projectile penetrated both the coverplate and model. Needless to say, the model was not recovered in a condition that allowed analysis of the failure mode. Therefore, none of these tests were instrumented tests of an actual bending failure. The measured data give information on the loading rise time and the peak stress level. These can be used to estimate the loading profile characteristics that produced bending failure. The rise time of a loading profile that has passed through a soil layer in increased to 5-12 μs. There is evidence that the rise time increases with with soil thickness, but enough data to quantify this has not been taken. As general rule, for the soil thickness of 8.6 cm used to produce the bending failure mode, the rise time is around 10-12 μs. This is the rise time assumed for the loading profile that produced the bending failure mode, and is discussed in Section III.1.a. This is approximately the time for a stress wave to propagate through the wall of the model, and is probably the reason that the failure mode becomes predominantly bending.

The peak loading that occurs in the bending failure mode is harder to estimate, because of the limited data. As previously stated, the peak stress as the shock enters the soil layer is believed to be known with reasonable accuracy. The attenuation through the soil layer is not known. The present data show an attenuation that ranges from 0 to 60 percent of the input stress on the soil. These data are given in Table 4, and there is considerable variation in shock attenuation between the different tests. There is not enough data to determine if the attenuation correlates with different soil conditions (porosity, wetness, grain size, packing density, etc), different input stress levels, projectile alignment, or if it is simply scatter in the tests. The data in which there is the most confidence indicate an attenuation of 30-60 percent. To provide an "order of magnitude" estimate, an attenuation of a constant value of 50 percent was used to calculate the peak stress on the model for the tests that produced the bending failure mode. This value is included in Table 3 as the

estimated peak stress on the model. If it is remembered that a higher stress level is required to fail the present square wall section as compared to the rectangular wall section used in larger scale tests, these values compare reasonably well with the peak stress that has been observed in one-third-scale (Reference 27) tests and with those in full-scale tests (Reference 28). This is particularly true when the possible variation in shock attenuation through the soil, which has been only approximated here, is included.

To have correct geometric scaling, the ground shock radius of curvature must be correctly scaled. A convenient way of comparing the scaled radius of curvature to that in a full- or larger-scale test is to nondimensionalize the shock radius of curvature, and then compare the non-dimensional radii. With correct scaling the nondimensional radii should be equal. Here, the ground shock radius of curvature is non-dimensionalized by the vertical length of the wall. If the shock radius is denoted by Rs, the nondimensional radius, Rs^* is obtained by dividing Rs by the wall length. If the model is scaled geometrically, as in these experiments, then the length ratio of any part of the model or prototype structure have the same ratio. Hence, nondimensionalization by any length on the structure is acceptable. This is because the magnitude of Rs^* may change with the length scale chosen to nondimensionalize Rs, but the ratio between scale and prototype tests remains the same. Therefore, the comparison between Rs^* in the scaled and the prototype test is still valid.

Two of the instrumented tests in Table 4 can be used to measure shock curvature. Shot M027 had two Manganin gages mounted on the model. One was on the model centerline and the other was located 3.8 cm off of the model center. A spherical shock shape was assumed, and the shock curvature was computed by the difference in arrival time at the two gages and the measured shock speed through the soil. The same procedure was used in shot M030, where a Manganin gage was mounted on the center of the model, and a polymer gage was mounted 2 cm off-center. Although the polymer gage calibration is not well-defined (which is discussed below),

the difference in arrival times can be used to measure shock curvature. The computed value of shock radius, Rs, and the nondimensional shock radius, Rs* are give in Table 5, below. In addition, the values from one-third-scale tests (Reference 27) are also given.

TABLE 5. GROUND SHOCK RADIUS OF CURVATURE - Rs

Test no.	Shock Radius Rs (M)	Non-Dim Radius Rs*
M027	.18	1.2
M030	.15	1.1
WES 1/3 Scale Tests		
7	1.52	1.0
7A	0.80	0.53

There is good agreement between the present gas gun tests and the WES one-third scale tests using explosives. The shock curvature in the gas gun is controlled by the ratio of projectile diameter to test model lateral (or vertical) dimension. These data indicate that this scaling is approximately correct. As data from additional instrumented tests are taken, the scaling of Rs* will be checked. However, at this time the shock radius appears to be properly scaled.

Work on the evaluation and dynamic calibration of the polymer gages has just begun. In preliminary tests, the polymer gages appear to withstand the large particle motion that occurs in shock loaded soil better than the Manganin gages. In addition, the polymer gages are more sensitive, and thus have greater signal-to-noise ratios at the lower stress levels that occur in soil layers. As previously stated, the correct calibration in soil is uncertain, given the results in Reference 23, which indicate a different

calibration in soil and a hydraulic oil bath. We are currently investigating this by attempting to make a dynamic stress measurement in a soil layer with both a Manganin gage and a polymer gage. Test M030 is the only test to date, and had a Manganin gage mounted on the center of the model, and the polymer gage mounted off-center. The polymer gage was mounted off-center because of its size, and this data was used to compute shock curvature. A graph of the loading profile as measured by each gage is given in Figure 16. In this figure the calibration constant for the polymer gage was taken from the NBS hydraulic calibration. The stress off-center is expected to be slightly lower than the stress at the center of the model, and as discussed in shock curvature calculation, begins slightly later. These data indicate that the hydraulic calibration is reasonably accurate, but may give a gage sensitivity that is slightly lower than that occurs under dynamic soil loading. Further testing can confirm the actual gage sensitivity for this type of loading

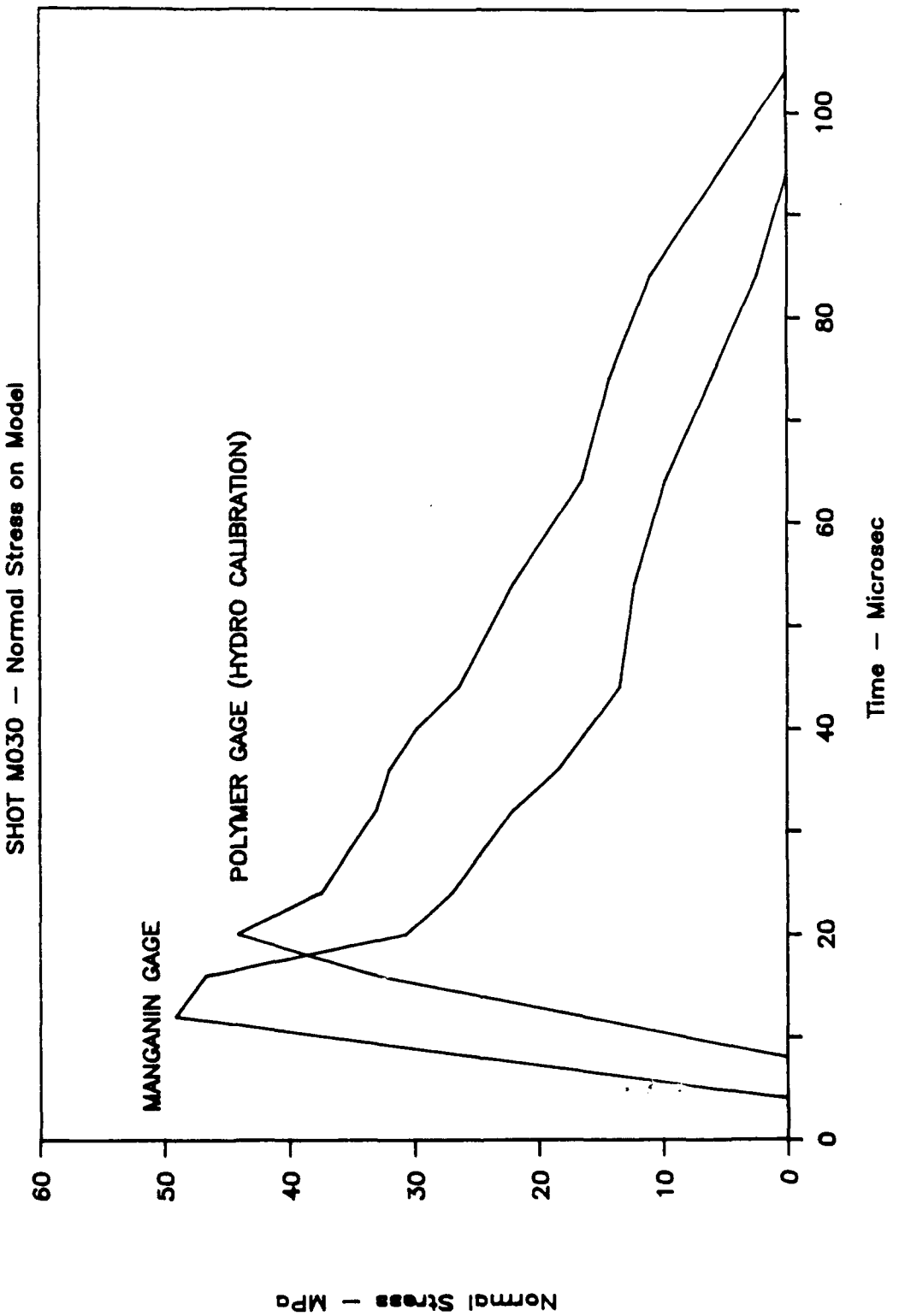

Figure 16. Normal Stress on the Model for Shot M030. The Curves Show the Normal Stress as Measured by a Manganin and a Polymer Gage.

REFERENCES

1. Abramson, N.H., Proceedings of the Second Symposium on the Interaction of Non-Nuclear Munitions with Structures (Panama City Beach, Florida, April 15-18,1985), University of Florida Graduate Engineering Center, Eglin AFB, Florida, April, 1985.
2. Baker, W.E., Westin, P.S., and Dodge, F.T., Similarity Methods in Engineering Dynamics, Hayden Book Co., New Rochelle, NJ, 1973.
3. Langhaar, H.L., Dimensional Analysis and Theory of Models, John & Sonms, New York, 1951.
4. Kline, S.J., Similitude and Approximation Theory, McGraw- Hill,New York, 1965.
5. Isaacson, E.de St Q., and Isaacson, M.de St Q., Dimensional Methods in Engineering and Physics, Edward Arnold, London, 1975.
6. Sedov, L.I., Similarity and Dimensional Methods in Mechanics, Academic Press, New York, 1959.
7. Harris, H.G.(ed.), Dynamic Modeling of Concrete Structures, Publication SP-73, American Concrete Institute, Detroit, MI, 1973.
8. Sabnis, G.M. and Harris, H.G, Structural Modelling and Experimental Techniques, Prentice Hall, New York, 1983.
9. Ross, C.A., Proceedings of the Symposium on the Interaction of Non-Nuclear Munitions with Structures, (U.S. Air Force Academy, CO, May 10-13, 1983), University of Florida Graduate Engineering Center, Eglin AFB, FL, 1983.
10. Abrahamson, G.R. Florence, A.L., and Colton, J.D., Scale Modeling in Structural Dynamics Involving Plastic Deformation and Fracture, Poulter Laboratory Technical Report, Stanford Research Institute, Menlo Park, 1975.
11. Abbott, P.A., Calibration of a Vertical Shock Tube and its Associated Soil Bin, Tech. Rept., AFWL-TR-66-134, U.S. Air Force Weapons Laboratory, Kirtland AFB, NM, 1966.
12. Dorris, A.F. and Albritton, G.E., Response of a Buried Prototype Communications Conduit to Static and Dynamic Loading, U.S. Army Water Ways Experiment Station, Vicksburg, MS, Tech. Rept., 1-750, 1966.

13. Murphy, M., Young, D.F., and McConnell, K.G., Similitude of Dynamically Loaded Buried Structures, Tech. Rept., AFWL-TR- 64-142, U.S. Air Force Weapons Laboratory, Kirtland AFB, NM, 1965.

14. Cowin, S.C., and Carroll, M.M., "The Effects of Voids on Material Deformation," AMD-Vol. 16, Am. Soc. Mech. Eng., New York, 1976.

15. Clyens, S. and Johnson, W., "The Dynamic Compaction of Powdered Materials," Mat. Sci. Eng., 30, 121, 1979.

16. Nelson, I., Constitutive Models for Use in Numerical Computations, Proceeding of DMSR 77,(Karlsruhe, September 5-16, 1977, West Germany), Volume 2, Balkema, Rotterdam, Belgium, 1977.

17. Nelson, I., Baron, M.L., and Sandler, I.S., Shock Waves and the Mechanical Properties of Solids, Syracuse University Press, Syracuse, New York, 1971.

18. Fowles, G.R., et al. 1970. Gas Gun Impact Studies. Review of Scientific Instruments. 41(7): 984-996.

19. Seigel, A.E. 1965. Agardograph 91. U.S. Naval Ordnance Laboratory. Silver Spring, Maryland.

20. Shigley, J.E. 1977. Mechanical Engineering Design, 3rd Edition. McGraw-Hill Book Company, Inc., New York.

21. Juvinall, Robert C. 1967. Engineering Considerations of Stress, Strain, and Strength. McGraw-Hill Book Company, Inc., New York.

22. Jeelani, S. 1970. Design of Powder Accelerator Systems for Impact Studies. North Carolina State University. Raleigh, North Carolina.

23. Chung, R.M., Bur, A.J and Reasoner, E. Development of an NBS Polymer Gage for Dynamic Soil Stress Measurement, NBSIR 85-3135, April, 1985

24. Zia, P., White, R.N., and Vanhorn., D.A. Principles of Model Analysis. Am. Concrete Inst. Pub. SP 24-2

25. Sabnis, G.M., Harris, H.G., White, R.N., and Mirza, M.S. Structural Modeling and Experimental Techniques. Prentice-Hall, 1983.

26. Cunningham, C.H., Townsend, F.C. and Fagundo, F.E. The Development of Micro-Concrete for Buried Structures. Report for AF Engineering and Services Ctr., Contract F08635-83-C-0136

27. Draft Tech Rept. WES 1/3 Scale Tests. Title and Authors Unknown

28. Kiger, S.A., and Albritton, G.E. Response of Buried Hardened Box Structures to the Effects of Localized Explosions. U.S. Army Engineer Waterways Experiment Station. TR SL-80-1. March, 1980.

APPENDIX A
SIX-INCH DIAMETER GUN SYSTEM

This Appendix contains a detailed design of the 6-inch diameter gun system, shown in Figures A-1 and A-2, being used for simulated blast wave studies in the Shock Laboratory at North Carolina State University. The facility is designed to accelerate a projectile mass of a maximum of 2.72 kg (6 Lbm) to a velocity of approximately 450 m/s (1500 ft/s) using helium or nitrogen as the propellant gas at a maximum breech pressure of 20 MPa (3000 psi). A horizontally oriented barrel is more common for light gas guns, but this system is vertically oriented because of two basic restraints. As the research emphasis of this project is blast wave studies in layered systems consisting of sand, gravel, and other types of soil cover, a horizontal target produced with these materials is much easier to handle and prepare than a vertical target. The horizontal target configuration is a consequence of a vertical gun and is more suitable for experimental logistics. Second, laboratory space is somewhat limited because this lab also houses a 3.8 cm diameter, 1.5 meter length gun, a 5 cm diameter, 7.3 meter length gun, experimental work space, and office space for the lab personnel. Therefore, the entire facility was designed and dimensioned to fit vertically in a 3.5 meter (11.5 foot) tall area. The 6-inch gun was constructed using English components and in a machine shop with English machine tools, therefore, for the remainder of the design discussion, dimensions will be given in English units.

A. DETAIL DESIGN

The detailed design of the facility are based on the following requirements with all parts designed with a minimum factor of safety of 1.5.

1. The most obvious requirement is that the parts must be designed to fit in the allotted space.
2. The barrel must be of sufficient length to produce the desired maximum velocity and of sufficient wall thickness to withstand the maximum pressure introduced.

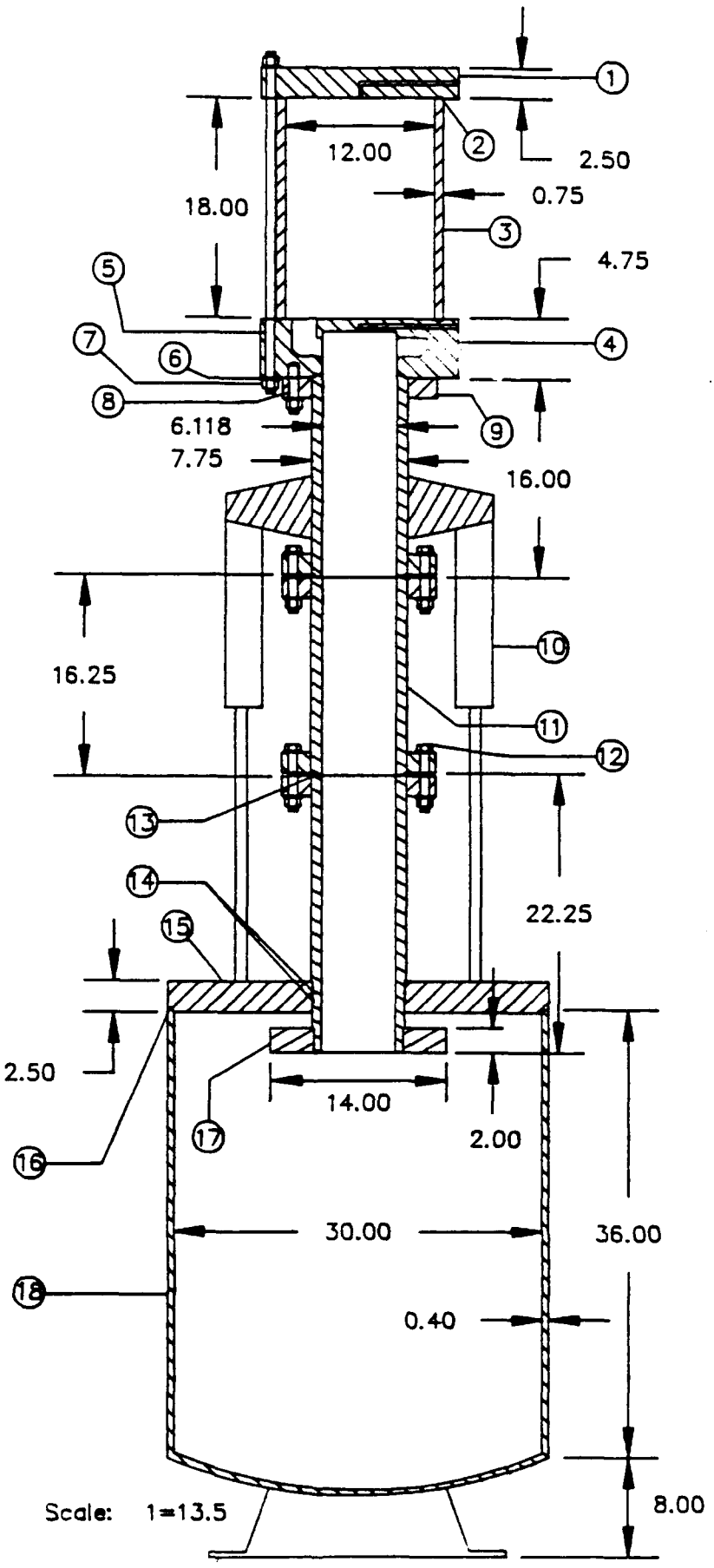

Figure A-1. View of 6 -Inch Diameter Gun.

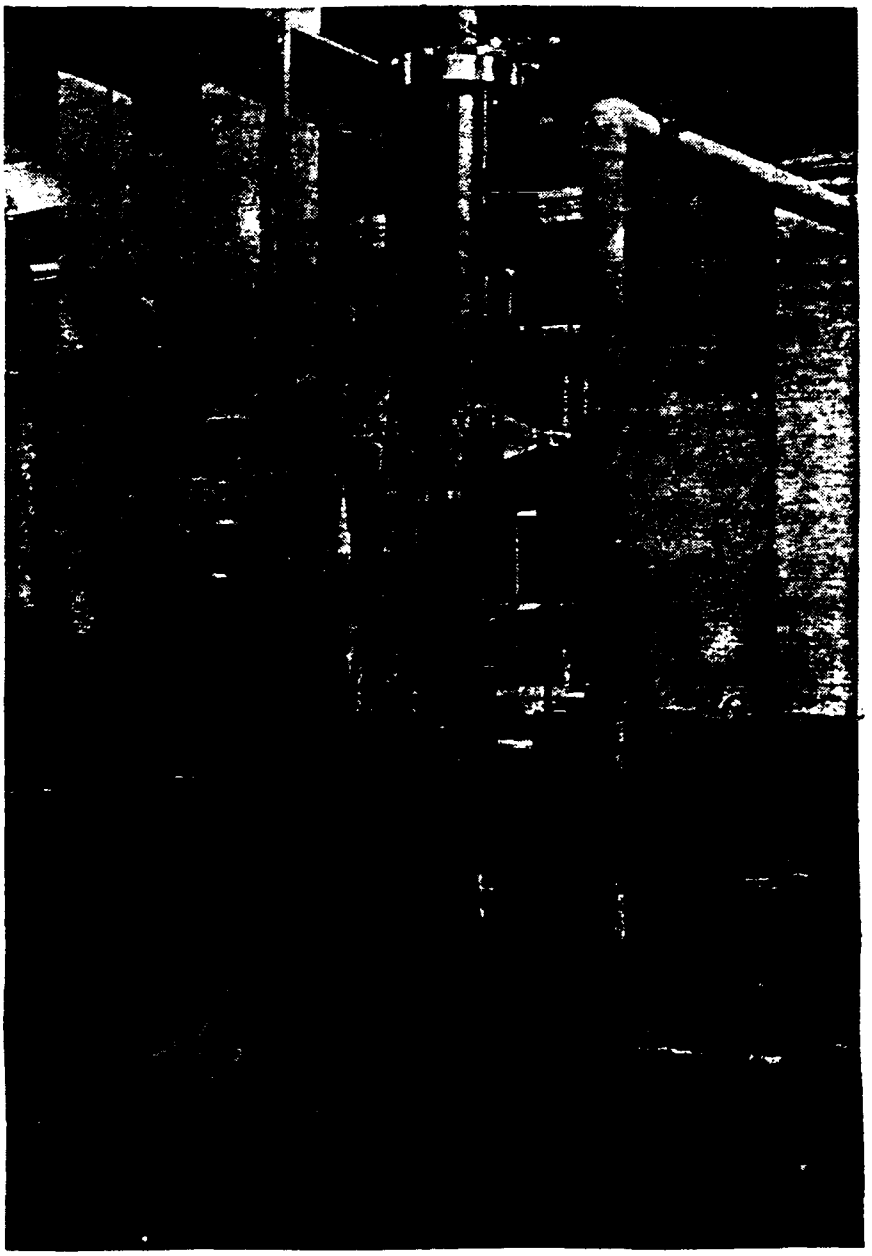

Figure A-2. Six-Inch Diameter Gun.

3. Tilt should be kept to a minimum through a combination of close tolerances on barrel manufacture and projectile design.
4. Breech diameter should be chosen to provide maximum chambrage which encourages a higher average pressure behind the projectile. The breech must also be of sufficient wall thickness to withstand the maximum pressure utilized.
5. Impact area must be sufficient to accommodate targets as large as 2 feet in diameter and 1 foot in thickness.
6. Catcher volume must be large enough to provide expansion room for the propellant gas before it is vented to the atmosphere. It also must have sufficient wall thickness to withstand the maximum final pressure of the gas and be deep enough to provide stopping distance for the projectile.
7. Adequate vacuum must be provided at three places: in the barrel to prevent air shocks, behind the projectile to help seal it and hold it in place, and in the catcher to reduce the total pressure it experiences.
8. An exhaust system must be provided to vent away the propellant gas from the system after successful firing or in the case of an aborted firing.
9. The entire system must be operated from a remote control panel to provide safety for the operator.
10. A recoil system must be provided to damp out the motion of the barrel when fired.
11. Electrical ports must be provided for the necessary experimental instrumentation.

PARTS LIST

ITEM	QTY	DESCRIPTION	MATERIAL	SPECIFICATION
1	1	BREECH END PLATE	A-16 HR	16" OD, 2.5" THICK
2	2	BREECH O-RINGS	BUNA	PARKER #2-279
3	1	BREECH TUBE	1026 HF	13.5" OD, 12" ID
4	1	BREECH FLOW PLATE	A-36 HR	16" OD, 4.75" THICK
5	18	BREECH RODS	A-449	3/4"-16 UNF, GRADE 8
6	96	WASHERS	LAMALLOY	3/4" ID, L9
7	72	NUTS	LAMALLOY	3/4"-16 UNF, L9
8	12	BARREL STUDS	A-449	3/4"-16 UNF, GRADE 8
9	5	BARREL FLANGES	STEEL	12.5" OD, 300# CLASS
10	4	SHOCK ABSORBERS	-	MONROE MODEL #74400
11	3	BARREL SECTIONS	1018 CD	7.75" OD, 6.118" ID
12	24	BARREL BOLTS	LAMALLOY	3/4"-16 UNF x 6", L9
13	4	BARREL O-RINGS	BUNA	PARKER #2-165
14	2	PLATE O-RINGS	BUNA	PARKER #2-263
15	1	MOUNTING PLATE	A-36 HR	30.90" OD, 7.505" ID
16	1	CATCHER TANK O-RING	BUNA	29.87" ID x 0.125"
17	1	TARGET COLLAR	A-36 HR	14.0" OD, 2.0" THICK

The barrel is constructed in three sections with lengths of 16, 16.25, and 22.25 inches (section 1, 2, and 3, respectively) for a total barrel length of 4.5 feet when assembled. Three barrel sections were chosen instead of one continuous length to facilitate holding a close tolerance on the barrel inside diameter. All major machining work on the barrel and breech was performed in the School of Engineering's shop, ERSD (Engineering Research Services Division). Available equipment in this shop was also a

factor in the choice of a sectioned barrel as their equipment would not adequately handle a 4.5-foot piece of material and, if it could, would still present difficulties in machining since there would be problems with excess deflections in such a long workpiece. The barrel sections were finished from a 1018 CD steel tubing with a 6-inch inside diameter and a 7.75-inch outside diameter. The finished inside diameter of the barrel was chosen as a consequence of the available projectile O-ring sizes which gave an acceptable squeeze range (as suggested by the O-ring manufacturer) between the barrel and projectile, based on a radial clearance of 4 to 5 thousandths. The inside diameter of the barrel was specified to be 6.118 inches, and the barrel sections were machined as indicated in Figure A-3. It is suggested that a different material be chosen for the barrel sections, if possible (such as 4140 or 4340 steel), to provide a heat-treatable workpiece. A 1018 CD steel does not heat treat without distortion and cannot be effectively nitrided. However, due to material availability and cost limitations, this material was used and has not shown excessive wear or damage.

Bayonet joints at each end of the barrel sections are used to connect the sections together. This design is modeled after an gun system used at Washington State University and described in Reference A.1. The joints are held together by flanges which are threaded onto each barrel section (Figures A-4 and A-5), and the flanges are, in turn, bolted together with 12 high strength cap screws (0.75-inch diameter, Grade 7). A standard 300-pound class steel, slip-on flange was chosen based on a standard design equation for a uniformly loaded flat circular plate (Reference A.2). The assembled barrel is pictured in Figure A-6. Each bayonet joint is vacuum sealed by a face O-ring in the barrel section ends.

The length of the barrel, 4.5 feet, was arrived at by an iterative computer program using the velocity equation, which is Equation (13) in Section III. Three barrel lengths, 4 feet, 4.5 feet, and 5 feet, were examined, checking each length for a suitable projectile velocity range with an upper limit of at least 1300 ft/sec (400 m/sec) for a 6-pound projectile. Some choices had to be made at random, such as projectile length, breech a-3

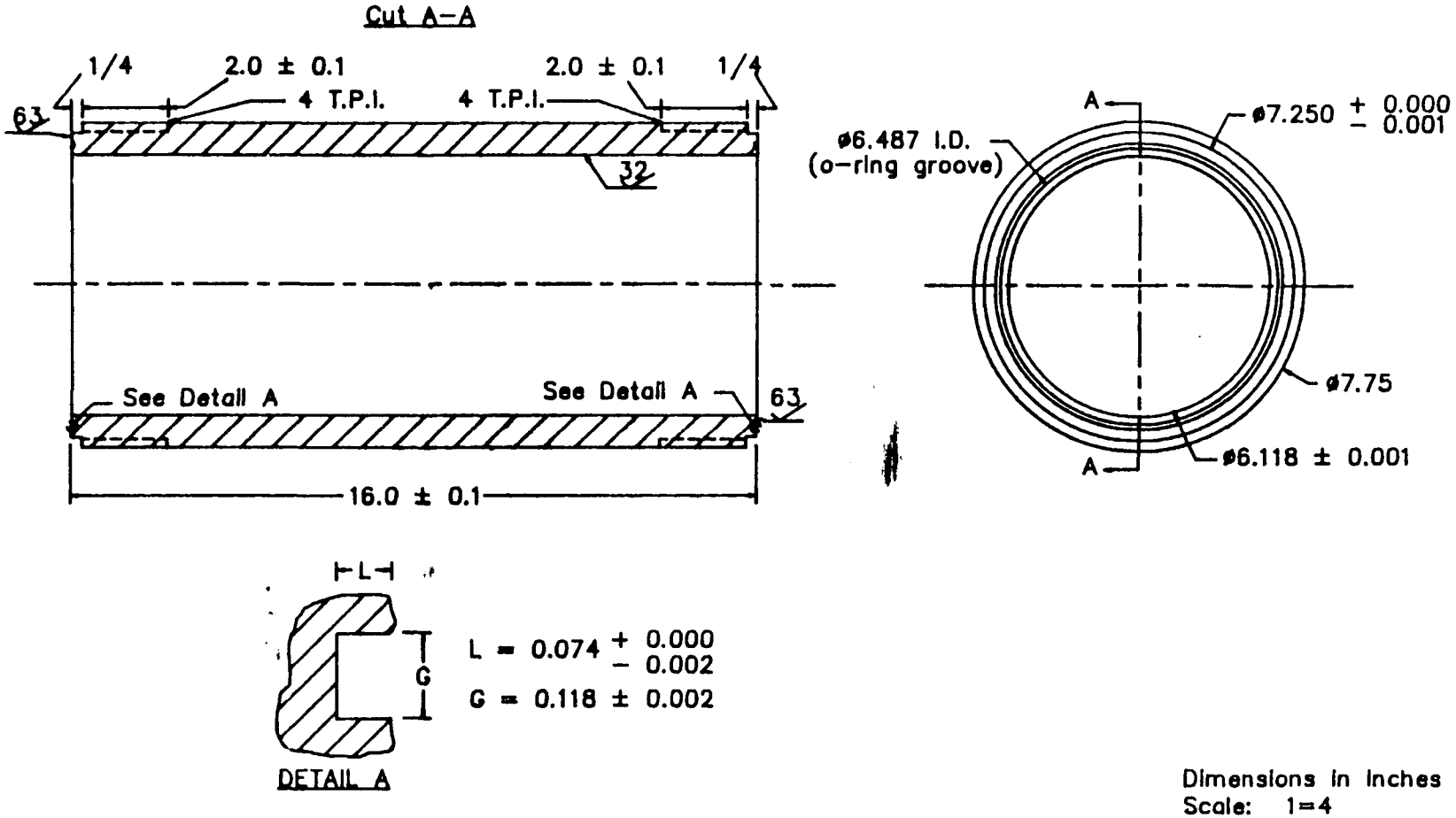

Figure A-3. View of Barrel Section #1 (Typical Barrel Section).

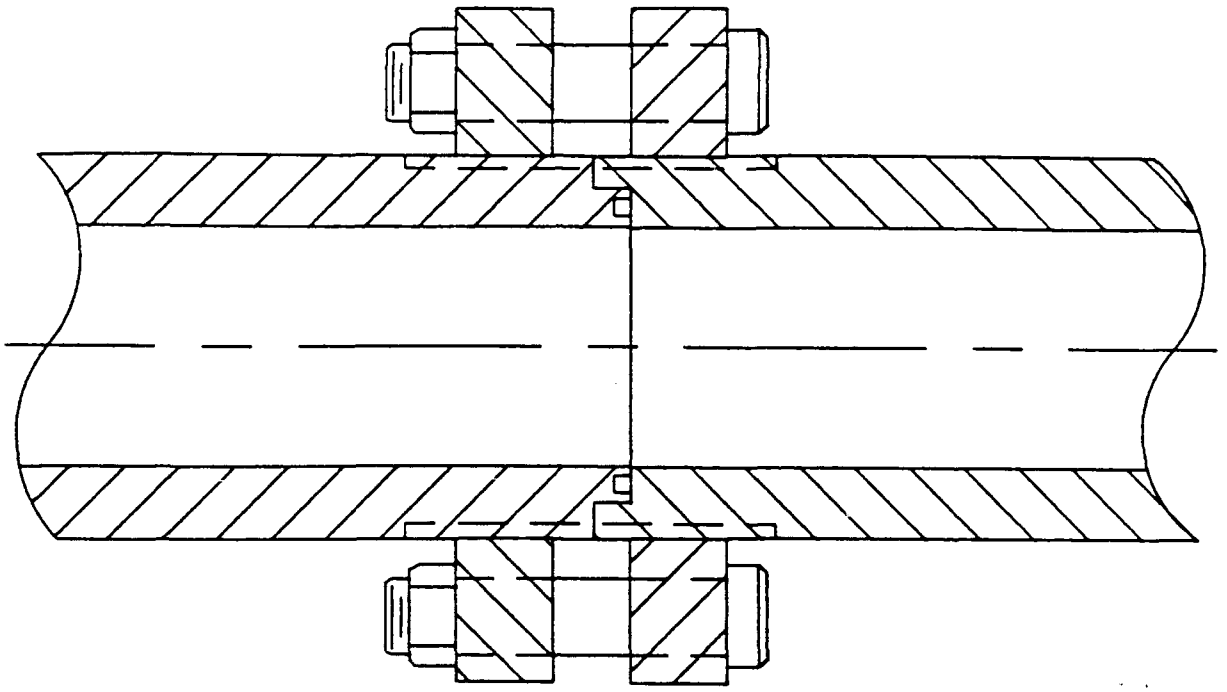

Figure A-4. View of Bayonet Joint.

Figure A-5. Bayonet Joint.

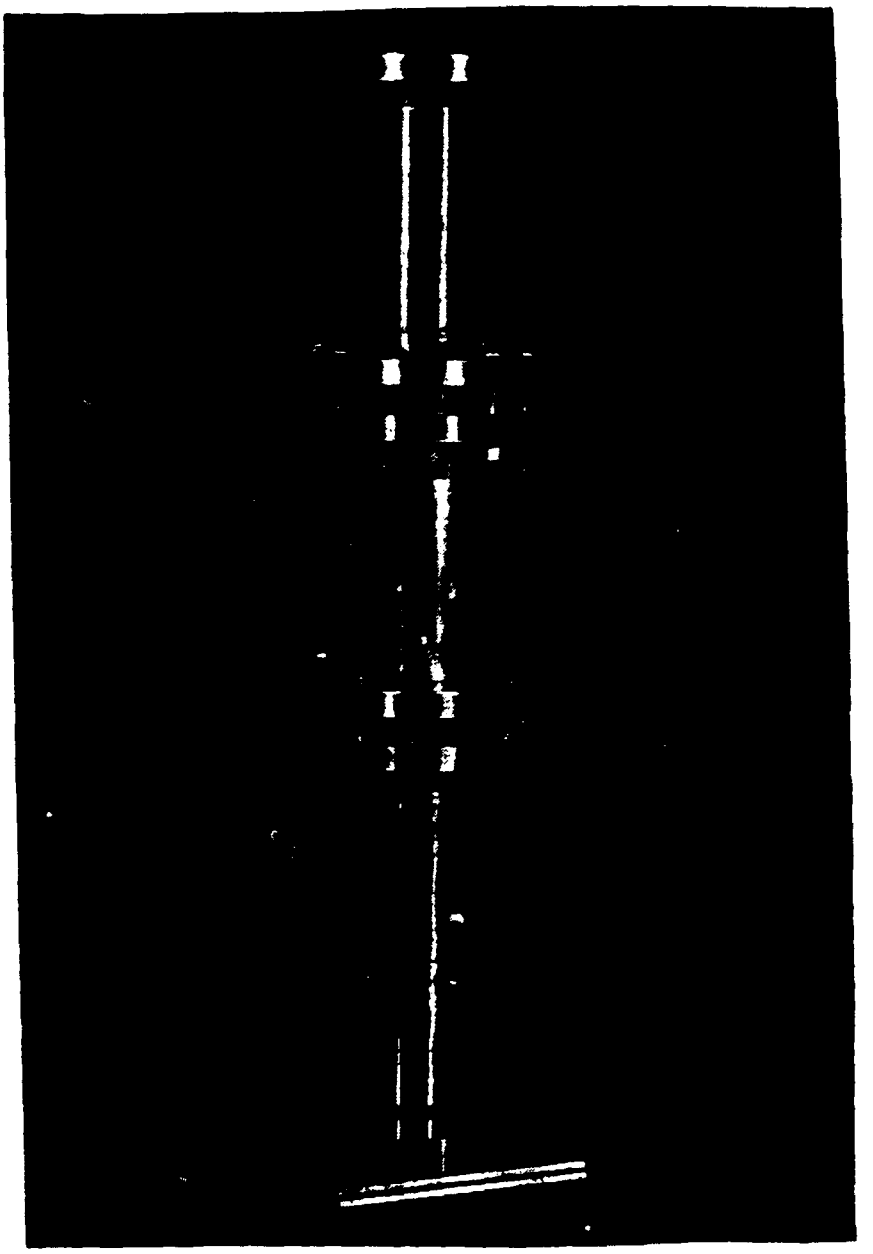

Figure A-6. Assembled Barrel.

diameter, and breech length, to begin the iterative process. Different parameters were adjusted and the solution obtained until a satisfactory set of data was achieved. The 4.5-foot length was decided upon because it only provided an acceptable velocity range, and best met the physical space requirements. Although the 4-foot barrel could provide an acceptable velocity range, a maximum barrel length was desired; somewhat lower pressures can be used in the 4.5-foot barrel to achieve the same projectile velocities which, in turn, reduce the amount of gas used and increase the safety. Coming as a consequence of the foregoing iterative process, a maximum breech pressure of 3000 psig was established. Even though this pressure pushes the projectile velocity predictions above that which is required, it provides flexibility for both the current research work and future endeavors.

With the maximum breech pressure of 3000 psig determined, it is now possible to calculate the principal stresses in the barrel and evaluate whether the barrel remains in an elastic or a plastic state during firing. The following system parameters are known with the symbols used having been previously defined:

$$P_{max} = 3000 \text{ psig}, \quad a = 3.059 \text{ inches}, \quad b = 3.875 \text{ inches}$$
$$t = 0.816 \text{ inches}, \quad S_y = 70{,}000 \text{ psi}$$

The principal stresses, σ_1 and σ_3, are calculated using Equations (19) and (21) in Section III and $\sigma_2 = \sigma_a = 0$. Substituting in the above parameters yields:

$$\sigma_1 = 4.308 * P_{max}$$
$$\sigma_2 = 0$$
$$\sigma_3 = -P_{max} \qquad \text{(A-1)}$$

Using first, the conservative maximum-shear-stress theory, a factor of safety against yielding by Equation (22) in Section III gives:

$$n = 4.396 \text{ at } P_{max} = 3000 \text{ psig} \qquad \text{(A-2)}$$

Second, the equivalent stress, σ', is calculated by Equation (23) in Section III, to be:

$$\sigma' = (23.867*P2_{max})1/2 = 4.885*P_{max} = 14,655 \text{ psi} \quad \text{(A-3)}$$

Therefore, the distortion-energy theory yields a factor of safety given by Equation (24) in Section III:

$$n = 4.777 \text{ at } P_{max} = 3000 \text{ psig} \quad \text{(A-4)}$$

Obviously, by both theories, the barrel material remains in an elastic state. These high factors of safety are a result of the heavy-walled tubing used to make the barrel. The larger than necessary tubing was used as it had the smallest outside diameter, with a 6-inch inside diameter, in available stock.

The gas reservoir or breech consists of three major components: (1) flow plate, (2) breech tube, and (3) back plate which is shown in figures A-7 and A-8. Of primary concern is the breech tube, which represents the major portion of the breech responsible for containing the high pressure gas. As a result of the discussion on breech chambrage and maintaining as high an average base pressure as possible on the projectile, a 12-inch diameter breech was chosen. This choice results in a breech diameter-to-barrel diameter ratio of two and therefore, more reliable performance than would be expected at a ratio of one. Referring back to the computer program mentioned in the previous section, the length of the breech was chosen after setting the breech diameter. Taking both the velocity requirements and limited space restrictions into consideration, the breech length was set at 18 inches. The breech volume capacity is 1.18 cubic feet of gas. The breech tube, constructed from 1026 steel tubing, has a 12-inch inside diameter and a 13.5 inch outside diameter.

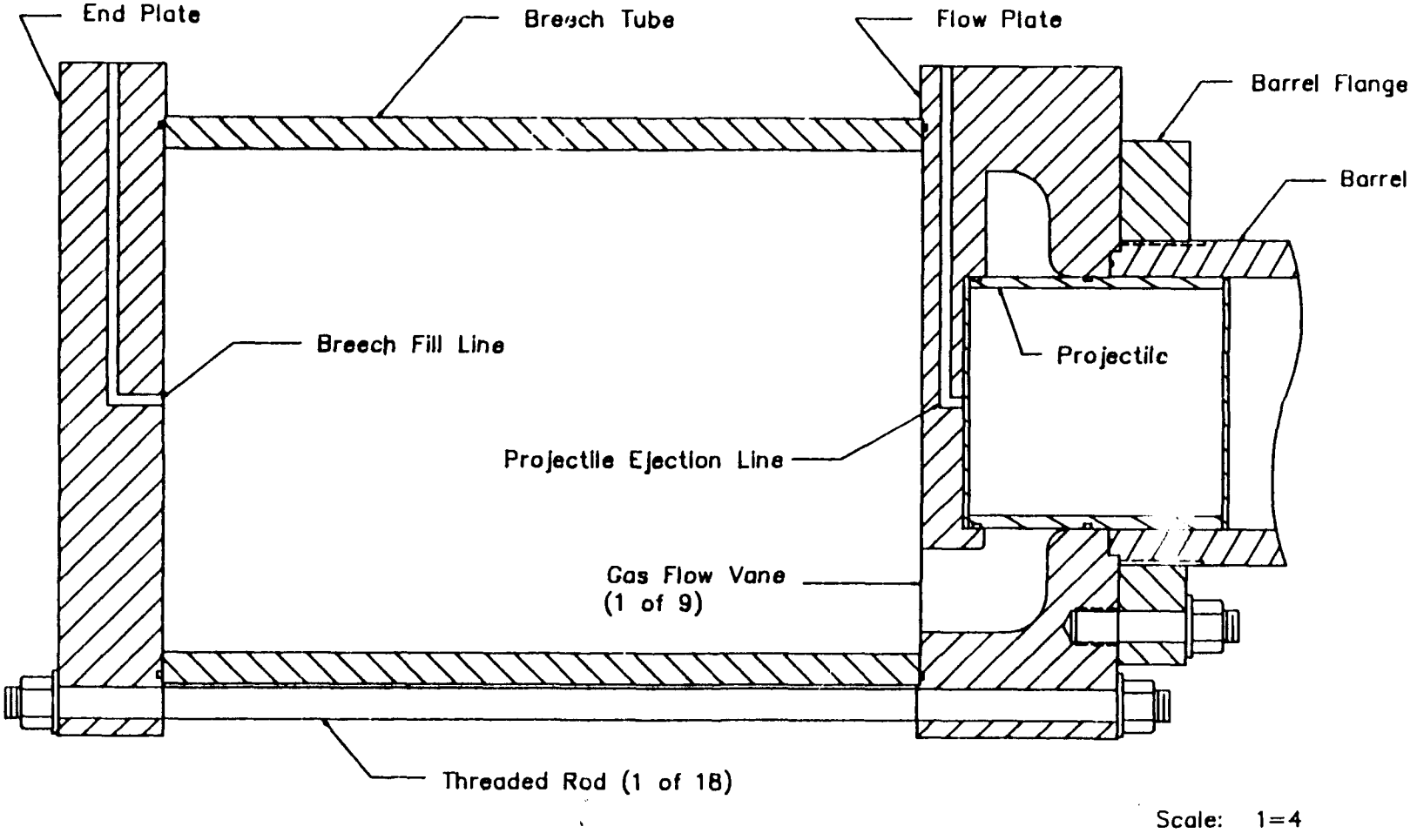

Figure A-7. View of Breech Assembly with Projectile in Place (Wrap-around Concept).

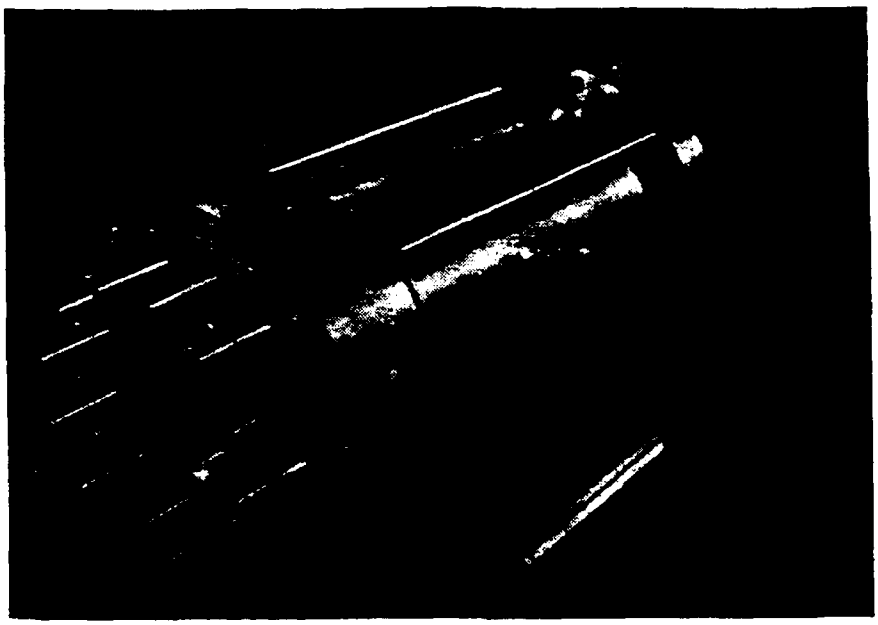

(a) Unassembled breech.

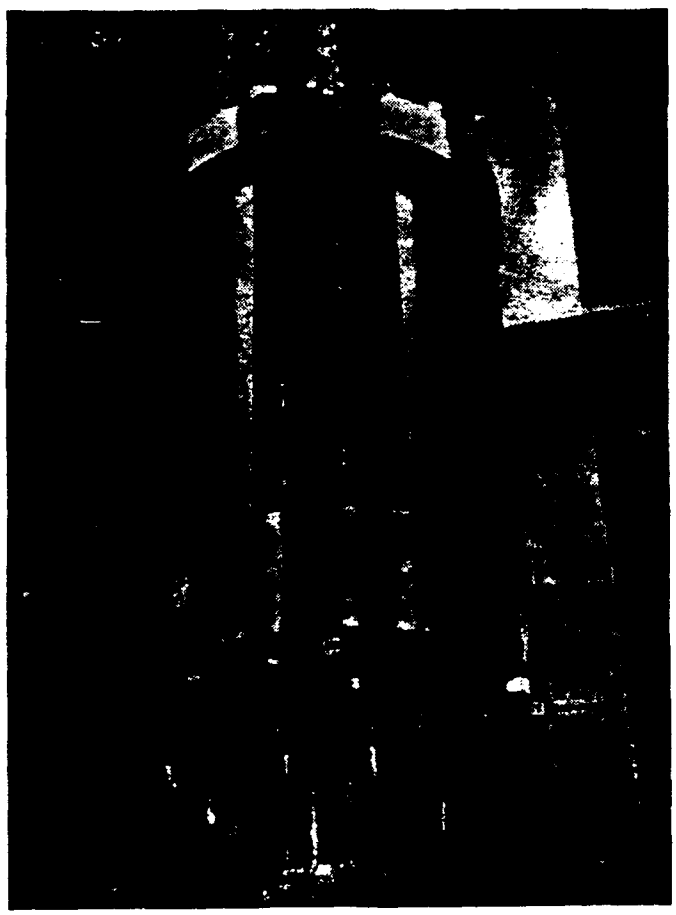

(b) Assembled breech.

Figure A-8. Breech Assembly.

With the breech tube dimensions and the maximum breech pressure set, the principal stresses in the tube can be calculated and the tube evaluated to determine whether it remains in an elastic or plastic state when under pressure. The known parameters are:

$$P_{max} = 3000 \text{ psig, } a = 6.00 \text{ inches, } b = 6.75 \text{ inches}$$
$$t = 0.75 \text{ inches, } Sy = 47{,}000 \text{ psi}$$

The principal stresses are calculated using Equations (19), (20), and (21) again in Section III. Substituting the above parameters produces:

$$\sigma_1 = 8.529 * P_{max}$$
$$\sigma_2 = 4. - 1000 * P_{max}$$
$$\sigma_3 = -P_{max} \qquad \text{(A-5)}$$

A factor of safety against yielding by the maximum-shear-stress theory is found by using Equation (22) in Section III:

$$n = 1.64 \text{ at } P_{max} = 3000 \text{ psig} \qquad \text{(A-6)}$$

The equivalent stress, σ', by Equation (23) in Section III, for the distortion-energy theory is:

$$\sigma' = (68.157 * P2_{max})1/2 = 8.256 * P_{max} = 24{,}767 \text{ psi} \qquad \text{(A-7)}$$

Therefore, by the distortion-energy theory, the factor of safety against yielding by Equation (24) in Section III is:

$$n = 1.90 \text{ at } P_{max} = 3000 \text{ psig} \qquad \text{(A-8)}$$

Again, both theories predict the tube remains in an elastic state. However, to assure safety and to protect the integrity of the breech tube, it absolutely should not be operated above a pressure of 3000 psig (also, flexible metal hoses which supply the breech with gas are only rated up to a working pressure of 3000 psig). A finite life for the breech tube was

established by standard finite-life equations in Reference A.3. For the breech described above, operating repeatedly under maximum load (fatigue strength taken to be equal to the maximum principal stress in the tube), a finite-life of 81,345 cycles would be expected (of course, the gun is not always operated at maximum conditions so this finite-life is conservative).

The basic breech design concept used for this facility, called a wrap-around breech, was used on a 2-inch diameter gun, which is already in place in the NCSU Shock Lab, and has proven itself to be a reliable means of gas containment and projectile firing. Serving as the front plate of the breech, the flow plate was designed to provide the "wrap-around" concept (see Figures A-9 and A-10). In the wrap-around design, the projectile serves as the gas release valve, thus eliminating the need for fast-opening valves which have a tendency to be inconsistent in their response (refer back to Figures A-7 and A-8). The projectile is seated in the flow plate such that the annular gas port surrounding the projectile periphery is sealed from the barrel by the projectile O-rings. Upon breech pressurization, the projectile remains in its initial seated position as it only experiences lateral pressure. Firing is effected by injecting a small amount of high-pressure gas behind the projectile which nudges it forward until the annular gas port is uncovered which, in turn, releases the gas stored in the breech reservoir. The only disadvantage of the wrap-around breech is the restriction on the projectile weight imposed by the requirement of sufficient strength to withstand the initial lateral pressure.

The cross-sectional area of the annular gas port and the total cross-sectional area of the nine gas inlet holes in the flow plate are equal to the cross-sectional area of the barrel to help promote unrestricted flow. Additionally, the annular gas port has rounded corners, as do the gas inlet holes, to reduce the effects of turbulent flow at sharp turns. A flow path for the gas, as smooth as possible, was machined to encourage maximum gas volume transfer from the breech with minimum disturbance.

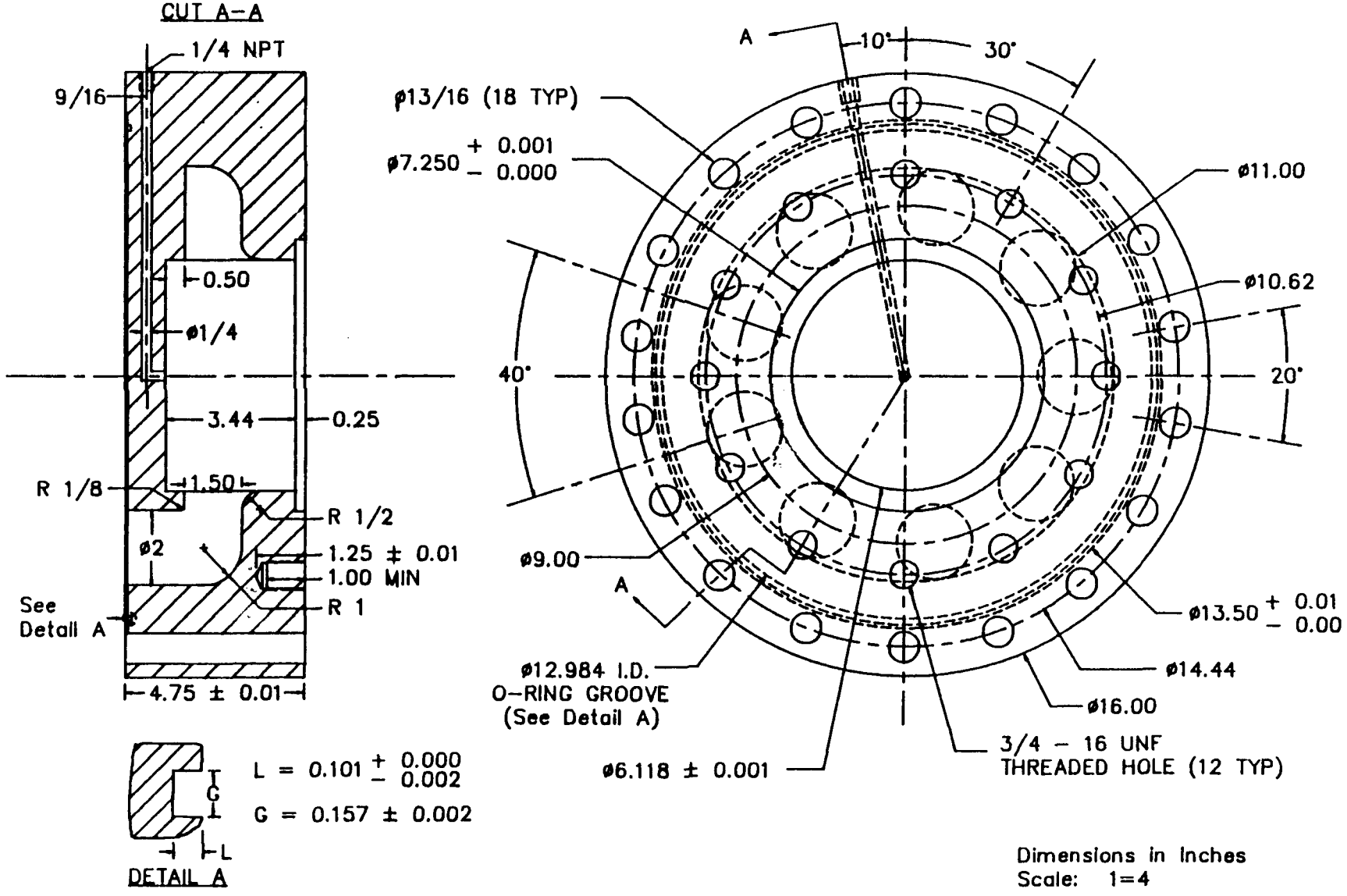

Figure A-9. View of Flow Plate.

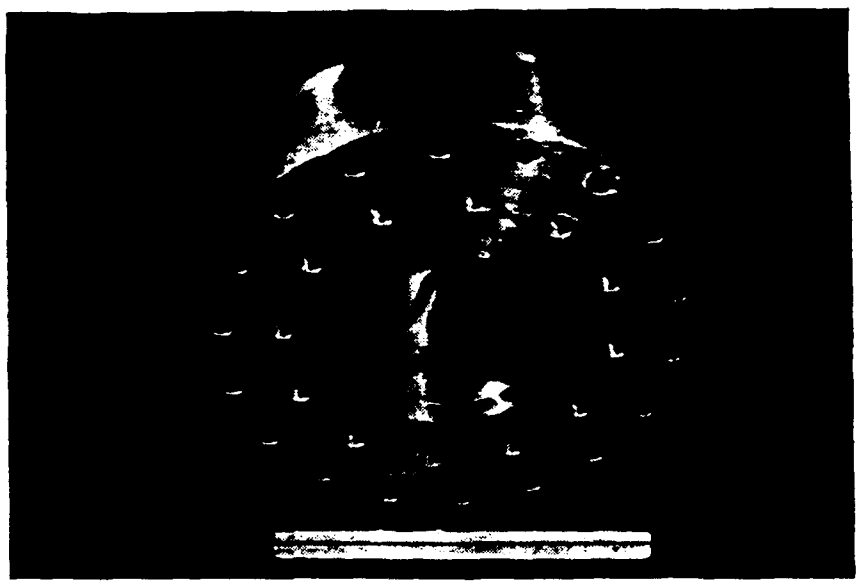

(a) Front view.

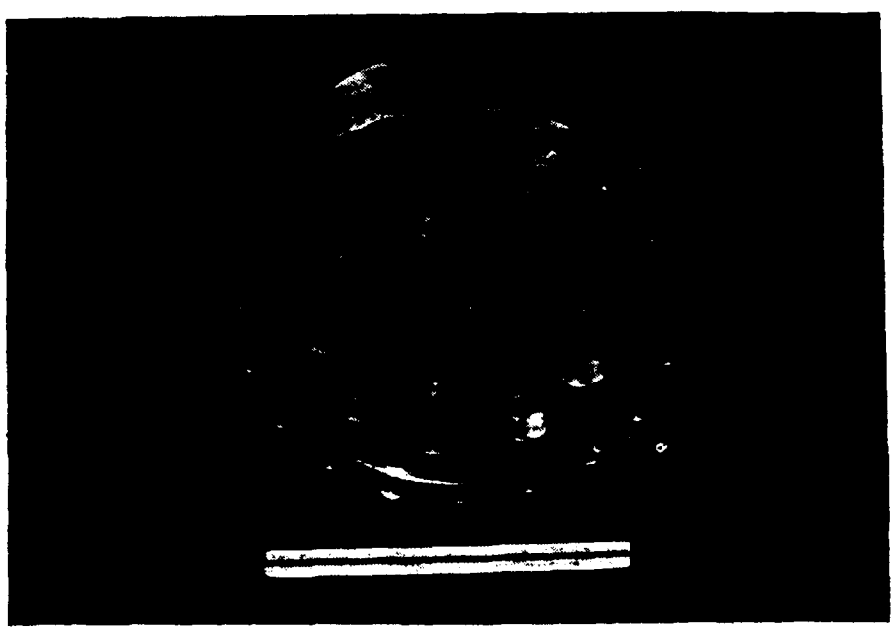

(b) Back view.

Figure A-10. Flow Plate.

Both the flow plate and end plate thicknesses were determined by engineering equations for solid plates in bending given in reference A.2, using a factor of safety against failure by a yielding of 2. These plates were machined from A-36 HR steel plate to a diameter of 16 inches. This diameter was needed to provide enough flange width on the plates to install threaded rods which are used to hold the entire breech assembly together. The flow plate was checked for shear between the gas inlet holes, at maximum pressure, and was found to have a factor of safety against shear in excess of 3.

Eighteen high-strength, SAE B-7, 3/4 inch-16 UNF threaded rods were used to assemble the breech. A tensile test on a representative rod was performed to verify the properties and integrity of the rods. This test indicated that the rods should not be subjected to a load exceeding 26,000 pounds, corresponding to a breech pressure of 4100 psi, to maintain a factor of safety of 1.5. A finite-life of 5986 cycles was calculated for the threaded rods operating continuously at maximum load conditions. Therefore, these rods should be replaced, for safety purposes, after the facility has been fired 5500 times. The assembled breech was hydraulically pressure tested to 3500 psi with a minute leak observed at the projectile/annular gas port interface. Otherwise, the breech was pressure-tight.

Twelve high-strength, SAE B-7, 3/4 inch-16 UNF threaded studs were used to connect the barrel to the breech. If this connection was disassembled every firing of the gun to load the projectile the studs would not be expected to fail. In fact, a plot against a Modified Goodman Line indicated a factor of safety against fatigue failure of 2.62. Additionally, a finite life in excess of 2.5 million cycles was calculated for the 12 threaded studs undergoing repeated assembly and disassembly.

The impact area is located at the muzzle end of the barrel inside the catcher chamber. The catcher chamber serves a dual role as both the target/impact chamber and the catcher/gas expansion chamber. Barrel Section 3 extends down through the mounting plate, sealed vacuum tight by two O-rings on the barrel, into the target area, as in Figure A-11. A target 11

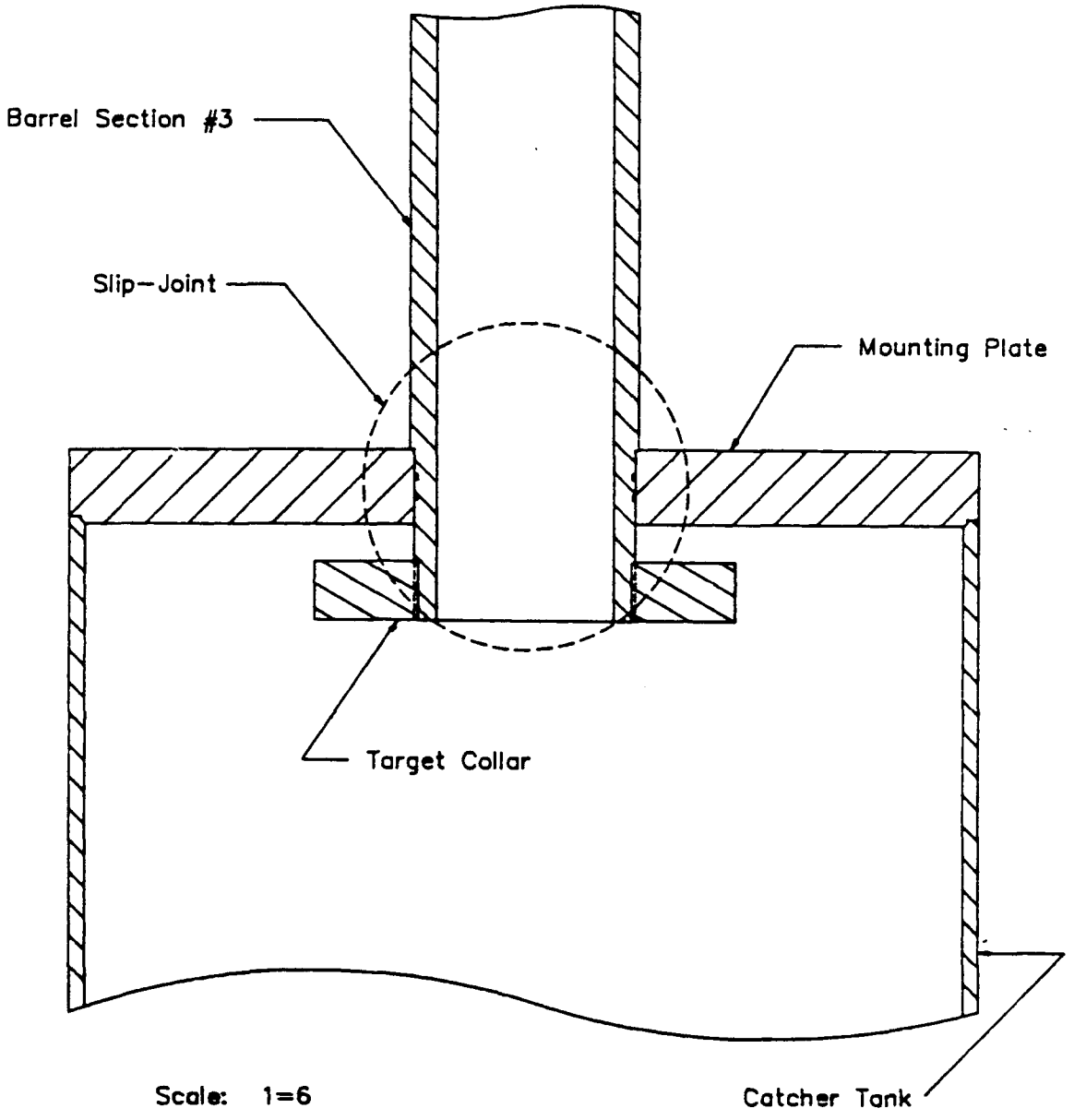

Figure A-11. View of Barrell Slip-joint in Mounting Plate.

plate threads onto the end of the barrel to a positive stop (see Figure A-11; see target plate on the bottom of the assembled barrel, Figure A-6). This assembly, of Barrel Section 3 and target collar, was machined simultaneously to provide a very flat reference surface between the projectile and target. The target collar was fabricated from A-36 HR steel plate with a 14 inch outside diameter and a 2 inch thickness.

The impact area has a diameter limited only by the inside diameter of the catcher chamber, 29.87 inches. Therefore, there is ample room for targets as large as 2 feet in diameter. Also, when final dimensions were set for each part of the facility, a maximum 1-foot target thickness was calculated into the final assembled height of 10+ feet. Although the gun is located in an 11+ foot area, the extra foot is required for the target so it can be attached to the target collar and then lowered into the catcher by a 1-ton Coffing hoist (the hoist lifts the assembly, from breech to mounting plate, by an eyebolt threaded in the back plate of the breech).

The mounting plate, pictured in Figure A-12, was designed to provide a closed end for the catcher chamber, a resting surface for the barrel, and electrical ports for the experimental instrumentation. It was fabricated from A-36 HR steel plate with an outside diameter of 30.90 inches and a thickness of 2.5 inches. The thickness is sufficient to withstand the maximum expansion pressure experienced in the catcher chamber. The plate also has a recessed lip which fits down inside the catcher chamber to provide structural rigidity under vacuum and to serve as a guide for placing the mounting plate onto the chamber. A vacuum seal between the mounting plate and catcher chamber is accomplished by an O-ring located on the mounting plate at the interface of the two surfaces. A lip, machined on Barrel Section 3, rests directly on the mounting plate supporting the weight of the entire breech/barrel assembly. Eleven BNC-type electrical connectors are provided on the mounting plate for instrumentation hook-up between the target and appropriate equipment (counters, oscilloscopes, etc.).

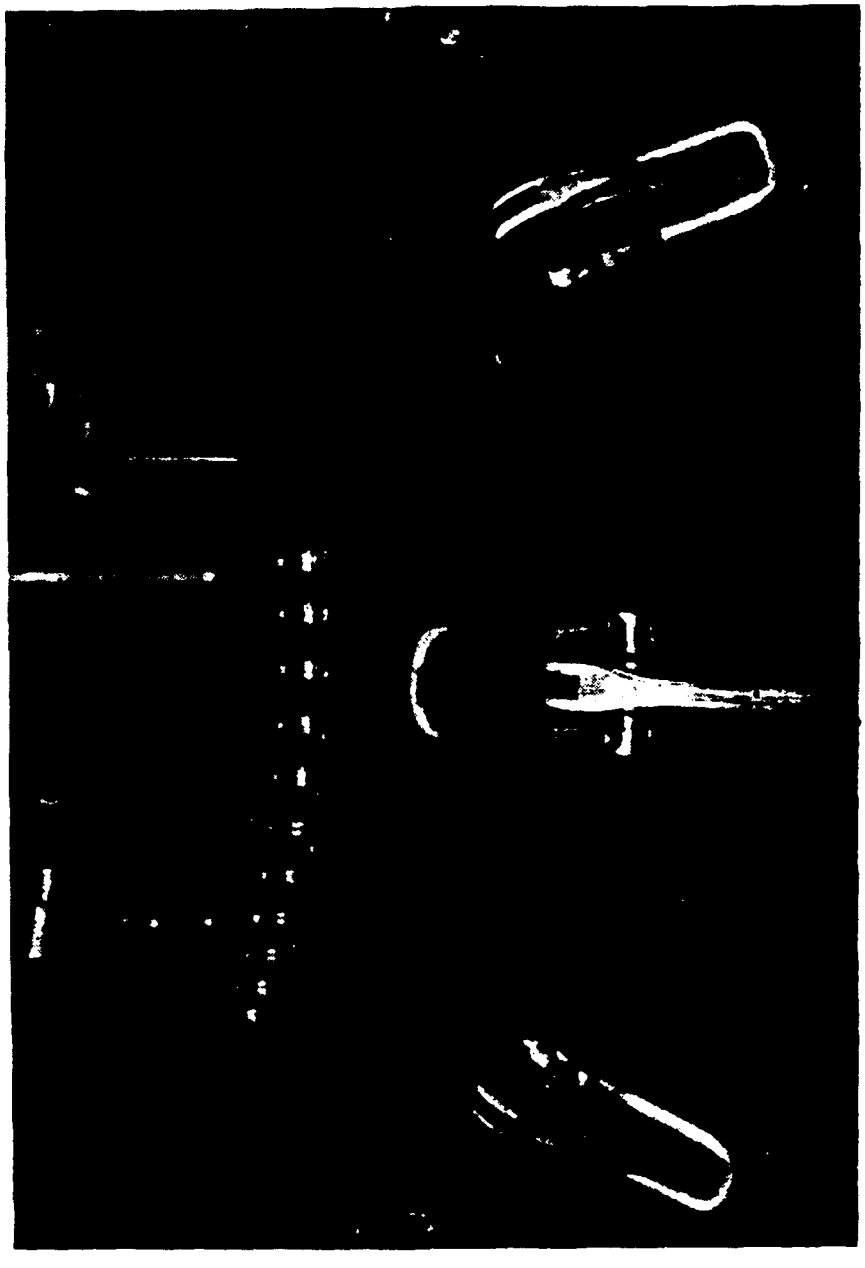

Figure A-12. Mounting Plate.

The catcher chamber was fabricated from a salvaged helium storage tank which was rated for maximum working pressure of 300 psi. Pictured in Figure A-13, the catcher has a wall thickness of 0.400 inches which, according to the tank rating and a check by the same equations used to determine the barrel and breech wall thicknesses, is more than sufficient to withstand the maximum expansion pressures (maximum predicted catcher pressure w 73 psig). Total expansion volume in the catcher is approximately 15 cubic feet which was set by the iteration on the barrel length, physical space restrictions, and projectile stopping distance. Total height of the catcher, including the flanged pedestal on which it rests, is 44 inches. The catcher is permanently attached to the concrete lab floor through the flange by eight 2 inch long, 5/8-inch diameter lag bolts. Quick-release toggle-action clamps are used to fasten the mounting plate to the catcher tank and to hold the mounting plate down when the force of the catcher pressure acts against it. Ten posi-power latch clamps with a load rating of 7500 pounds resisting force each are welded onto the periphery of the catcher. The ten latch plates are welded onto the mounting plate, shown in Figure A-12.

After the projectile impacts with the target the catcher chamber must be deep enough to provide adequate stopping distance for the projectile. Again, based on space restrictions, the catcher height was maximized with a resulting total stopping distance of 36 inches. The requirement for stopping of the projectile is dependent on the particular experimental goal. In a recovery shot the projectile needs to be stopped after the desired impact with the target occurs to prevent further damage to the target. In the case of a nonrecovery gaged shot the requirement is only that the projectile be stopped before impacting the bottom surface of the catcher. The current experimental program employs a 1.5-inch diameter nose protruding through the front plate of the 6-inch diameter projectile. The 6-inch projectile body is stripped away from the 1.5-inch nose by the stripping mechanism pictured in Figure A-14 (the stripper sits just above the target). The 1.5-inch nose passes through the middle of the stripper and impacts the target. Upon impact with the tripper, the 6-inch projectile is sheared into numerous pieces which fall to the bottom of the tank. A great deal of the projectile's kinetic energy is dissipated in the shearing process such that

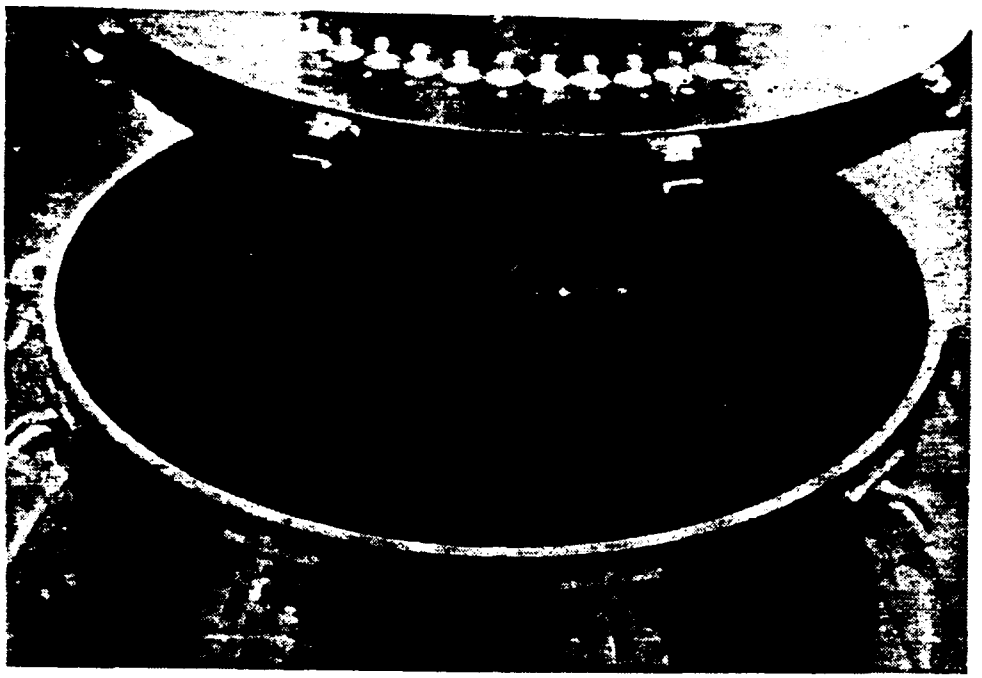

(a) Top view.

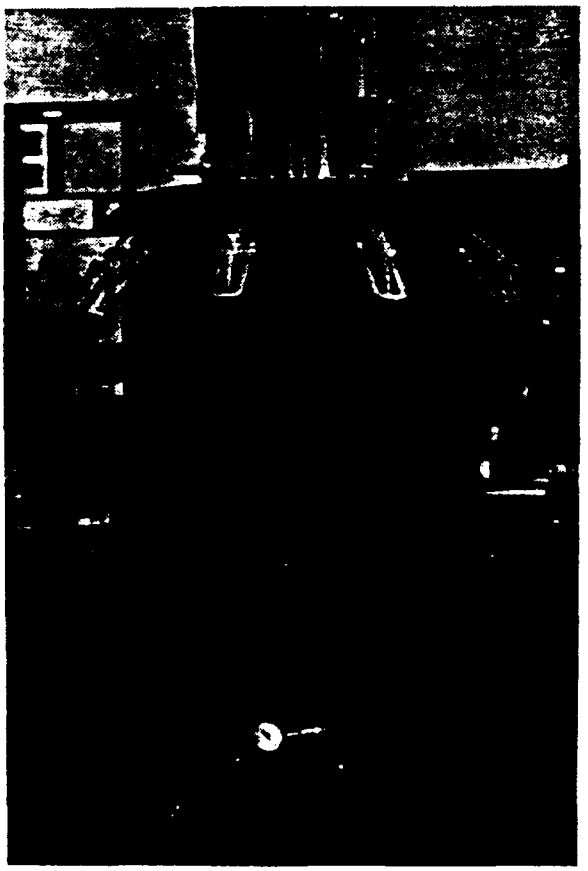

(b) Side view.

Figure A-13. Catcher Tank.

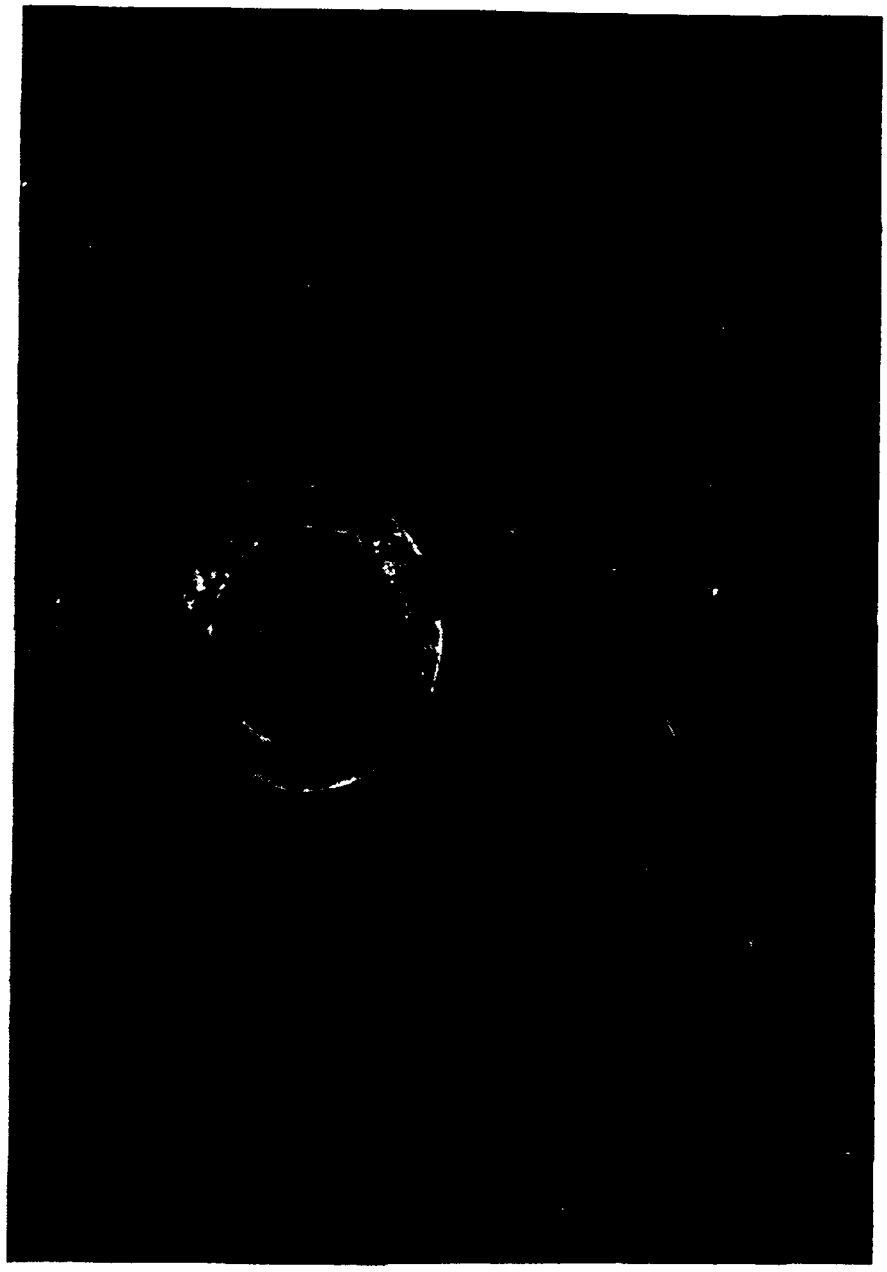

Figure A-14. Projectile Shell Stripping Mechanism.

there is no difficulty in stopping the small fragments. Once the 1.5-inch nose has impacted the target, it either penetrates the target and its motion is stopped or it bounces off the target and falls to the bottom of the tank. However, future experiments may require that the entire 6-inch diameter projectile impact the target. Methods for stopping the projectile which were tried in preliminary test shots and other possibilities for absorbing the projectile's kinetic energy are listed below:

1. Multiple layering of plywood sheets (1/2" to 1" thickness).
2. Alternating layers of aluminum or soft steel plates (1/4"thickness) and plywood sheets (1/4" to 1" thickness).
3. Deformable material such as parachute cloth or tightly packed rags, discarded computer paper, or a combination of these materials to encourage soft recovery.
4. Identical target to projectile (i.e., same mass) which upon impact reduces the kinetic energy to one half of its initial value, followed by another equal mass if necessary and then into deformable material as above.
(5) Filling of catcher with hydraulic oil or other viscous medium. A reduction in the projectile's kinetic energy can be effected by weight minimization through shorter length projectiles, reduced wall thicknesses, and varied material choices which, in turn, reduces the kinetic energy absorbing requirements of the catcher.

Projectile velocity is measured just before impact with the target by measuring the time interval between electrical signals generated by contact of the projectile face with a set of pins held in a velocity pin block, Figure A-15. The velocity pin block is attached directly to the target collar. The front pair of pins starts a set of counters and the second pair stops the counters. The velocity pins are made from 24-gage copper wire which is cut to the proper length and bent slightly so that the rounded tip of the wire strikes the projectile first. The two pairs of pins are spaced approximately 1 inch apart, and the precise separation is measured with an optical comparator (Photoelastic, Inc., Model 051) to an accuracy of ± 0.09 percent.

Figure A-15. Velocity Pin Block.

Each pair of pins terminates on a BNC connector; each BNC jack is connected by matched 8-foot coaxial cables (RG 58/U) to a Triune counter which records the time interval between pin contact. The overall counter accuracy has been calculated to be + 0.25 percent. A back-up counter, Fluke Model 7261A, is used in addition to the Triune counter to provide an alternate reading should the Triune malfunction. The total accuracy, as shown in Reference A.4, of the velocity measurements is better than ± 0.4 percent. Therefore, by accurately measuring pin spacing and by counting times between pin contacts, the projectile velocity can be readily determined.

The vacuum system for the gun is divided into three parts: (1) the region immediately behind the projectile, (2) the region between the projectile and the target (barrel assembly), and (3) the region inside the catcher chamber. A vacuum is drawn behind the projectile as the initial vacuuming procedure to seat the projectile in the breech. Vacuuming is accomplished through the same port used to inject the high pressure gas behind the projectile when firing. A Model 1400, Sargent Welch Duo-Seal vacuum pump is used to produce a vacuum, behind the projectile, of approximately 5 microns (pump capability as checked by a McLeod Gage). To protect the pump from the high-pressure gas, a mechanically actuated, Hoke Rotoball Valve, is closed just before breech pressurization. Also, to protect the pump in the event of an accidental pressure release, a check valve is located in the line between the valve and the pump.

After a satisfactory vacuum is achieved behind the projectile, the in-barrel vacuum is drawn through a fitting in the barrel wall using a Model 1402, Sargent Welch Duo-Seal vacuum pump. This in-barrel vacuum helps reduce the effect of air shocks on the instrumentation and also reduces the resisting force to the projectile's forward acceleration (i.e., this vacuum eliminates the air cushion between the front of the projectile and the target). The in-barrel vacuum level, verified by a McLeod Gage (Gilmont, Model S-39820), was found to be typically 5 microns or less. An O-ring, located on the target end of the barrel, helps provide a good seal between the barrel and the target. A thermocouple gage (Veeco, Type DV-1M) is used

to measure the barrel vacuum and monitor it throughout the firing sequence. The thermocouple gage is protected from pressure damage by a Circle Seal Gage Protector (Model 1159B-2PP-15). The pump is also protected from the high-pressure gas by a mechanically actuated Hoke Rotoball Valve which is closed just prior to breech pressurization.

The catcher chamber vacuum is drawn lastly through a fitting in the chamber wall using a Model 1397, Sargent Welch Duo-Seal vacuum pump. An electrical solenoid valve, closed just prior to breech pressurization, protects the pump from high pressure pulses. Typically, a vacuum of approximately 30 inches Hg is achieved and it is monitored by a Pacific Scientific Dial Pressure Gage; this gage also indicates the maximum pressure experienced in the catcher chamber after firing. The catcher vacuum not only provides more room for gas expansion but also reduces the impact noise.

The exhaust system for the gun facility is rather simple but effective. Propellant gas exits the catcher chamber by first rupturing a Mylar diaphragm (0.003 inches thick) and then expanding further as it vents to atmosphere through a 4-inch diameter PVC pipe. A muffler, attached to the end of the PVC piping and located outside the laboratory walls, reduces the noise produced by gas expansion.

Just as a rifle recoils when fired, in a like manner the breech/barrel assembly reacts when fired. The shock absorbing or recoil damping system was designed to connect the stationary mounting plate (when clamped for firing) to the breech/barrel assembly through velocity sensitive shock absorbers. Pictured in Figure A-16, the shock-absorbing mechanism employs four Monroe, Model 74400, heavy-duty shock absorbers attached at one end by a collar around Barrel Section 1 and at the other end to the mounting plate by high-strength threaded rods. The shock absorbers have a travel capacity of 8 inches, but only 1.25 inches maximum recoil distance is allowed, since that is the distance between the mounting plate and target plate. From information supplied by Monroe, a curve of rebound force versus velocity was plotted and used to predict the stopping distance of the recoiling body.

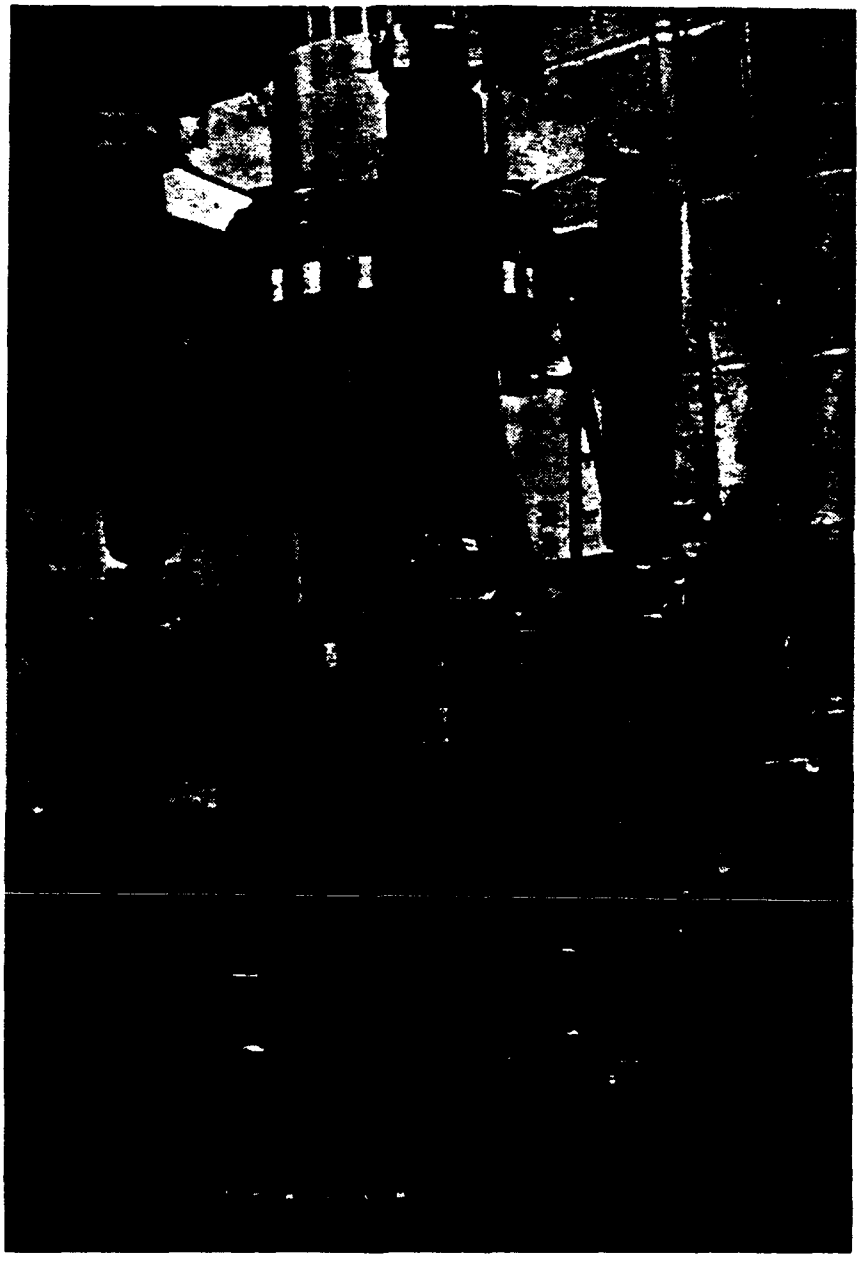

Figure A-16. Shock Absorber Assembly.

The recoil damping mechanism was designed for the worst conditions anticipated, i.e., a projectile of maximum mass propelled at the maximum anticipated velocity with a conservative maximum shock absorber rebounding force assumed. The shock absorber reaction was taken as starting when the projectile reaches the end of the barrel. This effectively means that an instantaneous velocity is imparted to the barrel. However, the shock absorbers begin to work at the first hint of motion. Therefore, the assumption of an instantaneous velocity produces a predicted stopping distance greater than actually expected and a margin of safety. The velocity of the barrel was calculated by applying conservation of momentum to the breech/barrel assembly and the projectile (effects of friction not considered as they also add a margin of safety). The velocity of the barrel given by:

$$V_b = \frac{M_p V_p}{M_b} \qquad \text{(A-9)}$$

where V_b is the breech/barrel velocity, m_b is the breech/barrel mass, m_p the projectile mass, and V_p is the projectile velocity. With the following parameters set, the maximum velocity, Vb, can be calculated.

Breech/barrel assembly weight = 1300 lb
Maximum projectile weight = 6 lb
Maximum projectile velocity = 1150 ft/sec

Therefore, the maximum expected breech/barrel velocity is 5.31 ft/sec. This value, as well as the associated recoil energy, will be reduced as the projectile mass is reduced.

The velocity and mass of the breech/barrel assembly was used to calculate the recoil energy of this assembly as follows:

Recoil energy = $1/2(1300/32.2)(5.31)^2$ = 569 ft-lb

As the forces in the shock absorbers change with velocity, the reduction in the recoil energy by the four shock absorbers was checked incrementally to ensure that the appropriate force/velocity relationship was applied. This iterative process in the reduction of the recoil energy was performed by a computer program and the total energy was dissipated between 0.8 and 0.9 inches of motion. Therefore, the maximum recoil energy is expected to be absorbed in less than 1 inch of travel. In the experiments conducted to date, no recoil motion has been observed indicating a great deal of frictional force is present which prohibits the motion. Recoil damping does not appear to pose any problems.

The control panel, which operates the gas and vacuum system for the gun, is shown in Figure A-17. All vacuum valves, vacuum pumps, and gas supply lines acting on the facility when fired are remotely activated from this control panel. Therefore, it is not necessary for the operator to be physically at the gun during a test. The panel has red and green lights associated with each electrical switch which controls valves and pumps; all lights must be green before firing. Control valves are also installed on the panel for an emergency system dump if required. In short, the control panel contains the valves and electrical switches needed to evacuate the system, pressurize the breech, and fire the projectile.

Projectile design is an important consideration for predictable and successful experiments. Proper projectile design is necessary to ensure proper operation of the wrap-around breech and to maintain acceptable tilt control. After a few design prospects were tried, two standard designs were selected: one for lower pressure shots, Figure A-18, and one for higher pressure shots, Figure A-19. Two projectile wall thicknesses were chosen to withstand lateral pressures up to (1) 1500 psig with a factor of safety of 1.8 against yielding for the low pressure projectile, and (2) 3000 psig with a factor of safety of 1.5 against yielding for the high pressure projectile. The front portion of the projectile wall, for both designs, was thinned to remove excess weight. O-rings, used on the projectile to prohibit the propelling gas from bypassing the projectile upon firing, are located so as

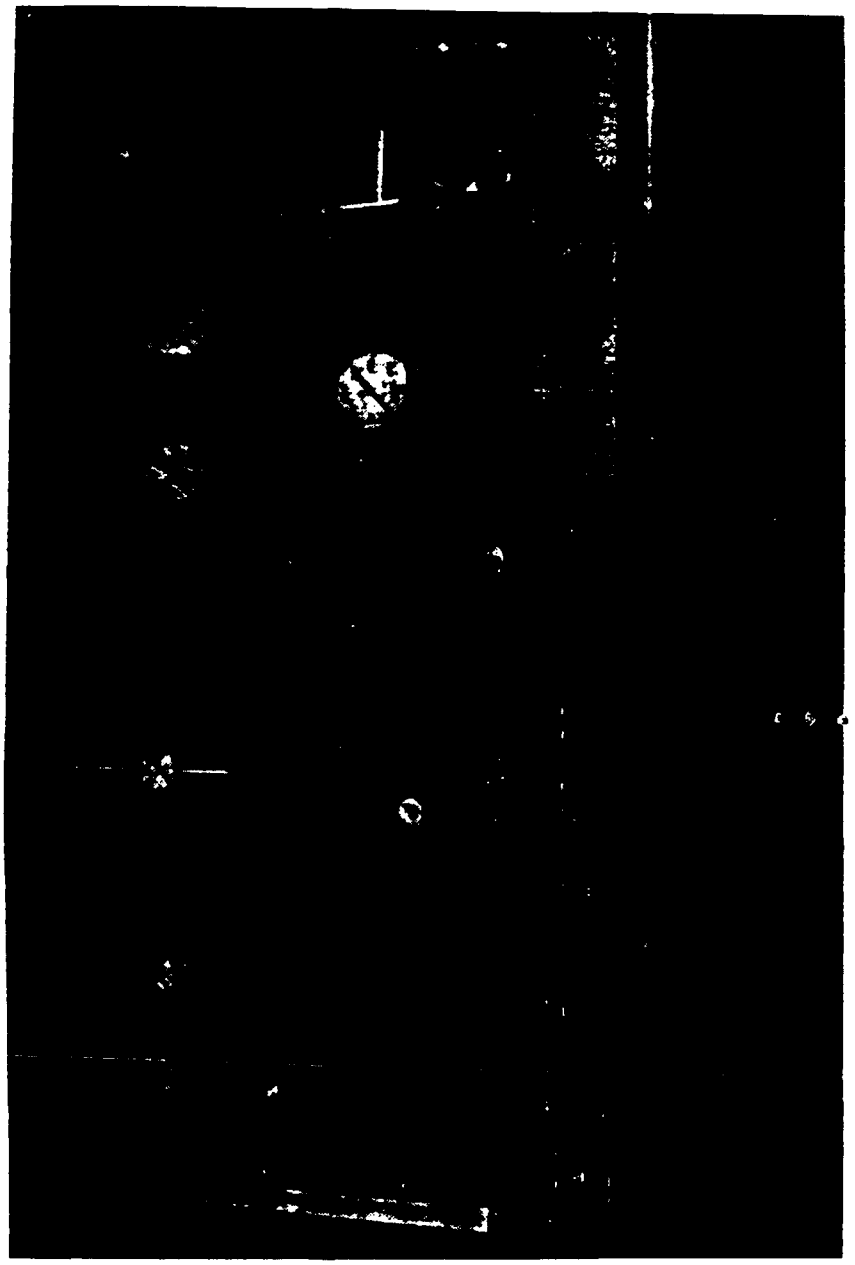

Figure A-17. Control Panel.

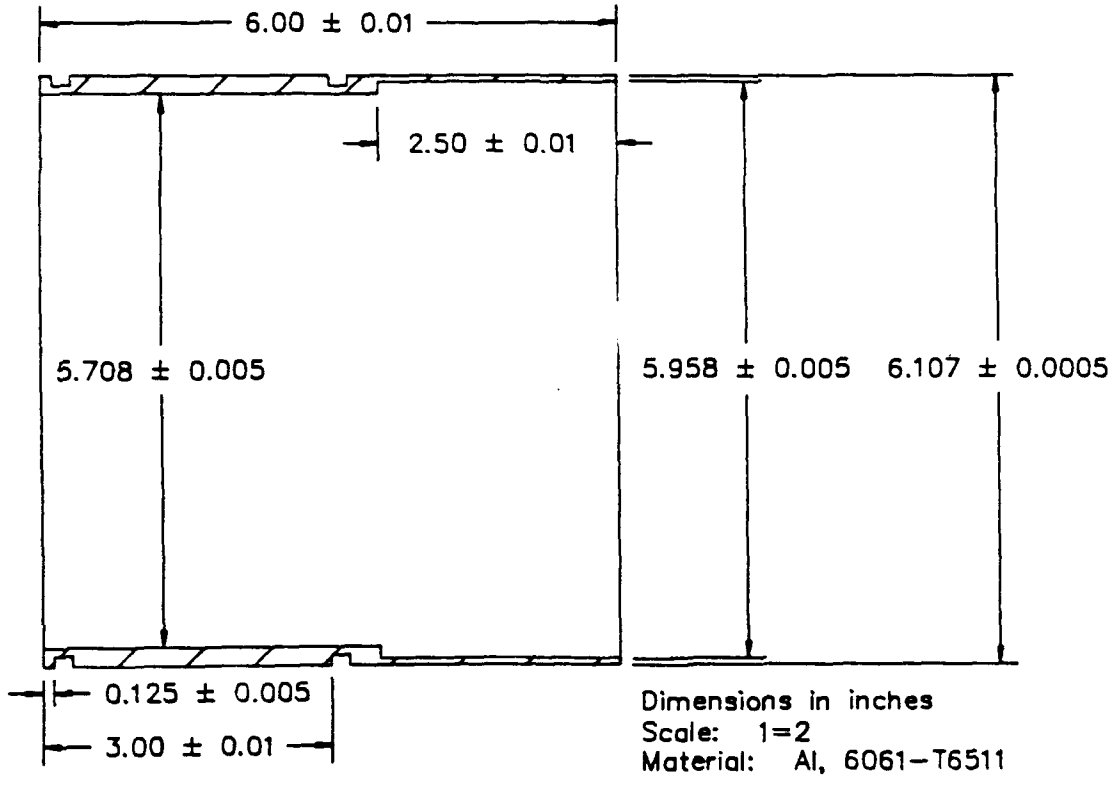

Figure A-18. View of Low Pressure (Below 1500 psi) Projectile Shell.

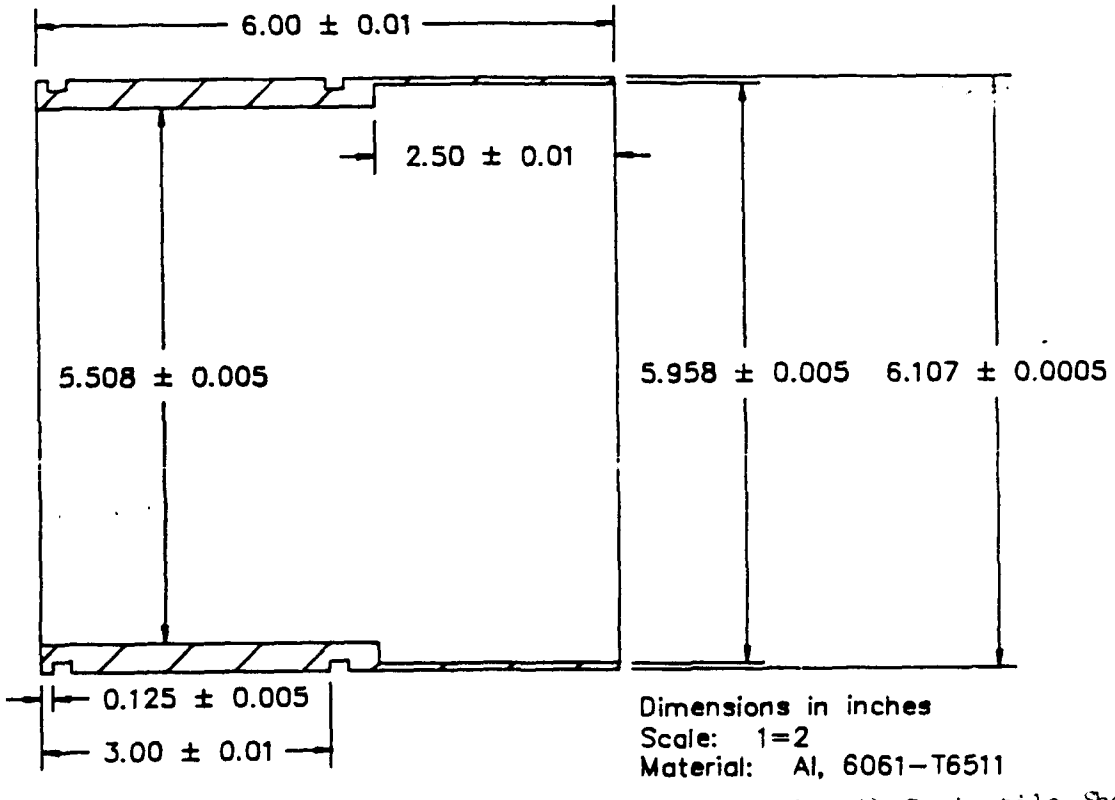

Figure A-19. View of High Pressure (1500 to 3000 psi) Projectile Shell.

to seal the gas at both ends of the annular gas port from the barrel. These O-rings are rated at 3000 psig maximum but, as indicated in Reference A.4, for non-rotary motion they have been found to be reliable up to 4200 psi.

Projectile length was determined as a compromise between keeping the projectile weight to a minimum and allowing sufficient length for tilt control. The projectile shell, pictured in Figure A-20, typical of both high and low pressure shells, has a length-to-diameter ratio of one which allows a maximum angular rotation of 0.005 inches. Therefore, the contribution to tilt from the allowed clearance between the projectile and barrel at this length-to-diameter ratio is approximately 0.83 mrad. Improvements in tilt, if demanded by experimental constraints, can probably be achieved with tighter fitting or longer projectiles. The projectile shell must also have a front and back plate before firing, but these are dependent again on the experimental constraints. A 0.25-inch thick aluminum back plate has been employed for all shots to date. Front plate material and thickness are dependent upon the goal of each particular experiment. The front plate should be ground flat and perpendicular to the projectile shell, to minimize its contribution to tilt.

B. SIX-INCH GUN OPERATION

Firing of the gun system must be accomplished through careful preparation and execution. This facility should always be approached and used with a great deal of respect for its energy producing capability; therefore, any operator must be totally familiar with the proper operation of the entire system. A "Firing Procedure" is presented below and must be completely read and understood before attempting to fire the gun.

1. Pretest Checklist

a. Ensure that all gas cylinders are valved off at the cylinder.
b. Ensure that the control panel main power is in the off position and that all toggle switches are in the down (remotely operated valves open) or off (pumps off) position.

(a) Projectile shell.

(b) Projectile shell with end plates.

Figure A-20. Projectile.

c. Close all valves on the control panel (Valves 1-10).

d. Ensure that all vacuum hoses are properly secured.

e. Check all electrical connections to assure they are in the proper outlet on the labeled outlet box.

f. Ensure that the quick-disconnect hoses to the breech and flow plate are properly connected.

2. Test Setup

a. Unclamp the mounting plate from the catcher tank and raise the gun assembly and mounting plate with the 1-ton electric hoist. This assembly may be moved away from the catcher tank if necessary.

b. Load the projectile from the muzzle end of the barrel using a ramrod of known length, ensuring that the rear of the projectile is completely inserted into the flow plate (verify by marking and measuring the ramrod).

c. Attach the target to the target collar.

d. Place the gun assembly back over the catcher tank and lower in place making sure the mounting plate O-ring seats properly and that the arrows scribed on the plate and tank are aligned.

e. Securely clamp the mounting plate to the catcher tank.

f. Hookup all instruments needed for the test and recheck all electrical connections and vacuum hoses.

g. Ensure that the shock absorbers are in the fully compressed position.

3. Vacuum Sequence

a. Turn on control panel main power. All indicator lights should be red (all remotely operated valves are open when red light indicators are on).

b. Start breech vacuum pump and let it run until the vacuum pump has a sound change (indicating vacuum has been achieved).

c. Start barrel vacuum pump and let it run until a satisfactory vacuum reading is achieved on the thermocouple gage before beginning the next step.

c. Start catcher vacuum pump and allow it to run until the tank gage indicates 20 inches of Hg vacuum or better before proceeding to the Firing Procedure.

4. Firing Sequence

a. Hang warning signs and lock both laboratory doors. Notify main office of imminent shot if necessary.

b. Ensuring that control panel Valves 1-5 are closed, fully open all gas cylinders to be used. The cylinder gages on the control panel should be registering the pressure in each open cylinder.

c. Open Valve 7 to access the 0-3000 psi breech pressure gage.

d. Check instruments and vacuum levels. If vacuum is acceptable, close the catcher valve, barrel valve, and breech valve and leave all pumps running.

e. All indicator lights should be green at this point.

f. Making sure that the main regulator (Valve 5) knob is in the fully decreased position, begin the fill procedure by first opening the shutoff valve located under the control panel on the regulator.

g. Open the desired cylinder valve (1,2,3, or 4) according to the pressure required for the experiment. The regulator inlet pressure gage should agree with the cylinder pressure.

h. Open breech fill Valve 6 and pressurize the breech using the regulator increase knob while observing the thermocouple gage for O-ring leakage. If sustained leakage is sensed by the gage, see Part E, Abort Procedure.

i. If an EMERGENCY DUMP is required, IMMEDIATELY CLOSE THE PRESSURE REGULATOR (VALVE 5) and see Part E, Emergency Dump.

j. Continue breech pressurization until the pressure in the breech is equal to the cylinder pressure or is equal to the pressure needed. If the breech pressure is greater than needed, see Part F.

k. If the cylinder cannot supply the needed pressure, close the valve on the cylinder that is open and open the valve for the cylinder with a pressure greater than the previously achieved breech pressure.

l. Increase the regulator pressure until the needed pressure is reached.

m. Repeat steps 10 and 11 with other cylinders if necessary.

n. When the desired breech pressure is achieved, close Valve #6 and Valve #5 (regulator).

o. Quickly open Valve #9 which will launch the projectile.

p. Close Valve #9, then close Valves #1-4.

q. See Part G for purging entire system after successful firing.

5. Emergency Dump and Abort Procedure

An emergency dump may be required if a misfire occurs, if gas leakage from the breech is detected, or if some component of the gun fails to function properly. Of course, other experimental circumstances may require an emergency dump. Sound engineering judgment should be exercised in evaluating unusual or potentially dangerous experimental conditions.

a. Emergency Dump

(1) Valve 5 should already be closed.

(2) Immediately open Valve 8 followed by Valves 6,9, and 10 to begin dumping to the atmosphere.

(3) Close Valves 1-4.

(4) When gas has been dumped, go to Part G for system purge.

b. Abort Procedure

(1) Close Valves 1-5.

(2) Open Valve 8 to dump gas to the atmosphere.

(3) See Part G for system purge.

6. Breech Pressure Reduction

a. Close Valve 6.

b. Crack open Valve 8 to vent some gas to the atmosphere until the desired breech pressure is achieved.

c. Close Valve 8 and continue with the Firing Sequence.

7. System Purce

a. Close gas cylinder valves at the cylinder.

b. Open Valves 8 and 10.

c. Open Valves 5,6, and 9.

d. Open Valves 1-4 one at a time.

e. All gas should now be out of the system and Valves 1-10 should be closed as well as the shutoff valve on the pressure regulator.

f. All panel toggle switches should be positioned for all red indicator lights.

g. Turn off control panel main power.

Proper care of this experimental facility includes cleanup and maintenance of the system after firing. A "Cleaning Procedure" is presented below.

After a firing of the facility is complete and the proper steps have been taken to purge the system of any gas and to shut off all valves and electrical operations, the facility must be cleaned. The best procedure to adopt is one in which the cleanup comes immediately after the experiment is completed. Use the following steps as guidelines to this operation.

(1) Clean the barrel, using dry rags wrapped around the plunger, which was made especially for this use. (The plunger consists of a rod long enough to reach to the top of the barrel with a round plastic plate on the end somewhat smaller than the barrel ID.)

(2) After several passes using dry rags, make a couple of passes with rags dampened with isopropyl alcohol or some other nonabrasive cleaning fluid.

(3) If the barrel is satisfactorily clean, coat it with silicone spray or some other form of lubrication.

(4) Make an inspection of the barrel ID (visual and by touch) to check for scoring and also inspect the target collar for any damage.

(5) Clean out the catcher by removing any debris created by the experiment and remove the ruptured diaphragm in the exhaust line (it would be a good practice to go ahead and replace the diaphragm at this time).

(6) The inside of the catcher tank should be coated periodically with some type of low vapor pressure oil or lubrication to help prevent rust.

(7) A visual check of all O-rings and O-ring joints should be made to check for any wear or damage. Replace O-rings as needed.

(8) Finally, keep all parts lubricated as a rust preventative measure.

REFERENCES: APPENDIX A

A.1 Fowles, G.R., et al. 1970. Gas Gun Impact Studies. Review of Scientific Instruments. 41(7): 984-996.

A.2 Roark, R.J., and Young, E. M., 1975. Formulas for Stress and Strain. Mcgraw-Hill Book Co. New York.

A.3 Shigley, J.E. 1977. Mechanical Engineering Design, 3rd Edition. McGraw-Hill Book Co. New York.

A.4 Hoy, D.E.P. 1985. The Shock Compaction of Ti-Al Elemental Powder Mixtures and Accompanying Alloy Formation. North Carolina State University. Raleigh, North Carolina.